NUMERICAL STUDY ON THE STEADY STATE NATURAL CONVECTION IN A PARTIALLY HEATED INCLINED SQUARE CAVITY CONTAINING ADIABATIC CIRCULAR CYLINDER

BY

MD. NURUL HUDA
Student No. 040809002P
Registration No. 040809002, Session: April- 2008

MASTER OF PHILOSOPHY
IN
MATHEMATICS

DEPARTMENT OF MATHEMATICS
BANGLADESH UNIVERSITY OF ENGINEERING AND TECHNOLOGY
DHAKA-1000
February-2013

The thesis titled

NUMERICAL STUDY ON THE STEADY STATE NATURAL CONVECTION IN A PARTIALLY HEATED INCLINED SQUARE CAVITY CONTAINING ADIABATIC CIRCULAR CYLINDER

Submitted by

MD. NURUL HUDA
Student No. 040809002P, Registration No. 040809002, Session: April- 2008

Board of Examiners

1. ____________________________________
Dr. Md. Mustafa Kamal Chowdhury — Chairman (Supervisor)
Professor
Department of Mathematics,
BUET, Dhaka-1000

2. ____________________________________
Dr. Md. Elias — Member (Ex-Officio)
Professor and Head
Department of Mathematics
BUET, Dhaka-1000

3. ____________________________________
Dr. Md. Abdul Maleque — Member
Professor
Department of Mathematics,
BUET, Dhaka-1000

4. ____________________________________
Dr. Md. Abdul Alim — Member
Professor
Department of Mathematics
BUET, Dhaka-1000

5. ____________________________________
Dr. Sujit Kumer Sen — Member (External)
Professor
Research Centre for Mathematics and Physical Sciences (RCMPS)
University of Chittagong, Chittagong

Author's Declaration

I am here by declaring that the work in this dissertation was carried out in accordance with the regulations of Bangladesh University of Engineering and Technology (BUET), Dhaka, Bangladesh. The work is also original except where indicated by and attached with special reference in the context and no part of it has been submitted for any attempt to get other degrees or diplomas.

All views expressed in the dissertation are those of the author and in no way or by no means represent those of Bangladesh University of Engineering and Technology, Dhaka. This dissertation has not been submitted to any other University for examination either in home or abroad.

(MD. NURUL HUDA)

Date: 02 February 2013

Permit of Research

This is to endorse that the work presented in this thesis is carried out by the author under the supervision of Dr. Md. Mustafa Kamal Chowdhury, Professor, Department of Mathematics, Bangladesh University of Engineering & Technology [BUET], Dhaka.

-- ----------------------------

Dr. Md. Mustafa Kamal Chowdhury Md. Nurul Huda

Dedicated to my Parents

Acknowledgements

With great pleasure the author takes this opportunity to place on record his deepest respect and sincerest gratitude to Dr. Md. Mustafa Kamal Chowdhury, Professor, Department of Mathematics, Bangladesh University of Engineering and Technology, Dhaka for his expert guidance and valuable suggestions throughout this work. It would not have been possible to carry out this study successfully without the continuous inspiration and encouragement from supervisor.

I am also deeply indebted to Prof. Dr. Md. Elias, Head of the Department of Mathematics, Prof. Dr. Md. Abdul Maleque and Professor Dr. Md. Abdul Alim, Department of Mathematics, BUET for their wise and liberal co-operation in providing me all necessary help from the department during my course of M.Phil. Degree.

I would also like to extend my thanks to Associate Professor Dr. Md Zafor Iqbal Khan and all other teachers and concerned of this department for their thoroughly help and co-operation.

I would like to extend my warmest gratitude to Mohammed Nasir Uddin, Assistant Professor, Department of Mathematics, Bangladesh University of Business and Technology, Dhaka for his constant inspiration and co-operation at all stages.

Finally I express my devoted affection to my beloved wife Mrs. Anoara Akter and son & daughter for creating a delightful atmosphere to complete the courses, research studies and final production of the thesis work.

Abstract

In this thesis under the title “Numerical Study on the Steady State Natural Convection in a Partially Heated Inclined Square Cavity Containing Adiabatic Circular Cylinder” two problems have been studied. The study as well depending on various locations of cylinder and boundary conditions are abstracted below.

Numerical analysis of two-dimensional laminar steady state natural convection in a tilted partially heated square cavity with adiabatic circular cylinder has been investigated. An adiabatic circular cylinder is placed at the top, centre and bottom of the cavity and the opposite wall to the aperture is placed at iso-flux heat source. The top and bottom walls are adiabatic and the opposite of the heat flux wall is partially heated with temperature T_h (right wall). The fluid is concerned with Prandtl numbers 0.72, 3.0 and 10.0. The properties of the fluid are assumed to be constant. The physical problems are represented mathematically by different sets of governing equations along with the corresponding boundary conditions. The obtained results are presented in terms of isotherms and streamlines, heat transfer characteristics Nusselt numbers for Rayleigh numbers from 10^3 to 10^6 and for inclination angles of the cavity from 0º to 45º. The obtained results are also presented with the variation of different diameter ratios of the cylinder. The results show that the Nusselt numbers increase with the increase of Rayleigh numbers. The computational results also indicate that the average Nusselt number at the hot wall of the cavity is depending on the dimensionless parameters.

Contents

Nomenclature

g	gravitational acceleration (ms^{-2})
Ra	Rayleigh number
k	thermal conductivity of the fluid ($Wm^{-1}K^{-1}$)
L	height and width of the enclosure (m)
Nu	Nusselt number
p	pressure (Nm^{-2})
P	non-dimensional pressure
Pr	Prandtl number, υ/α
q	heat flux (Wm^{-2})
dr	Diameter ratio
T	temperature (K)
u, v	velocity components (ms^{-1})
U, V	non-dimensional velocity components
x, y	Cartesian coordinates (m)
X, Y	non-dimensional Cartesian coordinates

Greek symbols

α	thermal diffusivity, (m^2s^{-1})
β	thermal expansion coefficient (K^{-1})
ρ	density of the fluid (kgm^{-3})
υ	kinematic viscosity of the fluid (m^2s^{-1})
θ	non-dimensional temperature
Φ	inclination angle of the cavity

List of Tables

List of Figures

CHAPTER 1

Introduction and Historical Review

1.1 Introduction

Heat has always been perceived to be something that produces in us a sensation of warmth, and one would think the nature of heat is one of the first things understood by mankind. The ancients viewed, heat as that related to fire. In the middle of nineteenth century that we had a true physical understanding of the nature of heat. The term heat and the associated phrases such as heat flow, heat addition, heat rejection, heat absorption, heat gain, heat loss, heat storage, heat generation, electrical heating, latent heat, body heat, and heat source are in common use today, and the attempt to replace heat in these phrases by thermal energy had only limited success. It is a basic science that deals with the rate of transfer of thermal energy. Heat is the form of energy that can be transferred. The transfer of heat is normally from a high temperature object to a lower temperature object. In the simplest of terms, the discipline of heat transfer is concerned with only two things; those are temperature and the flow of heat. Temperature represents the amount of thermal energy available; whereas heat flow represents the movement of thermal energy from place to place.

Heat transfer is that science which seeks to predict the energy transfer which may take place between material bodies as a result of a temperature difference. Thermodynamics teaches that this energy transfer is defined as heat. The science of heat transfer seeks not merely to explain how heat energy may be transferred, but also to predict the rate at which the exchange will take place under certain specified conditions.

The phenomenon of heat transfer was known to human being even in the primitive age when they used to use solar energy as a source of heat. Heat transfer in its initial stage was conceived with the invention of fire in the early age of human civilization. Since then its knowledge and use has been progressively increasing each day as it is directly related to the growth of human civilization. With the invention of steam engine by James watt in 1765 A. D., the phenomenon of heat transfer got its first industrial recognition and after that its use extended to a great extent and spread out in different spheres of engineering fields. In the past three decades, digital computers, numerical techniques and development of numerical models of heat transfer have made it possible to calculate heat transfer of considerable complexity and thereby create a new approach to the design of heat transfer equipment.

The study of temperature and heat transfer is of great importance to the engineers because of its almost universal occurrence in many branches of science and engineering. Although heat transfer analysis is most important for the proper sizing of fuel elements in the nuclear reactors cores to prevent burnout, the performance of aircraft also depends upon the case with which the structure and engines can be cooled. The design of chemical plants is usually done on the basis of heat transfer analysis and the analogous mass transfer processes. The transfer and conversion of energy from one form to another is the basis to all heat transfer process and hence, they are governed by the first as well as the second law of thermodynamics. Heat transfer is commonly associated with fluid dynamics. The knowledge of temperature distribution is essential in heat transfer studies because of the fact that the heat flow takes place only wherever there is a temperature gradient in a system. The heat flux which is defined as the amount of heat transfer per unit area in per unit time can be calculated from the physical laws relating to the temperature gradient and the heat flux.

Natural convection in a square cavity has received considerable attention because of its importance in several thermal engineering problems. It is used in the design of electronic devices, solar thermal receivers, uncovered flat plate, solar collectors having rows of vertical strips, geothermal reservoirs, etc. Several experiments and numerical calculations have been carried out for describing the phenomenon of natural convection in open cavities, during the past two decades. The present work studies the effect on the flow and heat transfer for different Rayleigh numbers, Prandtl numbers, diameter ratios and inclined angles.

Natural convection in an air filled, differentially heated, inclined square cavity with a diathermal partition placed at the middle of its cold wall has numerically been studied for Rayleigh numbers 10^3 to 10^5. It is observed that due to suppression of convection, heat transfer reductions up to 47 percent in comparison to the cavity without partition by Frederick [11]. Laminar natural convection and conduction in enclosures with multiple vertical partitions were studied theoretically by Kangni et al. [18]. The study covered Rayleigh number Ra in the range 10^3–10^7, Pr = 0.72 (air) aspect ratio 5–20, cavity width 0.1–0.9 and partition thickness 0.01–0.1. They found that the heat transfer decreases with increasing partition number at high Rayleigh number for all conductivity ratios Kr and heat transfer decreases with increasing partition thickness C at all Ra except in the conduction regime where the effect is negligibly small. The offender partitions are less effective in decreasing the heat transfer. Nusselt number is also a decreasing function in the aspect ratio. Tasnim and Collins [35] determined the effect of a horizontal baffle placed on hot (left) wall of a differentially heated square cavity. It has been found that adding baffle on the hot wall can increase the rate of heat transfer by as much as 31.46 percent compared with a wall without baffle for Ra = 10^4. When Ra = 10^5 the increase in heat transfer is 15.3 percent for the same baffle length and the increases in heat transfer is 19.73 percent, when the longest baffle is attached at the middle of the cavity. Bilgen and Oztop [2] studied numerically the steady-state heat transfer by natural convection in partially open inclined square cavities.

1.2 Historical Review

Natural convection in fluid-filled rectangular enclosures has received considerable attention over the past several years due to the wide variety of applications that involve natural convection processes. These applications span such diverse fields as solar energy collection, nuclear reactor operation and safety, the energy efficient design of building, room, and machinery, waste disposal, and fire prevention and safety. The oscillation-induced heat transport has been studied by a number of researchers due to its many industrial applications, such as bioengineering, chemical engineering, and so forth. Kuhn and Oosthuizen [19] numerically studied unsteady natural convection in a partially heated rectangular cavity. They concluded that as the heated location moves from the top to the bottom, the Nusselt number increases up to a maximum and then decreases. Lakhal et al. [21] studied the transient natural convection in a square cavity partially heated from side. In the first, the temperature is varied sinusoidal with time while in the second; it varies with a pulsating manner. The results showed that the mean values of heat transfer and flow intensity are considerably different with those obtained in stationary regime. Le Quere et al [22] investigated the effect on the flow field and heat transfer for the Grashof number as it was varied from 10^4 to $3x10^7$; the temperature difference between the cavity walls and ambient changed from 50 to 500 K, the aspect ratio varied between 0.5 and 2, and the inclination angle of the cavity was modified from 0^0 to 45^o (for 0^o the wall opposite the aperture was vertical and the angles were taken clockwise). The results of the paper showed that the Nusselt number diminishes with the increase in the inclination angle, and that the unsteadiness in the flow takes place for values of the Grashof number greater than 10^6 and inclination angles of 0^o. Showole and Tarasuk [33] investigated, experimentally and numerically, the natural steady state convection in a two dimensional isothermal open cavity. They obtained experimental results for air, varying the Rayleigh number from 10^4 to 5.5 $x10^5$, cavity aspect ratios of 0.25, 0.5 and 1.0, and inclination angles of 0^0, 30^o, 45^o and 60^o (for 0^o, the wall opposite the aperture was horizontal and the angles were taken clockwise). The numerical results were calculated for Rayleigh numbers between 10^4 and $5.5x10^5$, inclination angles of 0^0 and 45^o, and an aspect ratio equal to one. The results showed that, for all Rayleigh numbers, the first inclination of the cavity caused a significant increase in the average heat transfer rate, but a further increase in the inclination angle caused very little increase in the heat transfer rate. Another result observed that, for 0^o, two symmetric counter rotating eddies were formed, while at inclination angles greater than 0^o, the symmetric flow and temperature patterns disappear.

Mohamad [25] studied numerically the natural convection in an inclined two-dimensional open cavity with one heated wall opposite the aperture and two adiabatic walls. The author analyzed the influence on fluid flow and heat transfer, with the inclination angle in the range 10^o-90^o (for 90^o the wall opposite the aperture was vertical and the angles were taken clockwise), the Rayleigh number from 10^3 to 10^7, and the aspect ratio between 0.5 and 2. The study concludes that the inclination angle did not have a significant effect on the average Nusselt number from the isothermal wall, but a substantial one on the local Nusselt number. Polat and Bilgen [31] made a numerical study of the conjugate heat transfer by conduction and natural convection in an inclined, open shallow cavity with a uniform heat flux in the wall opposite to the aperture. The parameters studied were: the Rayleigh number from 10^6 to 10^{12}, the conductivity ratio from 1 to 60, the cavity aspect ratio from 1 to 0.125, the dimensionless wall thickness from 0.05 to 0.20, and the inclination angle from 0^0 to 45^0 from the horizontal (for 0^o, the wall opposite the aperture was vertical and the angles were taken counterclockwise).

Le Quere et al [22] investigated thermally driven laminar natural convection in enclosures with isothermal sides, one of which facing the opening. They used primitive variables and finite difference expressions suitable for treating problems with large temperature and density variations. The computational domain was an enlarged domain comprising a square open cavity and a far field surrounding it. Penot [29] studied a similar problem using stream function-vortices formulation. He also used an enlarged computational domain similar to that of Le Quere et al [22] with approximate boundary conditions. Chan and Tien [4] studied numerically a square open cavity, which had an isothermal vertical heated side facing the opening and two adjoining adiabatic horizontal sides. The boundary conditions at far field were approximated to obtain satisfactory solutions in the open cavity. Chan and Tien [3] studied numerically shallow open cavities and also made a comparison study using a square cavity in an enlarged computational domain. They found that for a square open cavity having an isothermal vertical side facing the opening and two adjoining adiabatic horizontal sides, satisfactory heat transfer results could be obtained, especially at high Rayleigh numbers. In a similar way, Mohamad [25] studied inclined open square cavities, by considering a restricted computational domain. Different from those by Chan and Tien [4], gradients of both velocity components were set to zero at the opening plane. It was found that heat transfer was not sensitive to inclination angle and the flow was unstable at high Rayleigh numbers and small inclinations angles. Polat and Bilgen [31] studied numerically inclined open shallow cavities in which the side facing the opening was heated by constant heat flux, two adjoining walls were insulated and the opening was in contact with a reservoir at constant temperature and pressure. The computational domain was restricted to the cavity.

The finite element method is one of the numerical methods that have received popularity due to its capability for solving complex structural problems (Cook, [6], Zienkiewicz,[37]). The method has been extended to solve problems in several fields such as in the field of heat transfer (Lewis et al., [23], Dechaumphai, [8]), electromagnetics (Jini, [17]), biomechanics (Gallagher et al., [13]), etc. In spite of the great success of the method in these fields, its application to fluid mechanics is still under intensive research. This is due to the fact that the governing differential equations for general flow problems consist of several coupled equations which are inherently nonlinear. Accurate numerical solutions thus require a vast amount of computer time and data storage. One-way to minimize the amount of computer time and data storage used is to employ an adaptive meshing technique (Dechaumphai, [8], Peraire et al., [30]). The technique places small elements in the regions of large change in the solution gradients to increase solution accuracy, and at the same time, uses large elements in the other regions to reduce the computational time and computer memory.

Goutam Saha et al [14] studied a numerical simulation of two-dimensional laminar steady-state natural convection in a square tilt open cavity. The opposite wall to the aperture was kept at either constant surface temperature or constant heat flux, while the surrounding fluid interacting with the aperture was maintained at an ambient temperature. The two remaining walls were assumed to be adiabatic. The fluid concerned is air with Prandtl number fixed at 0.71. The governing mass, momentum and energy equations are expressed in a normalized primitive variables formulation. A finite element method for steady-state incompressible natural convection flows has been developed. The streamlines and isotherms are produced, heat transfer characteristics is obtained for Rayleigh numbers from 10^3 to 10^6 and an inclination angles of the cavity ranges from 0^o to 60^o.

In experimental studies of Ozoe et al. [26], Arnold et al. [1], Linthorst et al. [24] and Hamady et al. [15] found as the tilt angle changes from 0° to 90°, the heat transfer decreases until a minimum point was reached, and then gradually increases again and the minimum point occurs at the angle where flow changes its mode from the three-dimensional roll pattern caused by the thermal instability to the two-dimensional circulation caused by the hydrodynamic effect. Most of these experimental researches only studied cavities with small to medium aspect ratios, with the maximum aspect ratio 15.5. In the study of Elsherbiny et al. [10], six aspect ratios between 5 and 110 were examined experimentally to find the influence of the tilt angle and the aspect ratio on the heat transfer rate. A correlation for tilt angle 60° was developed, and a suggestion of a straight-line interpolation between 60° and 90° was proposed. A lot of numerical studies were also performed. Most of them are two dimensional and only studied flow in an inclined square cavity, such as Ozoe et al. [27], Chen et al. [5], Kuyper et al. [20] and Zhong et al.[36]. However, these two-dimensional numerical studies could not work well at small tilt angles close to horizontal position. In the recent paper of Soong et al. [34], the same model of square cavity from Ozoe et al. [27] was studied with the imperfect constant wall temperature boundary conditions, and the results showed good agreement with the experimental curve even at small tilt angles.

In the present thesis a numerical analysis of two-dimensional laminar steady-state natural convection in a partially heated square cavity have numerically been studied. Adiabatic circular cylinders are placed at top, center and bottom of the cavity and the opposite wall to the aperture is heated by a constant heat flux. The top and bottom walls have kept as an adiabatic. The fluid is concerned with Prandtl number at 0.72, 3.0 and 10.0. The governing mass, momentum and energy equations are expressed in a normalized primitive variables formulation. In this thesis, a finite element method for steady-state incompressible natural convection flows has been developed. The streamlines and isotherms are produced; heat transfer characteristics are obtained for Rayleigh numbers from 10^3 to 10^6 and inclination angles of the cavity from 0º to 45º. The results show that the Nusselt number increases with the Rayleigh numbers. Also the Nusselt number has changed substantially with the inclination angle of the cavity while better thermal performance is also sensitive to the boundary condition of the heated wall.

1.3 Heat Transfer Mechanism

Heat transfer is the transport of thermal energy from one system to another. In order for heat transfer to occur, there must be a temperature difference between the two systems. The transfer of energy as heat is always from the higher temperature medium to the lower temperature one and it stops when the two mediums reach the same temperature. A heat transfer analysis would tell us how long it takes the medium reach the high temperature and also how long it takes to reach any temperature along the way. If the temperature is no longer changing with time, heat transfer occurs at steady conditions, it is called steady heat temperature. Again if the temperature changes with the time, this type of heat transfer is called time dependent or unsteady heat temperature.

Heat transfer mechanism can be grouped into three broad categories or modes: Conduction, Convection, and Radiation. All modes of heat transfer require the existence of a temperature difference and all modes are from the high temperature medium to a lower temperature one. In reality, the combined effect of these three modes of heat transfer control temperature distribution in a medium. A brief description of convection mode is given below.

1.3.1 Convection

Convection is the mechanism by which thermal energy is transferred between a solid surface and a fluid moving over that surface. Convection processes occur all around us, and we are very familiar with some of them. We learn in our childhood that we can cool hot food by blowing air over it. As we have already seen, a hot beverage left on the table will cool as thermal energy is transferred to the surroundings by conduction, convection and radiation. When we are outdoors on a warm summer day, our bodies feel cooler when a breeze blows. A similar, and sometimes dangerous, situation occurs when a wind makes us feel much colder in the winter time.

Convection is the transfer of heat energy between a solid surface and the nearby liquid or gas in motion. As fluid motion goes more quickly the convection heat transfer increases. The presence of bulk motion of fluid enhances the heat transfer between the solid surface and the fluid. The convective mode of heat transfer is divided into two basic processes. If the motion of the fluid arises due to an external agent, such as the externally imposed flow of fluid stream over a heated object, the process is termed as forced convection. The fluid flow may be the results of, for instance, a fan a blower, the wind or the motion of the heated object itself. Such problems are very frequently encountered in technology where heat transfer to, or from, a body is often due to an imposed flow of a fluid at a temperature different from that of the body. It has wide applications in compact heat exchanger, central air conditioning system, cooling tower, gas turbine blade, internal cooling passage, chemical engineering process industries, nuclear reactors, and many other cases. If, on the other hand, no such externally-induced flow is provided and the flow arises “naturally” simply due to the effect of a density difference, resulting from a temperature difference, in a body force field, such as gravitational field, the process is termed as natural or free convection. Natural Convection is when the fluid motion is caused by buoyancy forces that result from the density variations due to variations of temperature in the fluid. For example in the absence of an external source, when the mass of the fluid is in contact with a hot surface its molecules separate and scatter causing the mass of fluid to become less dense. When this happens, the fluid is displaced vertically or horizontally while the cooler fluid gets denser and the fluid sinks. Thus the hotter volume transfers heat towards the cooler volume of that fluid. The density deference gives rise to buoyancy effects due to which the flow is generated. A heated body cooled in ambient air generates such as flow in the region surrounding it. Similarly, the buoyant flow arising from heat rejection to the atmosphere and to other ambient media. Heat transfer by free convection occurs in many engineering applications, such as heat transfer from hot radiators, refrigerator coils, transmission lines, electric transformers, electric heating elements, and electronic equipment etc.

Internal and external flow can also classify convection. Internal flow occurs when the fluid is enclosed by a solid boundary such as a flow through a pipe. An external flow occurs when the fluid extends indefinitely without encountering a solid surface. Both these convections, either natural or forced, can be internal or external as they are independent of each other.

1.3.2 Conduction

Conduction is the transfer of heat by direct contact of particles of matter. The transfer of energy could be primarily by elastic impact as in fluids or by free electron diffusion as predominant in metals or phonon vibration as predominant in insulators. In other words, heat is transferred by conduction when adjacent atoms vibrate against one another, or as electrons move from atom to atom. For example, a spoon in a cup of hot soup becomes warmer because the heat from the soup is conducted along the spoon. Conduction is greater in solids, where atoms are in constant contact. In liquids (except liquid metals) and gases, the molecules are usually further apart, giving a lower chance of molecules colliding and passing on thermal energy. Heat transfer by conduction can occur in gases, liquids, and solids. In general, liquids have higher conductivities than gases, and solids have higher conductivities than liquids. Conduction is the flow of heat through solids and liquids by vibration and collision of molecules and free electrons. For example, a cold canned drink in a warm room eventually warms up to the room temperature as a result of heat transfer from the room to the drink through the aluminum can by conduction. The molecules of a portion of a system at a higher temperature vibrate faster than the molecules of other regions of the same or of another-system at lower temperature. The molecules with a high movement collide with the molecules less energized and transfer part of their energy to the less energized molecules of the colder regions of the structure. For example, the heat transfers by conduction through the bodywork of a car.

In gases the molecules move about in a random manner, colliding with other molecules and thereby exchanging kinetic energy and momentum. If a molecule moves from a high-temperature region to a low-temperature region, energy is transported by that molecule as it collides with other molecules in the low-temperature region.

In liquids the mechanism of heat conduction is essentially the same as it is in gases, except that the molecules are more closely spaced, so molecular forces affect the exchange of energy as collisions occur.

Conduction of heat in solids occurs by one of several mechanisms, depending upon the type of solid. In metals the primary mode of heat conduction is by the drift of free electrons in the valence band of the atoms. This is the same mechanism that is responsible for electrical current. To a lesser degree, heat is conducted in metals by the vibratory motion of the atomic lattice structure. For nonmetallic solids having a crystalline structure, such as quartz, the primary conduction mechanism is the vibratory motion of the lattice structure. In amorphous solids-i.e., solids that do not have crystalline structure, such as plastic, rubber etc -heat conduction occur by random molecular collisions.

The rate of heat conduction through a medium depends on the geometry of the medium, its thickness, and the material of the medium, as well as the temperature difference across the medium. We know that wrapping a hot water tank with glass wool (an insulating material) reduces the rate of heat loss from the tank. The thicker the insulation, the smaller the heat loss. We also know that a hot water tank loses heat at a higher rate when the temperature of the room housing the tank is lowered. Further, the larger the tank, the larger the surface area and thus the rate of heat loss.

1.3.3 Thermal Conductivity

Thermal conductivity of a material can be defined as the rate of heat transfer through a unit area per unit temperature difference. The thermal conductivity of a material is a measure of the ability of the material to conduct heat. As the definition we have the property specific heat c_p as a measure of a material's ability to store thermal energy. For example, C_p=4.18 kJ/kg °C for water and C_p=0.45 kJ/kg °C for iron at room temperature, which indicates that water can store almost 10 times the energy that iron can per unit mass. Similarly, the thermal conductivity k is a measure of a material's ability to conduct heat. For example, k= 0.607 W/m °C for water and k = 80.2 W/m °C for iron at room temperature, which indicates that iron conducts heat more than 100 times faster than water can. Thus we say that water is a poor heat conductor relative to iron, although water is an excellent medium to store thermal energy. A high value for thermal conductivity indicates that the material is good heat conductor, and a low value indicates that the material is a poor heat conductor or insulator. The thermal conductivity of pure copper at room temperature is k = 401 W/m, °C, which indicates that a 1-m-thick copper wall will conduct heat at a rate of 401 W per m^2 area per °C temperature difference across the wall. Note that material such as copper and silver that are good electric conductors, and have high values of thermal conductivity. Material such as rubber, wood, and Styrofoam are poor conductors of heat and have low conductivity values.

If the thermal conductivity is low, the temperature gradient is large, whereas if the thermal conductivity is high, the temperature gradient is small. Thermal conductivities between these extremes yield moderate temperature gradients.

1.3.4 Thermal Diffusivity

The time dependent heat conduction equation for constant k contains a quantity α, called the thermal diffusivity. Thermal diffusivity represents how fast heat diffuses through a material and is defined as

$$\alpha = \frac{\kappa}{\rho C_p}$$

Here the thermal conductivity κ represents how well a material conducts heat, and the heat capacity ρC_p represents how much energy a material stores per unit volume. Therefore, the thermal diffusivity of a material can be viewed as the ratio of the heat conducted through the material to the heat stored per unit volume. A material that has a high thermal conductivity or a low heat capacity will obviously have a large thermal diffusivity. The larger thermal diffusivity means that the propagation of heat into the medium is faster. A small value of thermal diffusivity means the material mostly absorbs the heat and a small amount of heat is conducted further.

1.3.5 Internal and External Flows

A fluid flow is classified as being internal or external, depending on whether the fluid is forced to flow in a confined channel or over a surface. An internal flow is bounded on all sides by solid surfaces except, possibly, for an inlet and exit. Flows through a pipe or in an air-conditioning duct are the examples of internal flow. Internal flows are dominated by the influence of viscosity throughout the flow field. The internal flow configuration represents a convenient geometry for the heating and cooling of fluids used in the chemical processing, environmental control, and energy conversion areas. The flow of an unbounded fluid over a surface is external flow. The flows over curved surfaces such as sphere, cylinder, airfoil, or turbine blade are the example of external flow. In external flows the viscous effects are limited to boundary layers near solid surfaces.

1.3.6 Boundary Layer

Since fluid motion is the distinguishing feature of heat convection, it is necessary to understand some of the principles of fluid dynamics in order to describe adequately the processes of convection. When a fluid flows over a body, the velocity and temperature distribution at the immediate vicinity of the surface strongly influence by the convective heat transfer. In order to simplify the analysis of convective heat transfer the boundary layer concept frequently is introduced to model the velocity and temperature fields near the solid surface in order to simplify the analysis of convective heat transfer. So we are concerned with two different kinds of boundary layers, the velocity boundary layer and the thermal boundary layer.

The velocity boundary layer is defined as the narrow region, near the solid surface, over which velocity gradients and shear stresses are large, but in the region outside the boundary layer, called the potential-flow region, the velocity gradients and shear stresses are negligible. The exact limit of the boundary layer cannot be precisely defined because of the asymptotic nature of the velocity variation. The limit of the boundary layer is usually taken to be at the distance from the surface, at which the fluid velocity is equal to a predetermined percentage of the free stream value, U_∞. This percentage depends on the accuracy desired, 99 or 95% being customary. Although, outside the boundary layer region the flow is assumed to be inviscid, but inside the boundary layer the viscous flow may be either laminar or turbulent. In the case of laminar boundary layer, fluid motion is highly ordered and it is possible to identify streamlines along which particles move. Fluid motion along a streamline is characterized by velocity components in both the x and y directions. Since the velocity component v is in the direction normal to the surface, it can contribute significantly to the transfer of momentum, energy or species through the boundary layer. Fluid motion normal to the surface is necessitated by boundary layer growth in the x direction. In contrast, fluid motion in the turbulent boundary layer is highly irregular and is characterized by velocity fluctuations. These fluctuations enhance the transfer of momentum, energy and species and hence increase surface friction, as well as convection transfer rates. Due to fluid mixing resulting from the fluctuations, turbulent boundary layer thicknesses are larger and boundary layer profiles are flatter than in laminar flow. The thermal boundary layer may be defined (in the same sense that the velocity boundary layer was defined above) as the narrow region between the surface and the point at which the fluid temperature has reached a certain percentage of ambient temperature T_∞. Outside the thermal boundary layer the fluid is assumed to be a heat sink at a uniform temperature of T_∞.The thermal boundary layer is generally not coincident with the velocity boundary layer, although it is certainly dependent on it. If the fluid has high thermal conductivity, it will be thicker than the velocity boundary layer, and if conductivity is low, it will be thinner than the velocity boundary layer.

1.3.7 Flow within an Enclosure

The flow within an enclosure consisting of two horizontal walls, at different temperatures, is an important circumstance encountered quite frequently in practice. In all the applications having this kind of situation, heat transfer occurs due to the temperature difference across the fluid layer, one horizontal solid surface being at a temperature higher than the other. If the upper plate is the hot surface, then the lower surface has heavier fluid and by virtue of buoyancy the fluid would not come to the lower plate. Because in this case the heat transfer mode is restricted to only conduction. But if the fluid is enclosed between two horizontal surfaces of which the upper surface is at lower temperature, there will be the existence of cellular natural convective currents which are called as Benard cells. For fluids whose density decreases with increasing temperature, this leads to an unstable situation.

1.3.8 Boussinesq Approximation

The governing equations for convection flow are coupled elliptic partial differential equations and are, therefore, of considerable complexity. The major problems in obtaining a solution to these equations lie in the inevitable variation of density with temperature, or concentration, and in their partial, elliptic nature. Several approximations are generally made to considerably simplify these equations. Among them Boussinesq approximation attributed to Boussinesq (1903) is considered here. In flows accompanied by heat transfer, the fluid properties are normally functions of temperature. The variations may be small and yet be the cause of the fluid motion. If the density variation is not large, one may treat the density as constant in the unsteady and convection terms, and treat it as variable only in the gravitational term. This is called the Boussinesq approximation.

1.4 Dimensionless Parameters

The dimensionless parameter is a quantity that is normalized as to negate the differences in properties from one substance to another. They are used to enable scientists and engineers to make direct comparisons between dissimilar substances. It can be thought of as measures of the relative importance of certain aspects of the flow. Some dimensionless parameters related to our study are discussed below:

1.4.1 Grashof Number *Gr*

The flow regime in free convection is governed by the dimensionless Grashof number, which represent the ratio of the buoyancy force to the viscous forces acting on the fluid, and is defined as

$$Gr = \frac{g\,\beta\,L^3\left(T_w - T_\infty\right)}{\nu^2}$$

where g is the acceleration due to gravity, β is the volumetric thermal expansion coefficient, T_w is the wall temperature, T_∞ is the ambient temperature, L is the characteristic length and ν is the kinematics viscosity. The Grashof number provides the main criterion in determining whether the fluid flow is laminar or turbulent in free convection. For vertical plates, the critical value of the Grashof number is observed to be about 10^9. Therefore, the flow regime on a vertical plate becomes turbulent at Grashof numbers greater than10^9.

1.4.2 Prandtl Number *Pr*

The relative thickness of the velocity and the thermal boundary layers is the best described by the dimensionless parameter. It is name after Ludwig Prandtl, who introduced the concept of boundary layer in 1904 and made significant contributions to boundary layer theory. The momentum equations with associated boundary conditions are the governing relations for the transport of momentum in the laminar boundary layer and the energy equations for the laminar boundary layer with the associated boundary conditions are the governing relations for the transport of thermal energy in the laminar boundary layer. There is a noticeable similarity between the momentum and thermal energy equations. In fact, the solution of two equations has the same form when the thermal diffusivity (α) equals the kinematics viscosity (ν). The ratio of these two properties is a dimensionless parameter called Prandtl number and is defined as:

$$\Pr = \frac{Molecular\, diffusivity\ of\ momentum}{Molecular\, diffusivity\ of\ heat} = \frac{\nu}{\alpha}$$

The Prandtl number is interpreted physically as the ratio of the rate at which momentum is transported to the rate at which thermal energy is transported in the laminar boundary layer. Therefore, the size of the Prandtl numbr is an indication of the relative rates of growth of the velocity and thermal boundary layers. A Prandtl number larger than 1 indicates that the rate of velocity boundary-layer growth exceeds that of the thermal boundary layer, whereas a Prandtl number smaller than 1 indicates that the thermal boundary layer is growing at a rate faster than the velocity boundary layer.

The Prandtl number controls the relative thickness of the momentum and thermal boundary layers. When *Pr* is small, it means that the heat diffuses very quickly compared to the velocity. This means that for liquid metals the thickness of the thermal Boundary layer is much bigger than the velocity Boundary Layer. The Prandtl numbers of gases are about 1, which indicates that both momentum and heat dissipate through the fluid at about the same rate. The Prandtl number for common liquids is normally greater than 1, but it varies considerable with temperature because of the strong temperature dependence of kinematics viscosity. Liquid metals such as mercury have low Prandtl numbers due to their high thermal conductivities. Consequently the thermal boundary layer is much thicker for liquid metals and much thinner for oils relative to the velocity boundary layer. For mercury, heat conduction is very effective compared to convection - thermal diffusivity is dominant. For engine oil, convection is very effective in transferring energy from an area, compared to pure conduction - momentum diffusivity is dominant. The Prandtl numbers of fluids range from less than 0.01 for liquid metals to more than 100,000 for heavy oils. Note that the Prandtl number is in the order of 7 for water. Prandtl numbers as a function of temperature for several liquids and gases.

1.4.3 Rayleigh Number *Ra*

The Rayleigh number for a fluid is a dimensionless number associated with buoyancy driven flow (also known as free convection or natural convection). In fluid mechanics When the Rayleigh number is below the critical value for that fluid, heat transfer is primarily in the form of conduction; when it exceeds the critical value, heat transfer is primarily in the form of convection. The latter can be laminar or turbulent. The Rayleigh number is named after Lord Rayleigh and is defined as the product of the Grashof number, which describes the relationship between buoyancy and viscosity within a fluid, and the Prandtl number, which describes the relationship between momentum diffusivity and thermal diffusivity. Hence the Rayleigh number itself may also be viewed as the ratio of buoyancy forces and (the product of) thermal and momentum diffusivities.

For convection near a vertical wall, this number is

$$Ra = Gr \,.\Pr = \frac{g\,\beta\left(T_w - T_\infty\right)L^3}{\nu\,\alpha}$$

For most engineering purposes, the Rayleigh number is large, somewhere around 10^6 and 10^8.

1.4.4 Nusselt Number *Nu*

The Nusselt number is named after Wilhelm Nusselt, who made significant contributions, to convective heat transfer in the first half of the twentieth century, and it is viewed as the dimensionless convection heat transfer coefficient. It represents the enhancement of heat transfer through a fluid layer as a result of convection relative to conduction across the same fluid layer. In heat transfer at a boundary surface within a fluid, the Nusselt number is the ratio of convective to conductive heat transfer across the boundary, and is defined as

$$Nu = \frac{hL}{k}$$

Where *k* is the thermal conductivity of the fluid, *h* is the convective heat transfer coefficient, and *L* is the characteristic length. The conductive component is measured under the same conditions as the heat convection by with a stagnant fluid.

The Nusselt number is interpreted physically as a dimensionless temperature gradient at the surface. A large Nusselt number indicates a large temperature gradient at the surface and, hence, high heat transfer by convection. The larger the Nusselt number, the more effective the convection. A Nusselt number close to unity, namely convection and conduction of similar magnitude, is characteristic of laminar flow. A larger Nusselt number correspondence to more active convection, with turbulent flow typically in the 100-1000 range

To under the significance of the Nusselt number, consider the following daily life problems. For example, we turn on the fan on hot summer days to help our body cool more effectively. The higher the fan speed, the better we feel. We stir our soup and blow on a hot slice of pizza take them cool faster.

Typically, for free convection, the average Nusselt number is expressed as a function of the Raleigh number and the Prandtl number, written as: Nu=f (Ra, Pr). Else, for forced convection, the Nusselt number is generally a function of the Reynolds number and the Prandtl number, or Nu = f (Re, Pr).

1.5 Enthusiasm behind the Selection of Current Work

From the historical review it is clear that during the past two decades, several experiments and numerical calculations have been presented for describing the phenomenon of natural convection in open cavities. Those studies have been focused to study the effect on flow and heat transfer for different Rayleigh numbers, aspect ratios, and tilt angles. Natural convection in open cavities has received considerable attention because of its importance in several thermal engineering problems, for example, in the design of electronic devices, solar thermal receivers, uncovered flat plate, solar collectors having rows or vertical strips, geothermal reservoirs, etc. In the present thesis, a numerical analysis of two-dimensional laminar steady-state natural convection in a partially heated square cavity has numerically studied. An adiabatic circular cylinder is placed at different locations such as top, center and bottom of the cavity and the opposite wall to the aperture by a constant iso-flux heat source. The top and bottom walls remain adiabatic. In this thesis, a finite element method for steady-state incompressible natural convection flows has been developed. Numerical studies are therefore essential to observe the variation in fluid flow and heat transfer due to the above physical changes with boundary conditions, which forms the basis of the motivation behind the present study.

1.6 Main Objectives of the Present Study

The present study has focused on the development of a mathematical model and numerical techniques regarding the effects of natural convection flow around an adiabatic circular cylinder placed in a square cavity in different locations.

The specific objectives of the present research work are as follows:

a. A mathematical model regarding the effect of natural convection flow around an adiabatic circular cylinder which is placed in various places in a square cavity will be developed.

b. To visualize the fluid flow and temperature distribution inside cavity.

c. To investigate the effects of Rayleigh number and Prandtl number on the heat transfer characteristics.

d. To investigate the effects of adiabatic circular cylinder placed at different locations on natural convection inside a square cavity.

e. To examine the effects of inclination angles of the cavity.

f. To investigate the effects of diameter ratio of an adiabatic circular center cylinder.

1.7 Outline of the Thesis

This dissertation contains four chapters. In this chapter a brief introduction is presented with aim and objectives. This chapter also consists of a literature review of the past studies on fluid flow and heat transfer in cavities. The different aspects of the previous studies have been mentioned categorically. This is followed by the post-mortem of a recent historical event for the illustration of fluid flow and heat transfer effects in cavities.

In Chapter 2, the computational technique of the problem has been discussed for viscous incompressible flow.

In Chapter 3, a detailed parametric study on Numerical simulation of two-dimensional laminar steady-state natural convection in an inclined partially heated square cavity with an adiabatic circular cylinder is placed at the top, center and bottom. Effects of the major parameters such as Rayleigh number, Prandtl number, different angles of the cavity and diameter ratio of the cylinder have been presented for a better understanding of the heat transfer mechanisms in square cavity. The results of isotherms and streamlines for

Rayleigh number, Prandtl number, different angle of the cavity and different diameter ratio of the cylinder with natural convection have been studied.

Finally, in Chapter 4 the study is rounded off with the conclusions, comparison of both cylinders and recommendations for further study of the present problem are outlined.

CHAPTER 2

COMPUTATIONAL TECHNIQUE

Computational Technique

Computational fluid dynamics (CFD) has been rapidly gaining popularity over the past several years for technological as well as scientific interests. For many problems of industrial interest, experimental techniques are extremely expensive or even impossible due to the complex nature of the flow configuration. Analytical methods are often useful in studying the basic physics involved in a certain flow problem, however, in many interesting problems; these methods have limited direct applicability. The dramatic increase in computational power over the past several years has led to a heightened interest in numerical simulations as a cost effective method of providing additional flow information, not readily available from experiments, for industrial applications, as well as a complementary tool in the investigation of the fundamental physics of turbulent flows, where analytical solutions have so far been unattainable. It is not expected (or advocated), however, that numerical simulations replace theory or experiment, but that they are to be used in conjunction with these other methods to provide a more complete understanding of the physical problem at hand.

Mathematical model of physical phenomena may be ordinary or partial differential equations, which have been the subject of analytical and numerical investigations. The partial differential equations of fluid mechanics and heat transfer are solvable for only a limited number of flows. To obtain an approximate solution numerically, we have to use a discretization method, which approximated the differential equations by a system of algebraic equations, which can then be solved on a computer. The approximations are applied to small domains in space and / or time so the numerical solution provides results at discrete locations in space and time. Much as the accuracy of experimental data depends on the quality of the tools used, the accuracy of numerical solutions depend on the quality of discretizations used. Computational fluid dynamics (CFD) computation involves the formation of a set numbers that constitutes a practical approximation of a real life system. The outcome of computation process improves the understanding of the performance of a system. Thereby, engineers need CFD codes that can make physically realistic results with good quality accuracy in simulations with finite grids. Contained within the broad field of computational fluid dynamics are activities that cover the range from the automation of well established engineering design methods to the use of detailed solutions of the Navier-Stokes equations as substitutes for experimental research into the nature of complex flows. CFD have been used for solving wide range of fluid dynamics problem. It is more frequently used in fields of engineering where the geometry is complicated or some important feature that cannot be dealt with standard methods.

2.1 Elements of Numerical Solution Methods

Several components of numerical solution methods are available in Ferziger and Perić [12], here only the main steps will be demonstrate in the following.

2.1.1 Mathematical Model

The starting point of any numerical method is the mathematical model, i.e. the set of partial differential equations and boundary conditions. A solution method is usually designed for a particular set of equations. Trying to produce a general purpose solution method, i.e. one which is applicable to all flows, is impractical, is not impossible and as with most general purpose tools, they are usually not optimum for any one application.

2.1.2 Discretization Process

After selecting the mathematical model, one has to choose a suitable discretization method, i.e. a method of approximating the differential equations by a system of algebraic equations for the variable at some set of discrete locations in space and time.

2.1.3 Numerical Grid

The numerical grid defines the discrete locations, at which the variables are to be calculated, which is essentially a discrete representation of the geometric domain on which the problem is to be solved. It divided the solution domain into a finite number of sub-domains (elements, control volumes etc). Some of the options available are structural (regular) grid, block structured grid, unstructured grids etc.

2.1.4 Finite Approximations

Following the choice of grid type, one has to select the approximations to be used in the discretization process. In a finite difference method, approximations for the derivatives at the grid points have to be selected. In a finite volume method, one has to select the methods of approximating surface and volume integrals. In a finite element method, one has to choose the functions and weighting functions.

2.1.5 Solution Technique

Discretization yields a large system of non-linear algebraic equations. The method of solution depends on the problem. For unsteady flows, methods based on those used for initial value problems for ordinary differential equation (marching in time) is used. At each time step an elliptic problem has to be solved. Pseudo-time marching or an equivalent iteration scheme usually solves steady flow problems. Since the equations are non-linear, an iteration scheme is used to solve them. These methods use successive linearization of the equations and the resulting linear systems are almost always solved by iterative techniques. The choice of solver depends on the grid type and the number of nodes involved in each algebraic equation.

2.2 Discretization Approaches

The first step to numerically solve a mathematical model of physical phenomena is its numerical discretization. This means that each component of the differential equations is transformed into a “numerical analogue” which can be represented in the computer and then processed by a computer program, built on some algorithm. There are many different methodologies were devised for this purpose in the past and the development still continues. In order to short them, we can at first divide the spatial discretisation schemes into the following three main categories: finite difference (FD), finite volume (FV), finite element (FE) methods, Boundary element (BE) method and Boundary volume (BV) method.

In the present numerical computation, Galerkin finite element method (FEM) is used. Detailed discussion of this method is available in Chung [7] and Dechaumphai [9].

2.2.1 Finite Element Analysis

The finite element method (FEM) is a powerful computational method for solving problems, which are described by partial differential equations. The fundamental idea of the finite element method is to outlook a given domain as an assemblage of simple geometric shapes, called finite elements, for which it is possible to systematically generate the approximation functions needed in the solution of partial differential equations by the weighted residual method. The computational domains with irregular geometries by a collection of finite elements makes the method a valuable practical tool for the solution of boundary value problems arising in various fields of engineering. The approximation functions, which satisfy the governing equations and boundary conditions, are often constructed using ideas from interpolation theory. Approximating functions in finite elements are determined in terms of nodal values of a physical field, which is required. A continuous physical problem is transformed into a discretized finite element problem with unknown nodal values. For a linear problem, a system of linear algebraic equations should be solved. Values inside finite elements can be recovered using nodal values.

The finite element method is one of the numerical methods that have received popularity due to its capability for solving complex structural problems. The method has been extended to solve problems in several other fields such as in the field of heat transfer, computational fluid dynamics, electromagnetic, biomechanics etc. In spite of the great success of the method in these fields, its application to fluid mechanics, particularly to convective viscous flows, is still under intensive research.

The major steps involved in finite element analysis of a typical problem are:

a. Discretization of the domain into a set of finite elements (mesh generation).
b. Weighted-integral or weak formulation of the differential equation to be analyzed.
c. Development of the finite element model of the problem using its weighted-integral or weak form.
d. Assembly of finite elements to obtain the global system of algebraic equations.
e. Imposition of boundary conditions.
f. Solution of equations.
g. Post-computation of solution and quantities of interest.

2.2.2 Mesh Generation

The area of numerical grid generation is relatively young in practice, although its roots in mathematics are old. The arrangement of discrete points throughout the flow field is simply called a grid. The determination of a proper grid for the flow through a given geometric shape is important. The way that such a grid is determined is called grid generation. The grid generation is a significant consideration in CFD. Finite element method can be applied to unstructured grids. This is because the governing equations in this method are written in integral form and numerical integration can be carried out directly on the unstructured grid domain in which no coordinate transformation is required. A two-dimensional domain may be triangulated as shown in Figure 2.1. In finite element method, the mesh generation is the technique to subdivide a domain into a set of sub-domains, called finite elements. Figure 2.1 shows a domain, Λ is subdivided into a set of sub-domains, Λ^e with boundary Γ^e. Detailed discussion of this issue is available in Chung [7].

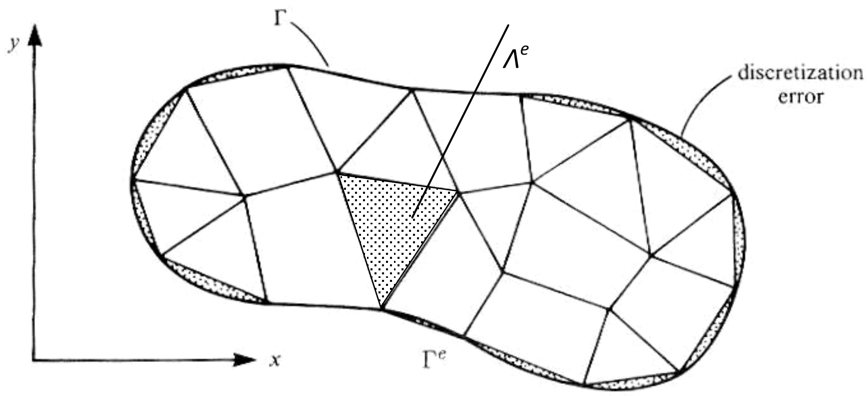

Figure 2.1: A typical FE discretization of a domain.

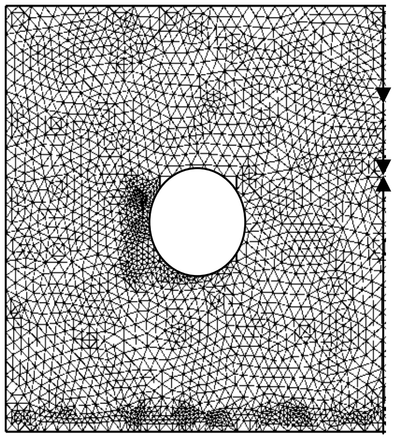

Figure 2.2: Current mesh structure of elements for partially heated square cavity.

2.2.3 Finite Element Formulation and Computational Technique

Viscous incompressible thermal flows have been the subject of our investigation. The problem is relatively complex due to the coupling between the energy equation and the Navier-Stokes equations, which govern the fluid motion. These equations comprise a set of coupled nonlinear partial differential equations, which is difficult to solve especially with complicated geometries and boundary conditions. The finite element formulation and computational procedure for Navier-Stokes equations along with energy equations will discuss in chapter 3.

2.2.4 Algorithm

The algorithm was originally put forward by the iterative Newton-Raphson algorithm; the discrete forms of the continuity, momentum and energy equations are solved to find out the value of the velocity and the temperature. It is essential to guess the initial values of the variables. Then the numerical solutions of the variables are obtained while the convergent criterion is fulfilled. The simple algorithm is shown by the flow chart in next page.

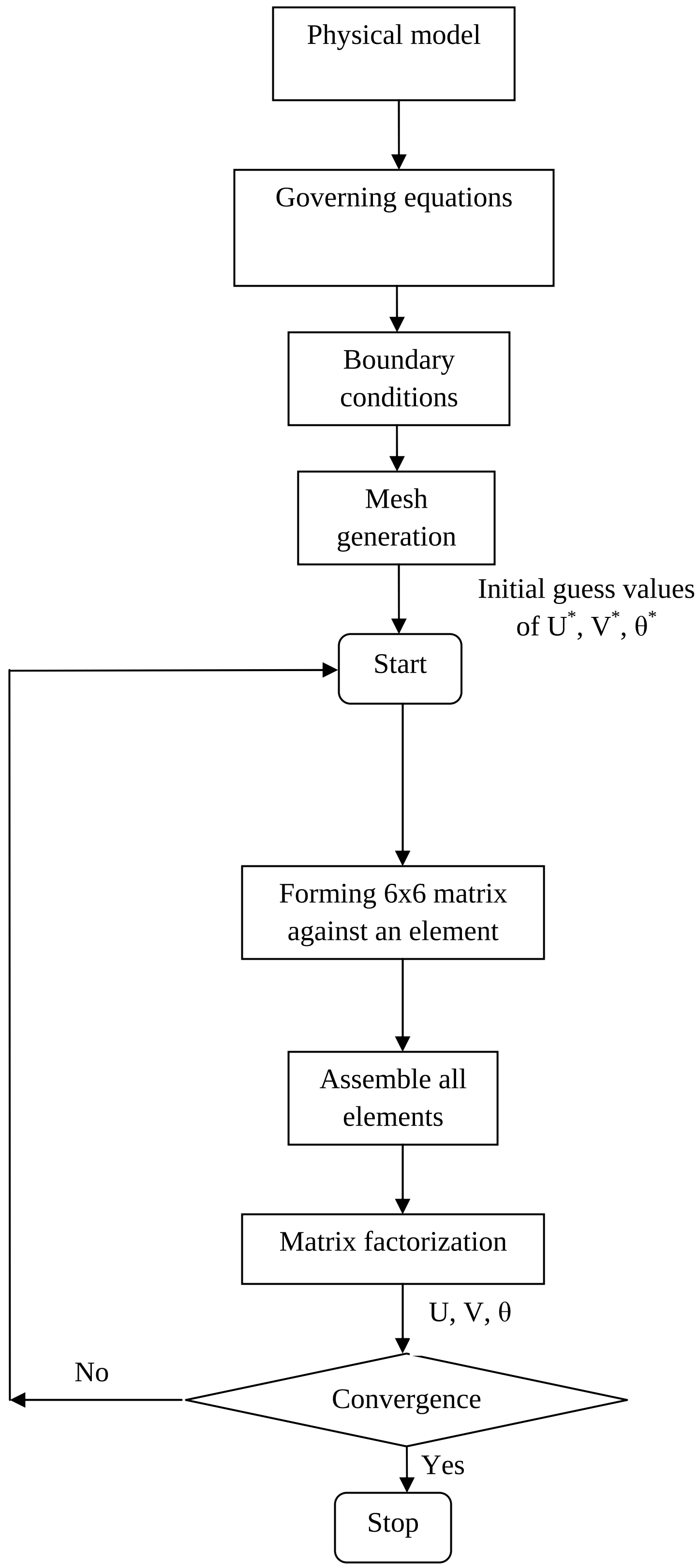

Figure 2.3: Flow chart of the computational procedure

2.2.5 Solution of System of Equations

A system of linear algebraic equations has been solved by the UMFPACK with COMSOL MULTIPHYSICS package interface. UMFPACK is a set of routines for solving asymmetric sparse linear systems $Ax = b$, using the Asymmetric Multi-Frontal method and direct sparse LU (Lower and Upper triangular) factorization. Five primary UMFPACK routines are required to factorize A or $Ax = b$:

a. Pre-orders the columns of A to reduce fill-in and performs a symbolic analysis.
b. Numerically scales and then factorizes a sparse matrix.
c. Solves a sparse linear system using the numeric factorization.
d. Frees the Symbolic object.
e. Frees the Numeric object.

Additional routines are:

a. Passing a different column ordering
b. Changing default parameters
c. Manipulating sparse matrices
d. Getting LU factors
e. Solving the LU factors
f. Computing determinant

UMFPACK factorizes PAQ, PRAQ, or $PR^{-1}AQ$ into the product LU, where L and U are lower and upper triangular respectively, P and Q are permutation matrices, and R is a diagonal matrix of row scaling factors (or R = I if row-scaling is not used). Both P and Q are chosen to reduce fill-in (new nonzero in L and U that are not present in A). The permutation P has the dual role of reducing fill-in and maintaining numerical accuracy (via relaxed partial pivoting and row interchanges). The sparse matrix A can be square or rectangular, singular or non-singular, and real or complex (or any combination). Only square matrices A can be used to solve $Ax = b$ or related systems. Rectangular matrices can only be factorized. UMFPACK first finds a column pre-ordering that reduces fill-in, without regard to numerical values. It scales and analyzes the matrix, and then automatically selects one of three strategies for pre-ordering the rows and columns: asymmetric, 2-by-2 and symmetric. These strategies are described below.

One notable attribute of the UMFPACK is that whenever a matrix is factored, the factorization is stored as a part of the original matrix so that further operations on the matrix can reuse this factorization. Whenever a factorization or decomposition is calculated, it is preserved as a list (element) in the factor slot of the original object. In this way a sequence of operations, such as determining the condition number of a matrix and then solving a linear system based on the matrix, do not require multiple factorizations of the intermediate results.

Conceptually, the simplest representation of a sparse matrix is as a triplet of an integer vector **i** giving the row numbers, an integer vector **j** giving the column numbers, and a numeric vector **x** giving the non-zero values in the matrix. The triplet representation is row oriented if elements in the same row were adjacent and column oriented if elements in the same column were adjacent. The compressed sparse row (CSR) or compressed sparse column (CSC) representation is similar to row oriented triplet or column oriented triplet respectively. These compressed representations remove the redundant row or column in indices and provide faster access to a given location in the matrix.

2.3 Chapter Summary

This chapter has presented an introduction to computational method with advantages of numerical investigation. Because numerical method has played a central role in this thesis. Various components of numerical method have been also explained. Finally, the major steps involved in finite element analysis of a typical problem have been discussed.

CHAPTER 3

Numerical study on the steady state natural convection in a partially heated inclined square cavity containing adiabatic circular cylinder

3.1 Problem Definition

The heat transfer and the fluid flow in a two-dimensional square cavity of length L is considered, as shown in the schematic diagram of figure 3.1. The top and bottom walls are adiabatic and right wall is partially heated with temperature T_h but upper and lower portion of right wall is adiabatic while the side wall in front of the breathing space to the aperture is kept constant heat flux q, and the surrounding fluid interacting with the aperture is maintained to an ambient temperature T_∞. The circular cylinder is assumed adiabatic. The fluid is assumed with Prandtl number (*Pr* = 0.72, 3.0, 10.0) and the fluid flow is considered to be laminar. The properties of the fluid are assumed to be constant.

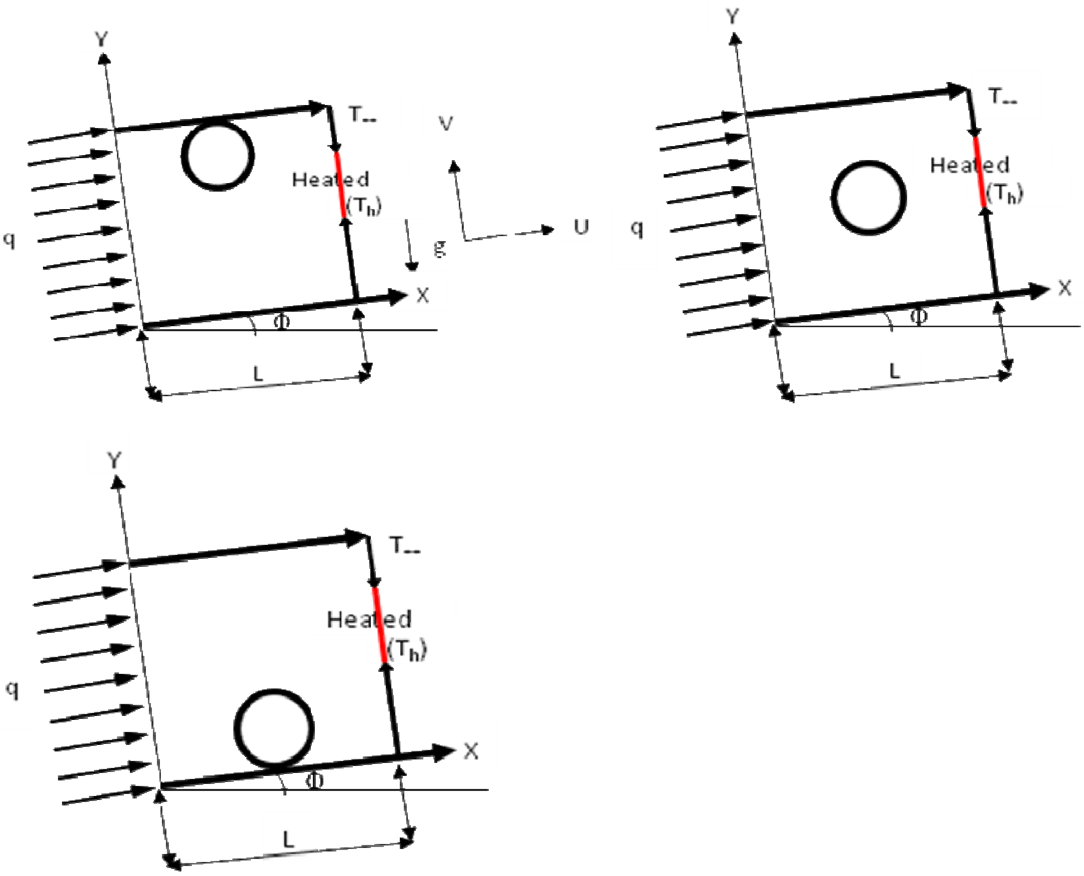

Fig-3.1: Schematic diagram of the physical system

3.2 Mathematical Modeling

The several steps of the mathematical formulation for the above physical configurations are shown as follows.

3.2.1 Governing Equations

Natural convection is governed by the differential equations expressing conservation of mass, momentum and energy. The present flow is considered steady, laminar, incompressible and two-dimensional. The viscous dissipation term in the energy equation is neglected. The Boussinesq approximation is invoking for the fluid properties to relate density changes to temperature changes, and to couple in this way the temperature field to the flow field. The governing equations for steady natural convection flow can be written as:

Continuity equation

$$\frac{\partial u}{\partial x} + \frac{\partial v}{\partial y} = 0 \tag{1}$$

Momentum equations in x-direction

$$u\frac{\partial u}{\partial x} + v\frac{\partial u}{\partial y} = -\frac{1}{\rho}\frac{\partial p}{\partial x} + \upsilon\left(\frac{\partial^2 u}{\partial x^2} + \frac{\partial^2 u}{\partial y^2}\right) + g\,\beta\left(T - T_\infty\right) Sin\,\Phi \tag{2}$$

Momentum equations in y-direction

$$u\frac{\partial v}{\partial x} + v\frac{\partial v}{\partial y} = -\frac{1}{\rho}\frac{\partial p}{\partial y} + \upsilon\left(\frac{\partial^2 v}{\partial x^2} + \frac{\partial^2 v}{\partial y^2}\right) + g\,\beta\left(T - T_\infty\right) Cos\,\Phi \tag{3}$$

Energy equation

$$u\frac{\partial T}{\partial x} + v\frac{\partial T}{\partial y} = \alpha\left(\frac{\partial^2 T}{\partial x^2} + \frac{\partial^2 T}{\partial y^2}\right) \tag{4}$$

3.2.2 Boundary Conditions

The boundary conditions for the present problem are specified as follows:

On the left wall at $x=0$

$$u=v=0,\ \frac{\partial T}{\partial x}=-\frac{q}{k}$$

On the right wall at $x=L=1$

$$u=v=0,\ \frac{\partial T}{\partial x}=0\ and\ T=T_h$$

On the bottom wall at $y=0$

$$u=v=0,\ \frac{\partial T}{\partial y}=0$$

On the upper wall at $y=L=1$

$$u=v=0,\ \frac{\partial T}{\partial y}=0$$

On the cylinder $u=v=0,\ \frac{\partial T}{\partial x}=0,\ \frac{\partial T}{\partial y}=0$

where x and y are the distances measured along the horizontal and vertical directions, respectively; u and v are the velocity components in the x- and y-direction, respectively; T denotes the temperature; ν and α are the kinematics viscosity and the thermal diffusivity respectively; p is the pressure and ρ is the density; T_h and T_∞ are heated and ambient temperatures respectively.

3.2.3 Dimensional Analysis

The governing equations in non-dimensional form are written as follows:

Continuity equation

$$\frac{\partial U}{\partial X}+\frac{\partial V}{\partial Y}=0 \tag{5}$$

Momentum equations

$$U\,\frac{\partial U}{\partial X}+V\,\frac{\partial U}{\partial Y}=-\frac{\partial P}{\partial X}+\sqrt{\frac{\Pr}{Ra}}\left(\frac{\partial^2 U}{\partial X^2}+\frac{\partial^2 U}{\partial Y^2}\right)+\theta\,\sin\,\Phi \tag{6}$$

$$U\,\frac{\partial V}{\partial X}+V\,\frac{\partial V}{\partial Y}=-\frac{\partial P}{\partial Y}+\sqrt{\frac{\Pr}{Ra}}\left(\frac{\partial^2 V}{\partial X^2}+\frac{\partial^2 V}{\partial Y^2}\right)+\theta\,\cos\,\Phi \tag{7}$$

Energy equation

$$U\,\frac{\partial\theta}{\partial X}+V\,\frac{\partial\theta}{\partial Y}=\frac{1}{\sqrt{\Pr.Ra}}\left(\frac{\partial^2\theta}{\partial X^2}+\frac{\partial^2\theta}{\partial Y^2}\right) \tag{8}$$

Equations (5)-(8) are made non-dimensional using the following dimensionless scales:

$$\mathrm{X}=\frac{\mathrm{x}}{\mathrm{L}},\ \mathrm{Y}=\frac{\mathrm{y}}{\mathrm{L}},\ \mathrm{U}=\frac{\mathrm{u}}{\mathrm{U_o}},\ \mathrm{V}=\frac{\mathrm{v}}{\mathrm{U_o}},\ P=\frac{p-p_\infty}{\rho U_o^2},\ \theta=\frac{T-T_\infty}{\Delta t},\ dr=\frac{D}{L},$$

$$\Pr=\frac{\nu}{\alpha},\ Gr=\frac{g\,\beta\,\Delta t\,L^3}{\nu^2},\ Ra=\Pr.Gr,\ \Delta t=(T_h-T_\infty),\ \Delta t=\frac{q\,L}{k}$$

Here Gr, Pr and Ra are Grashof, Prandtl and Rayleigh numbers respectively. The Rayleigh number is defined as the ratio of buoyancy forces and (the product of) thermal and momentum diffusivities. The reference velocity U_o is related to the buoyancy force term and is defined as $U_o=\sqrt{g\,\beta\,L\left(T_h-T_\infty\right)}$.

The Nusselt number Nu is one of the important dimensionless parameters to be computed for heat transfer analysis in natural convection flow. Also the Nusselt number for free convection is a function of the Raleigh number and the Prandtl number. The local Nusselt number can be obtained from the temperature field by applying

$$Nu = -\frac{1}{T(1, y)}$$

and the average or overall Nusselt number was calculated by integrating the temperature gradient over the heated wall as

$$Nu_{av} = -\int_0^1 \frac{1}{\theta(1, Y)} dY$$

with the boundary conditions

On the left wall at $X = 0$

$$U = V = 0, \ \frac{\partial \theta}{\partial X} = -1$$

On the right wall at $X = L = 1$

$$U = V = 0, \ \frac{\partial \theta}{\partial X} = 0 \ \ and \ T = T_h$$

On the bottom wall at $Y = 0$

$$U = V = 0, \ \frac{\partial \theta}{\partial Y} = 0$$

On the upper wall at $Y = L = 1$

$$U = V = 0, \ \frac{\partial \theta}{\partial Y} = 0$$

On the cylinder: $U = V = 0, \ \frac{\partial \theta}{\partial X} = 0 \quad and \ \frac{\partial \theta}{\partial Y} = 0$

3.3 Numerical Analysis

The governing equations along with the boundary conditions are solved numerically, employing Galerkin weighted residual finite element techniques discussed below.

3.3.1 Finite Element Formulation and Computational Technique

The numerical procedure used to solve the governing equations for the present work is based on the Galerkin weighted residual method of finite element formulation. The non-linear parametric solution method is chosen to solve the governing equations. This approach will result in substantially fast convergence assurance. A non-uniform triangular mesh arrangement is implemented in the present investigation especially near the walls to capture the rapid changes in the dependent variables.

The velocity and thermal energy equations (5)-(8) result in a set of non-linear coupled equations for which an iterative scheme is adopted. To ensure convergence of the numerical algorithm the following criteria is applied to all dependent variables over the solution domain

$$\sum \left| \psi_{ij}^{n} - \psi_{ij}^{n-1} \right| \leq 10^{-5}$$

Where, Ψ represents a dependent variable U, V, P and T; the indexes i, j indicate a grid point; and the index n is the current iteration at the grid level. The six node triangular element is used in this work for the development of the finite element equations. All six nodes are associated with velocities as well as temperature; only the corner nodes are associated with pressure. This means that a lower order polynomial is chosen for pressure and which is satisfied through continuity equation. The velocity component and the temperature distributions and linear interpolation for the pressure distribution according to their highest derivative orders in the differential Eqs (5)-(8) as

$$U(X,Y) = N_{\alpha} U_{\alpha} \tag{9}$$

$$V(X,Y) = N_{\alpha} V_{\alpha} \tag{10}$$

$$\theta(X,\ Y) = N_{\alpha} \quad \theta_{\alpha} \tag{11}$$

$$P(X,Y) = H_{\lambda} P_{\lambda} \tag{12}$$

where α = 1, 2, … …, 6; λ= 1, 2, 3; N_α are the element interpolation functions for the velocity components and the temperature, and H_λ are the element interpolation functions for the pressure.

To derive the finite element equations, the method of weighted residuals is applied to the continuity Eq. (5), the momentum Eqs (6)-(7), and the energy Eq. (8), we get

$$\int_A N_\alpha \left(\frac{\partial U}{\partial X} + \frac{\partial V}{\partial Y}\right) dA = 0 \tag{13}$$

$$\begin{aligned}\int_A N_\alpha \left(U\frac{\partial U}{\partial X} + V\frac{\partial U}{\partial Y}\right) dA &= -\int_A H_\lambda \left(\frac{\partial P}{\partial X}\right) dA \\ &+ \sqrt{\frac{\Pr}{Ra}} \int_A N_\alpha \left(\frac{\partial^2 U}{\partial X^2} + \frac{\partial^2 U}{\partial Y^2}\right) dA + \int_A N_\alpha \,(Sin\Phi)\, \theta \, dA\end{aligned} \tag{14}$$

$$\begin{aligned}\int_A N_\alpha \left(U\frac{\partial V}{\partial X} + V\frac{\partial V}{\partial Y}\right) dA &= -\int_A H_\lambda \left(\frac{\partial P}{\partial Y}\right) dA \\ &+ \sqrt{\frac{\Pr}{Ra}} \int_A N_\alpha \left(\frac{\partial^2 V}{\partial X^2} + \frac{\partial^2 V}{\partial Y^2}\right) dA + \int_A N_\alpha \,(Cos\Phi)\, \theta \, dA\end{aligned} \tag{15}$$

$$\int_A N_\alpha \left(U\frac{\partial \theta}{\partial X} + V\frac{\partial \theta}{\partial Y}\right) dA = \sqrt{\frac{1}{\Pr . Ra}} \int_A N_\alpha \left(\frac{\partial^2 \theta}{\partial X^2} + \frac{\partial^2 \theta}{\partial Y^2}\right) dA \tag{16}$$

where A is the element area. Gauss's theorem is then applied to Eqs (14)-(16) to generate the boundary integral terms associated with the surface tractions and heat flux. Then Eqs (14)-(16) become,

$$\begin{aligned}&\int_A N_\alpha \left(U\frac{\partial U}{\partial X} + V\frac{\partial U}{\partial Y}\right) dA + \int_A H_\lambda \left(\frac{\partial P}{\partial X}\right) dA + \sqrt{\frac{\Pr}{Ra}} \int_A \left(\frac{\partial N_\alpha}{\partial X}\frac{\partial U}{\partial X} + \frac{\partial N_\alpha}{\partial Y}\frac{\partial U}{\partial Y}\right) dA \\ &\quad - \int_A Sin\Phi \, N_\alpha \, \theta \, dA = \int_{S_0} N_\alpha S_x \, dS_0\end{aligned} \tag{17}$$

$$\begin{aligned}&\int_A N_\alpha \left(U\frac{\partial V}{\partial X} + V\frac{\partial V}{\partial Y}\right) dA + \int_A H_\lambda \left(\frac{\partial P}{\partial Y}\right) dA + \sqrt{\frac{\Pr}{Ra}} \int_A \left(\frac{\partial N_\alpha}{\partial X}\frac{\partial V}{\partial X} + \frac{\partial N_\alpha}{\partial Y}\frac{\partial V}{\partial Y}\right) dA \\ &\quad - \int_A Cos\Phi \, N_\alpha \, \theta \, dA = \int_{S_0} N_\alpha S_y \, dS_0\end{aligned} \tag{18}$$

$$\int_A N_\alpha \left(U\frac{\partial \theta}{\partial X} + V\frac{\partial \theta}{\partial Y}\right) dA + \sqrt{\frac{1}{\Pr . Ra}} \int_A \left(\frac{\partial N_\alpha}{\partial X}\frac{\partial \theta}{\partial X} + \frac{\partial N_\alpha}{\partial Y}\frac{\partial \theta}{\partial Y}\right) dA = \int_{S_0} N_\alpha q_w \, dS_w \tag{19}$$

Here (14)-(15) specifying surface tractions (S_x, S_y) along outflow boundary S_0 and (16) specifying velocity components and fluid temperature or heat flux that flows into or out from domain along wall boundary S_w. Substituting the element velocity component distributions, the temperature distribution, and the pressure distribution from Eqs (9)-(12), the finite element equations can be written in the form,

$$K_{\alpha\beta^x} U_\beta + K_{\alpha\beta^y} V_\beta = 0 \tag{20}$$

$$K_{\alpha\beta\gamma^x} U_\beta U_\gamma + K_{\alpha\beta\gamma^y} V_\gamma U_\gamma + M_{\alpha\mu^x} P_\mu + \sqrt{\frac{\Pr}{Ra}} \left(S_{\alpha\beta^{xx}} + S_{\alpha\beta^{yy}}\right) U_\beta$$
$$- Sin\Phi\, K_{\alpha\beta}\, \theta_\beta = Q_{\alpha^x} \tag{21}$$

$$K_{\alpha\beta\gamma^x} U_\beta V_\gamma + K_{\alpha\beta\gamma^y} V_\gamma V_\gamma + M_{\alpha\mu^x} P_\mu + \sqrt{\frac{\Pr}{Ra}} \left(S_{\alpha\beta^{xx}} + S_{\alpha\beta^{yy}}\right) V_\beta$$
$$- Cos\Phi\, K_{\alpha\beta}\, \theta_\beta = Q_{\alpha^y} \tag{22}$$

$$K_{\alpha\beta\gamma^x} U_\beta\, \theta_\gamma + K_{\alpha\beta\gamma^y} V_\beta\, \theta_\gamma + \sqrt{\frac{1}{\Pr . Ra}} \left(S_{\alpha\beta^{xx}} + S_{\alpha\beta^{yy}}\right) \theta_\beta = Q_{\alpha^{\Gamma y}} \tag{23}$$

where the coefficients in element matrices are in the form of the integrals over the element area and along the element edges S_0 and S_w as,

$$K_{\alpha\beta^x} = \int_A N_\alpha N_{\beta,x} dA\,, \tag{24a}$$

$$K_{\alpha\beta^y} = \int_A N_\alpha N_{\beta,y} dA\,, \tag{24b}$$

$$K_{\alpha\beta\gamma^x} = \int_A N_\alpha N_\beta N_{\gamma,x} dA\,, \tag{24c}$$

$$K_{\alpha\beta\gamma^y} = \int_A N_\alpha N_\beta N_{\gamma,y} dA\,, \tag{24d}$$

$$K_{\alpha\beta} = \int_A N_\alpha N_\beta dA\,, \tag{24e}$$

$$S_{\alpha\beta^{xx}} = \int_A N_{\alpha,x} N_{\beta,x} dA\,, \tag{24f}$$

$$S_{\alpha\beta^{yy}} = \int_A N_{\alpha,y} N_{\beta,y} dA\,, \tag{24g}$$

$$M_{\alpha\mu^x} = \int_A H_\alpha H_{\mu,x} dA\,, \tag{24h}$$

$$M_{\alpha\mu^y} = \int_A H_\alpha H_{\mu,y} dA \,, \tag{24i}$$

$$Q_{\alpha^u} = \int_{S_0} N_\alpha S_x dS_0 \,, \tag{24j}$$

$$Q_{\alpha^v} = \int_{S_0} N_\alpha S_y dS_0 \,, \tag{24k}$$

$$Q_\alpha \theta = \int_{S_w} N_\alpha \, q_w \, dS_w \,, \tag{24l}$$

These element matrices are evaluated in closed form ready for numerical analysis. Details of the derivation for these element matrices are omitted herein for brevity.

The derived finite element equations, Eqs (20)-(23), are nonlinear. These nonlinear algebraic equations are solved by applying the Newton-Raphson iteration technique (Dechaumphai, [9]) by first writing the unbalanced values from the set of the finite element Eqs (20)-(23) as,

$$F_{\alpha^p} = K_{\alpha\beta^x} U_\beta + K_{\alpha\beta^y} V_\beta \tag{25a}$$

$$\begin{aligned} F_{\alpha^u} = {} & K_{\alpha\beta\gamma^x} U_\beta U_\gamma + K_{\alpha\beta\gamma^y} V_\gamma U_\gamma + M_{\alpha\mu^x} P_\mu + \sqrt{\frac{\Pr}{Ra}} \left(S_{\alpha\beta^{xx}} + S_{\alpha\beta^{yy}} \right) U_\beta \\ & - Sin\Phi \, K_{\alpha\beta} \, \theta_\beta - Q_{\alpha^u} \end{aligned} \tag{25b}$$

$$\begin{aligned} F_{\alpha^v} = {} & K_{\alpha\beta\gamma^x} U_\beta V_\gamma + K_{\alpha\beta\gamma^y} V_\gamma V_\gamma + M_{\alpha\mu^x} P_\mu + \sqrt{\frac{\Pr}{Ra}} \left(S_{\alpha\beta^{xx}} + S_{\alpha\beta^{yy}} \right) V_\beta \\ & - Cos\Phi \, K_{\alpha\beta} \, \theta_\beta - Q_{\alpha^v} \end{aligned} \tag{25c}$$

$$F_{\alpha^T} = K_{\alpha\beta\gamma^x} U_\beta \, \theta_\gamma + K_{\alpha\beta\gamma^y} V_\beta \, \theta_\gamma + \sqrt{\frac{1}{\Pr . Ra}} \left(S_{\alpha\beta^{xx}} + S_{\alpha\beta^{yy}} \right) \theta_\beta - Q_{\alpha^T} \tag{25d}$$

This leads to a set of algebraic equations with the incremental unknowns of the element nodal velocity components, temperatures, and pressures in the form,

$$\begin{bmatrix} K_{uu} & K_{uv} & K_{u\theta} & K_{up} \\ K_{vu} & K_{vv} & K_{v\theta} & K_{vp} \\ K_{Tu} & K_{\theta v} & K_{\theta\theta} & 0 \\ K_{pu} & K_{pv} & 0 & 0 \end{bmatrix} \begin{Bmatrix} \Delta u \\ \Delta v \\ \Delta \theta \\ \Delta p \end{Bmatrix} = - \begin{Bmatrix} F_{\alpha^u} \\ F_{\alpha^v} \\ F_{\alpha^\theta} \\ F_{\beta^p} \end{Bmatrix} \tag{26}$$

where

$$K_{uu} = K_{\alpha\beta\gamma\,x} U_{\gamma} + K_{\alpha\gamma\beta\,x} U_{\gamma} + K_{\alpha\beta\gamma\,y} V_{\beta} + \sqrt{\frac{\Pr}{Ra}}\left(S_{\alpha\beta\,xx} + S_{\alpha\beta\,yy}\right)$$

$K_{uv} = K_{\alpha\beta\gamma y} U\gamma$,

$K_{u\theta} = -\sin\Phi \quad K_{\alpha\beta}$,

$K_{up} = M_{\alpha\mu} x$,

$K_{vu} = K_{\alpha\beta\gamma} x V\gamma$,

$$K_{vv} = K_{\alpha\beta\gamma\,x} U_{\beta} + K_{\alpha\gamma\beta\,y} V_{\gamma} + K_{\alpha\beta\gamma\,y} V_{\gamma} + \sqrt{\frac{\Pr}{Ra}}\left(S_{\alpha\beta\,xx} + S_{\alpha\beta\,yy}\right)$$

$K_{v\theta} = -\cos\Phi \quad K_{\alpha\beta}$,

$K_{vp} = M_{\alpha\mu} y$,

$K_{\theta u} = K_{\alpha\beta\gamma^{x}} \theta\gamma$,

$K_{\theta v} = K_{\alpha\beta\gamma^{y}} \theta\gamma$

$$K_{\theta\theta} = K_{\alpha\beta\gamma^{x}} U_{\beta} + K_{\alpha\beta\gamma^{y}} V_{\beta} + \sqrt{\frac{1}{\Pr . Ra}}\left(S_{\alpha\beta^{xx}} + S_{\alpha\beta^{yy}}\right)$$

$K_{\theta p} = 0$, $K_{pu} = K_{\alpha\beta} x$, $K_{pv} = K_{\alpha\beta} y$ and $K_{p\theta} = 0 = K_{pp}$.

The iteration process is terminated if the percentage of the overall change compared to the previous iteration is less than the specified value.

To solve the sets of the global non-linear algebraic equations in the form of matrix, the Newton-Raphson iteration technique has been adapted through PDE solver.

3.3.2 Grid Independence Test

Preliminary results are obtained to inspect the field variables grid independency solutions. Test for the accuracy of grid fineness has been carried out to find out the optimum grid number.

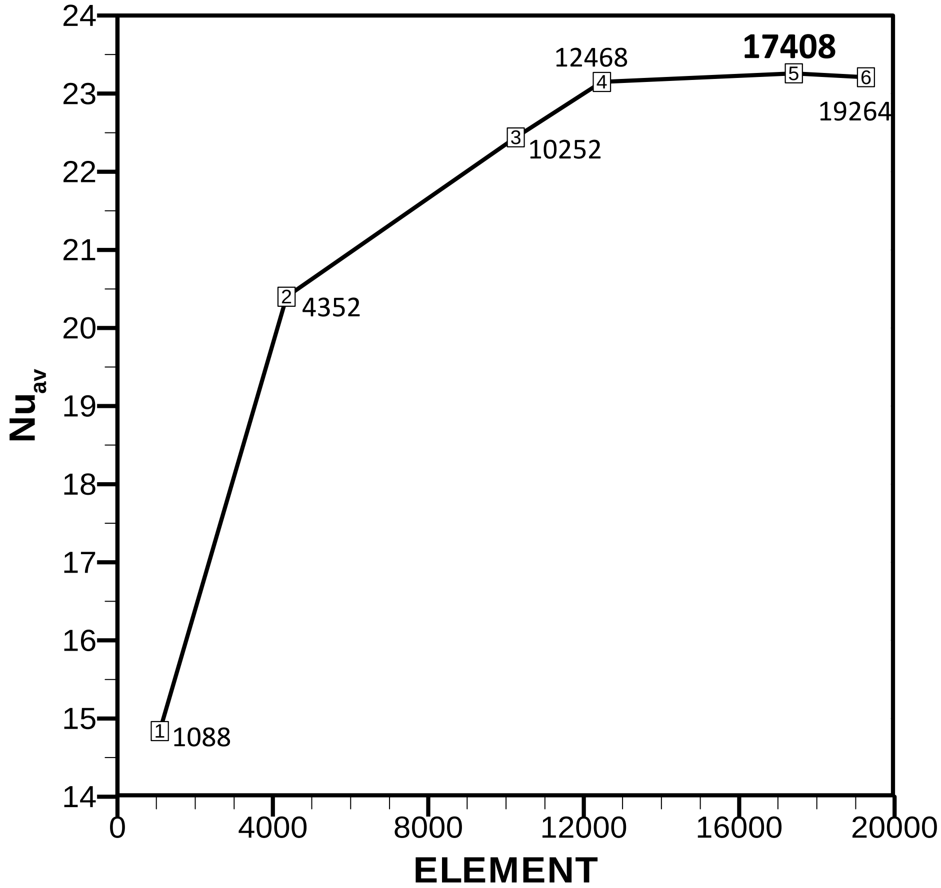

Fig-3.2: Convergence of average Nusselt number with grid refinement for Ra = 10^6 and dr = 0.2

In order to obtain grid independent solution, a grid refinement study is performed for a square cavity with Ra = 10^6 and dr = 0.2. Figure 3.2 shows the convergence of the average Nusselt number, Nu_{av} at the heated surface with grid refinement. It is observed that grid independence is achieved with 17408 elements where there is insignificant change in Nu with further increase of mesh elements. Six different non-uniform grids with the following number of nodes and elements were considered for the grid refinement tests: 7366 nodes, 1088 elements; 28876 nodes, 4352 elements; 67450 nodes, 10252 elements; 82029 nodes, 12468 elements; 114328 nodes, 17408 elements and

126476 nodes, 19264 elements. From these values, 114328 nodes, 17408 elements can be chosen throughout the simulation to optimize the relation between the accuracy required and the computing time.

Table 3.1: Grid Sensitivity Check at Pr = 0.72, dr = 0.2 and Ra = 10^6.

Elements	1088	4352	10252	12468	17408	19264
Nodes	7366	28876	67450	82029	114328	126476
Nu No	14.8433	20.4025	22.4768	23.1468	23.2553	23.2089
Time(s)	70.563	964.187	2022.547	1724.031	2432.344	2831.156

3.4 Results and Discussion

The problem is a partially heated square cavity with the left vertical wall is at iso-flux heat source, right wall is partially heated while the rest of the wall and circular cylinders are adiabatic, as shown in Fig 3.1. Two-dimensional forms of Navier-Stokes equations along with the energy equations are solved using Galerkin finite element method. Results are obtained for a range of Rayleigh number from 10^3 to 10^6 at Pr = 0.72, 3.00 and 10.00 with constant physical properties. The parametric studies for a wide range of governing parameters show consistent performance of the present numerical approach to obtain as temperature profiles and stream functions. The computational results indicate that the heat transfer coefficient is strongly affected by Rayleigh number. The use of Nusselt number and Rayleigh number develops an empirical correlation. Obviously for high values of Rayleigh number the errors encountered are appreciable and hence it is necessary to perform some grid size testing in order to establish a suitable grid size. Grid independent solution is ensured by comparing the results of different grid meshes for Rayleigh number 10^6, which is the highest Rayleigh number. The total domain is discretized into 17408 elements that results in 114328 nodes.

The effect of inclination angle is examined for Φ = 0º, 30º, 45º with aspect ratio A = 1. A comparison between the steady-state patterns of streamlines from Rayleigh numbers of 10^3 to 10^6 with different angles is presented in Figure 3.3 – 3.12. Also a comparison between the steady-state patterns of isotherms from Rayleigh numbers of 10^3 to 10^6 with different angles is presented in Figure 3.3 – 3.12. For the isotherm, the figures show that as the Rayleigh number and the inclination angle increase, the buoyancy force increases and the thermal boundary layers become thinner. We observe that the heat transfer in the cavity is qusi-conductive at Ra = 10^3 and becomes dominated by convective regime as

Ra increases to 10^6 in fig: 3.3-3.17. As Ra is increased to 10^6, the isotherms show that the fluid penetrates right to the heated wall, where steep temperature gradients exit. At Ra = 10^5 and 10^6 from the figure, shows that heat transfer rate increases and flow is boundary layer type-specially left and right walls. Then the isotherms and streamlines become more packed to the heated wall. This suggests that the flow moves faster as natural convection is rigorous. For the streamlines, the figures show that the fluid enters from the left of the aperture, circulates in a clockwise direction following the shape of the cavity, and leaves toward the mid part of the right aperture. At Ra = 10^3 and 10^4 , the streamlines in the cavity show that for quasi-conductive regime entrance and exit sections of the fluid at the right side of heated part are unequal. Streamlines show that as the inclination angle of the heated wall increases, the velocity gradient increases at heated wall, and also the strength of the circulation increases. The results are presented in terms of streamlines and isotherm patterns. The variations of the average Nusselt number are also highlighted. The results in the steady state are obtained for a Rayleigh range from 10^3 to 10^6 and for a range of 0^o-45^o for the inclination angles of the cavity. The results show that for high Rayleigh numbers, the Nusselt number changes substantially with the inclination angle of the cavity. The numerical model predicts Nusselt number oscillations for low angles and high Rayleigh numbers.

In order to validate the numerical code, pure natural convection with Pr = 0.72 in a partially heated square cavity was solved and the average Nusselt numbers is presented by graphically. The results are compared with those reported by Hinojosa et al. [16], obtained with an extended computational domain. In Table 3.2, a comparison between the average Nusselt numbers is presented. The results from the present experiment are almost same as Hinojosa et al.

Table 3.2: Comparison of the results for the constant surface temperature with Pr = 0.72.

Ra	Nu_{av}	
	Present work	Hinojosa et al. (2005)
10^3	1.33	1.30
10^4	3.42	3.44
10^5	7.40	7.44
10^6	14.41	14.51

3.4.1 Effects of Inclination Angle

With the increase of the Rayleigh number, complex flow pattern characteristics are found for some inclination angles. To show this, the profiles of isotherm, streamlines and inclination angles of 0^o, 30^o and 45^o are presented in Fig 3.3 to 3.12. For inclination angles of the cavity between 0^o and 45^o, the steady state cannot be reached; the instantaneous pictures show that the fluid enters and leaves in a very irregular way, indicating an unsteady convection. The velocity magnitude of the leaving fluid is greater than the incoming fluid, and thus the thermal boundary layer at the top wall becomes much thinner for bottom and centre cylinder but for top cylinder bottom wall becomes much thinner.

For Isotherm Patterns: When Pr=0.72 at angles 0^0 , 30^0 and 45^0 for bottom, centre and top cylinder, the flow patterns become more packed to left boundary wall with increase of Ra. As a result, Thermal Boundary Layer becomes thinner and also temperature gradient increases. Hence, qusi-conduction dominated at 10^3 and convection intensified. Besides, flow patterns have been gradually distorted for Ra = 10^3 - 10^5 and circulated at Ra = 10^6 and also for top cylinder at angles 0^0 - 45^0 for Ra=10^6 flow patterns distorted. Flow patterns from the right side become more horizontal for Ra = 10^3 - 10^5 but more dense to right wall at 10^6. Because of conduction intensified with increasing Rayleigh numbers. For Pr=3.0 and 10.0 at centre cylinder flow patterns behavior similar as the Pr=0.72 at centre cylinder.

For streamline Patterns: When Pr=0.72 at angles 0^0, 30^0 and 45^0 for bottom, centre and top cylinder, the streamline patterns become boundary type with increase of Ra. There are more vortices in the cavity for Ra=10^3-10^4 and vortex gradually converted to boundary type. As a result, Velocity Boundary Layer becomes thinner and also velocity gradient increases. Hence, conduction dominated at 10^3 and convection intensified with increase of Ra. Streamline patterns from the right side become more horizontal for Ra = 10^3 - 10^5 but circulate at 10^6. For Pr=3.0 and 10.0 at centre cylinder flow patterns behavior similar as the Pr=0.72 at centre cylinder.

From Table 3.3 – 3.7, The average Nusselt number for different cavity's inclination angles (0^o- 45^o) and Rayleigh numbers (10^3-10^6), obtained for different cylinder location (top, center and bottom) with different Prandtl number (Pr = 0.72, 3.0 and 10.0) is presented. For different angles and Rayleigh numbers, the average Nusselt number increases. Therefore, in Table 3.3 – 3.7, the average Nusselt numbers and their deviation are reported. In Fig.3.13 – 3.17, we observe that the heat transfer rate Nu increases with the increase of inclination angles because conduction dominated at 10^3 and convection intensified with increase of Ra.

Table 3.3: Average Nusselt number Nu for different angles Φ and Rayleigh numbers Ra when Pr =0.72 for top cylinder

Nu_{av}				
Φ	Ra=10^3	Ra=10^4	Ra=10^5	Ra=10^6
0^o	14.95883729	22.04043181	22.46611881	23.19581808
30^o	15.47878136	22.09227947	22.50535489	23.23131258
45^o	16.51195327	22.23765696	22.50841718	23.2414453

Table 3.4: Average Nusselt number Nu for different angles Φ and Rayleigh numbers Ra when Pr =0.72 for Centre cylinder

Nu_{av}				
Φ	Ra=10^3	Ra=10^4	Ra=10^5	Ra=10^6
0^o	20.17243983	21.30193788	21.51197329	22.36279026
30^o	20.23971823	21.57393913	21.91566822	22.4763611
45^o	20.40250621	21.58317925	22.29072279	22.48039619

Table 3.5: Average Nusselt number Nu for different angles Φ and Rayleigh numbers Ra when Pr =0.72 for bottom cylinder

Nu_{av}				
Φ	Ra=10^3	Ra=10^4	Ra=10^5	Ra=10^6
0^o	21.31163357	22.88931537	23.04394247	23.54447156
30^o	22.6864705	22.90042721	23.43104014	23.59416481
45^o	22.87433423	23.57987663	23.65229046	23.73532059

Table 3.6: Average Nusselt number Nu for different angles Φ and Rayleigh numbers Ra when *Pr* =3.0 for Centre cylinder

Nu_{av}				
Φ	Ra=10^3	Ra=10^4	Ra=10^5	Ra=10^6
0^o	12.63859595	20.07549464	21.44009634	22.24093084
30^o	13.99251657	20.75348129	21.51449017	22.44059645
45^o	14.96348202	21.3112681	21.50929871	22.47750561

Table 3.7: Average Nusselt number Nu for different angles Φ and Rayleigh numbers Ra when *Pr* =10.0 for Centre cylinder

Nu_{av}				
Φ	Ra=10^3	Ra=10^4	Ra=10^5	Ra=10^6
0^o	8.96380401	19.55421272	21.41617059	22.16082597
30^o	10.44347108	19.86945846	21.48540366	22.34484008
45^o	11.69442281	20.36985093	21.48010234	22.38447703

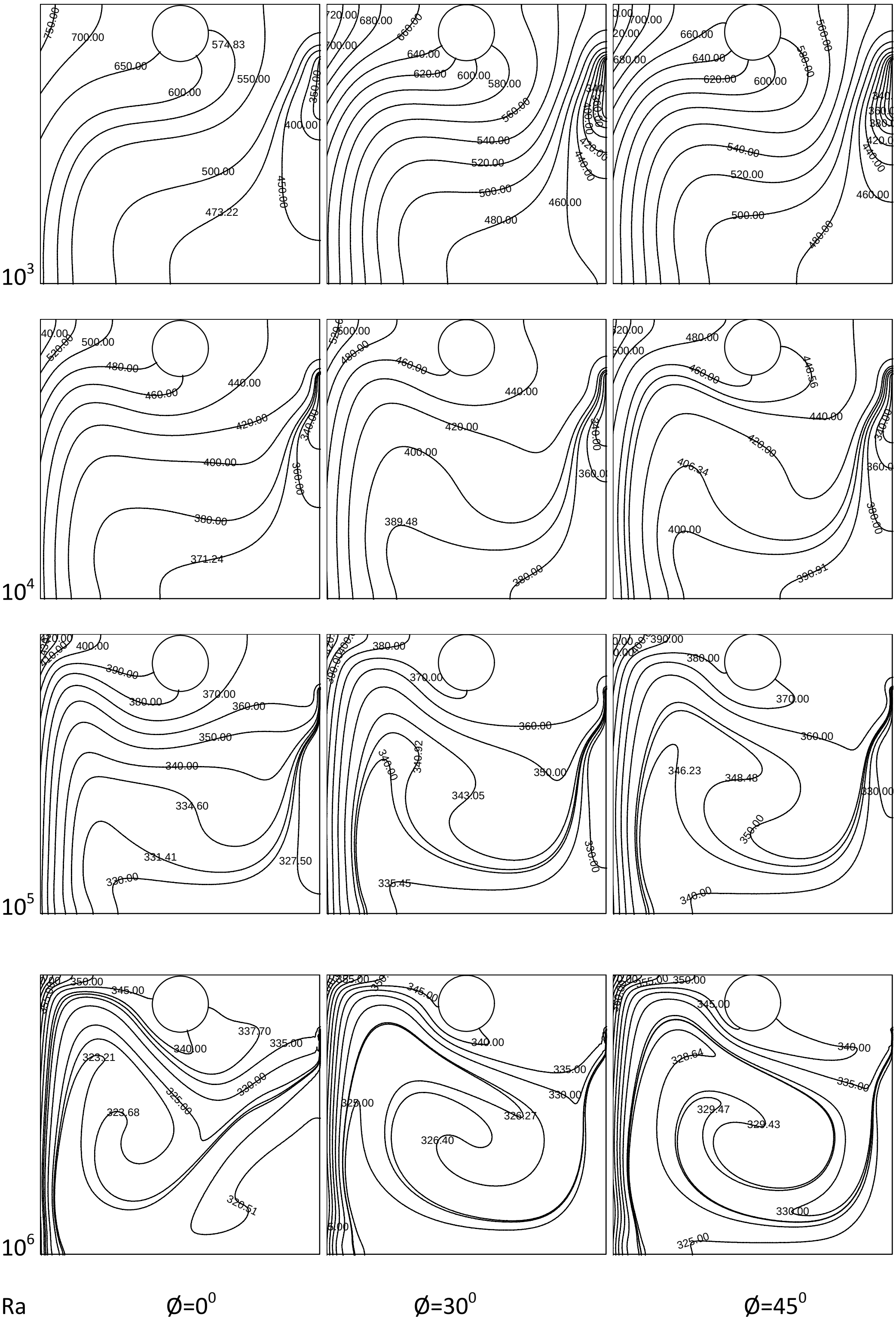

Fig-3.3: Isothermal patterns for different angles and Rayleigh numbers where circular cylinder at Top wall and Pr=0.72

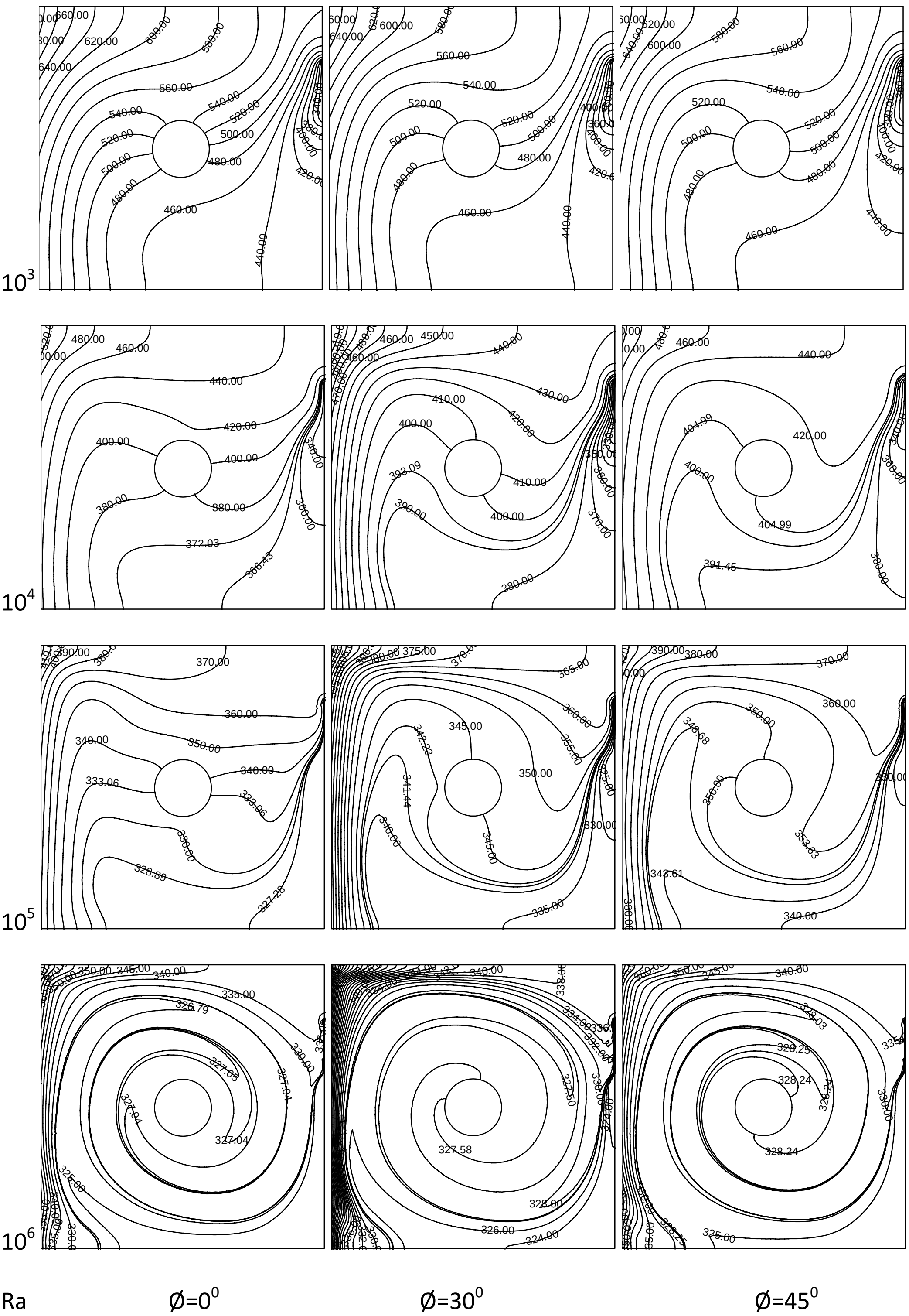

Fig-3.4: Isothermal patterns for different angles and Rayleigh numbers where circular cylinder at Centre and Pr=0.72

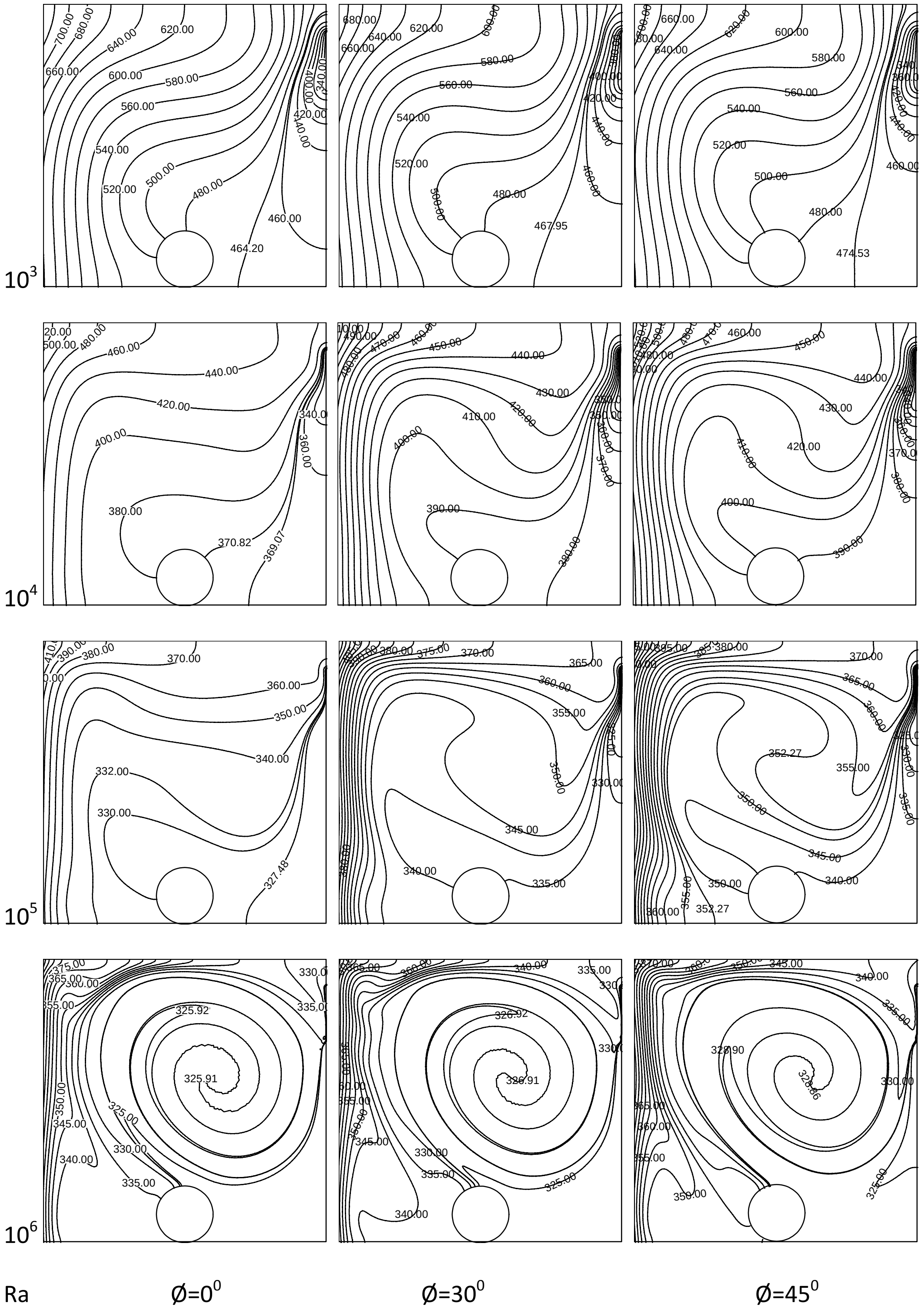

Fig- 3.5: Isothermal patterns for different angles and Rayleigh numbers where circular cylinder at Bottom wall and Pr=0.72

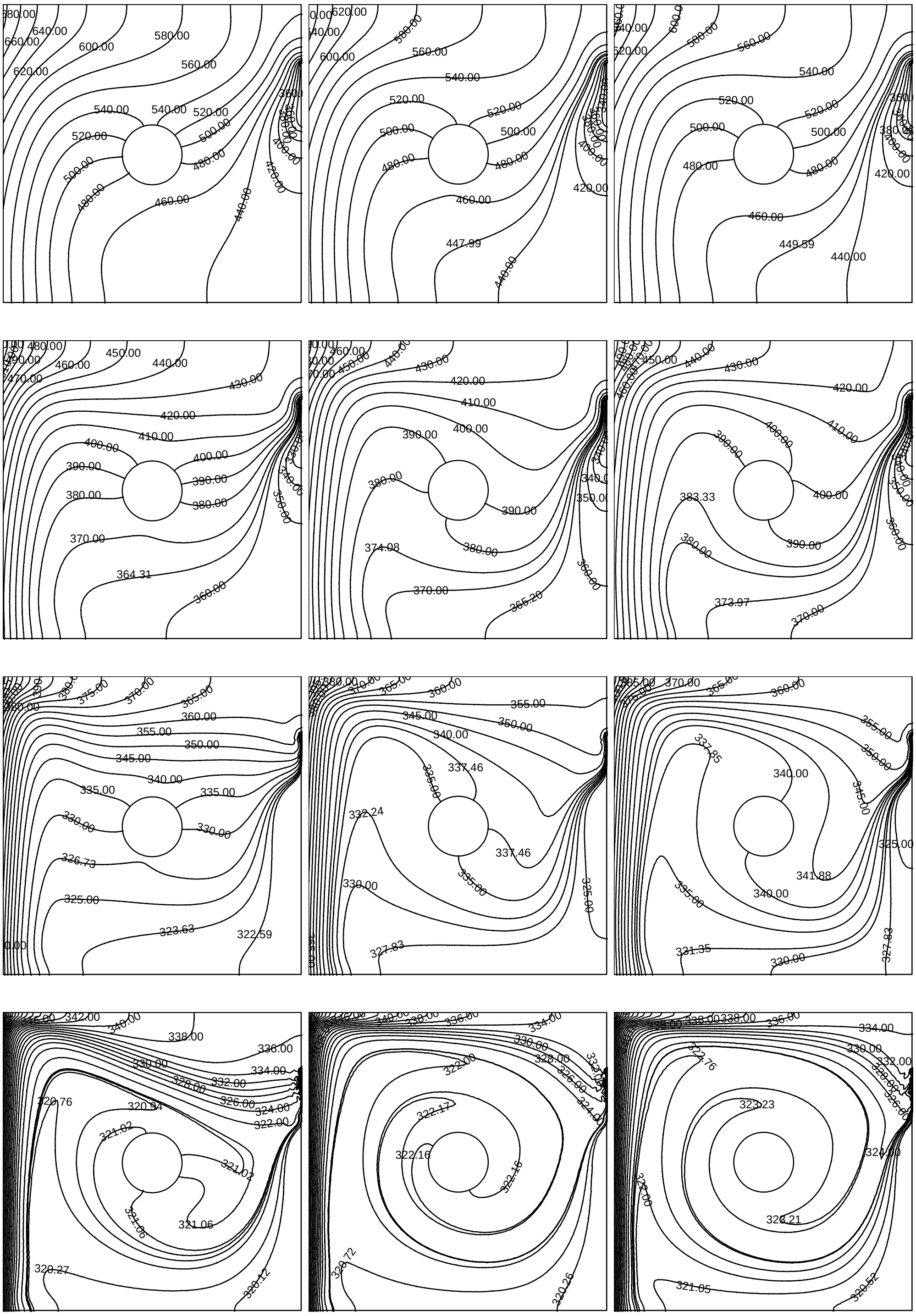

10^3

10^4

10^5

10^6

Ra $\quad Ø=0^0 \quad Ø=30^0 \quad Ø=45^0$

Fig-3.6: Isothermal patterns for different angles and Rayleigh numbers where circular cylinder at Centre and Pr=3.0

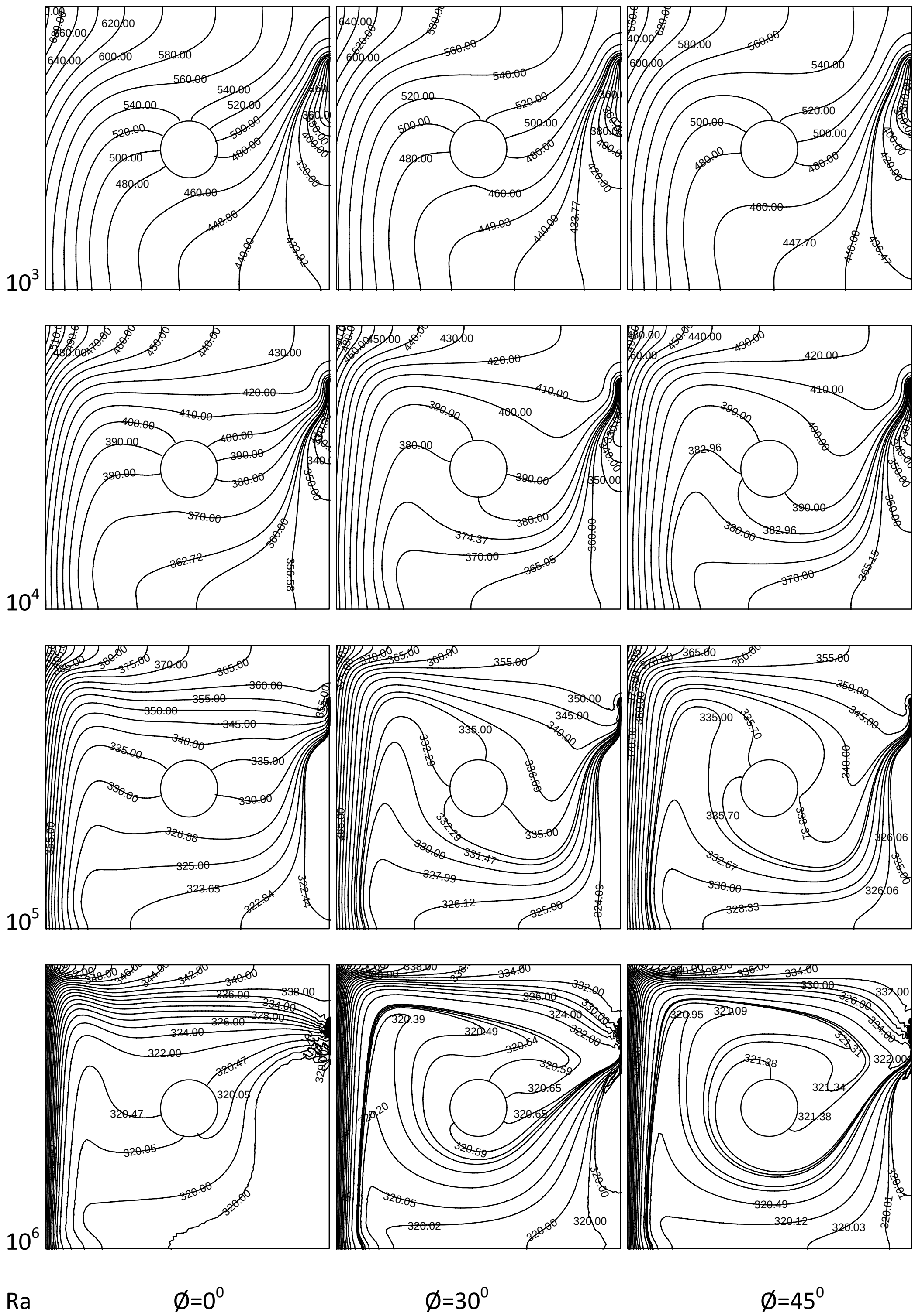

Fig-3.7: Isothermal patterns for different angles and Rayleigh numbers where circular cylinder at Centre and Pr=10.0

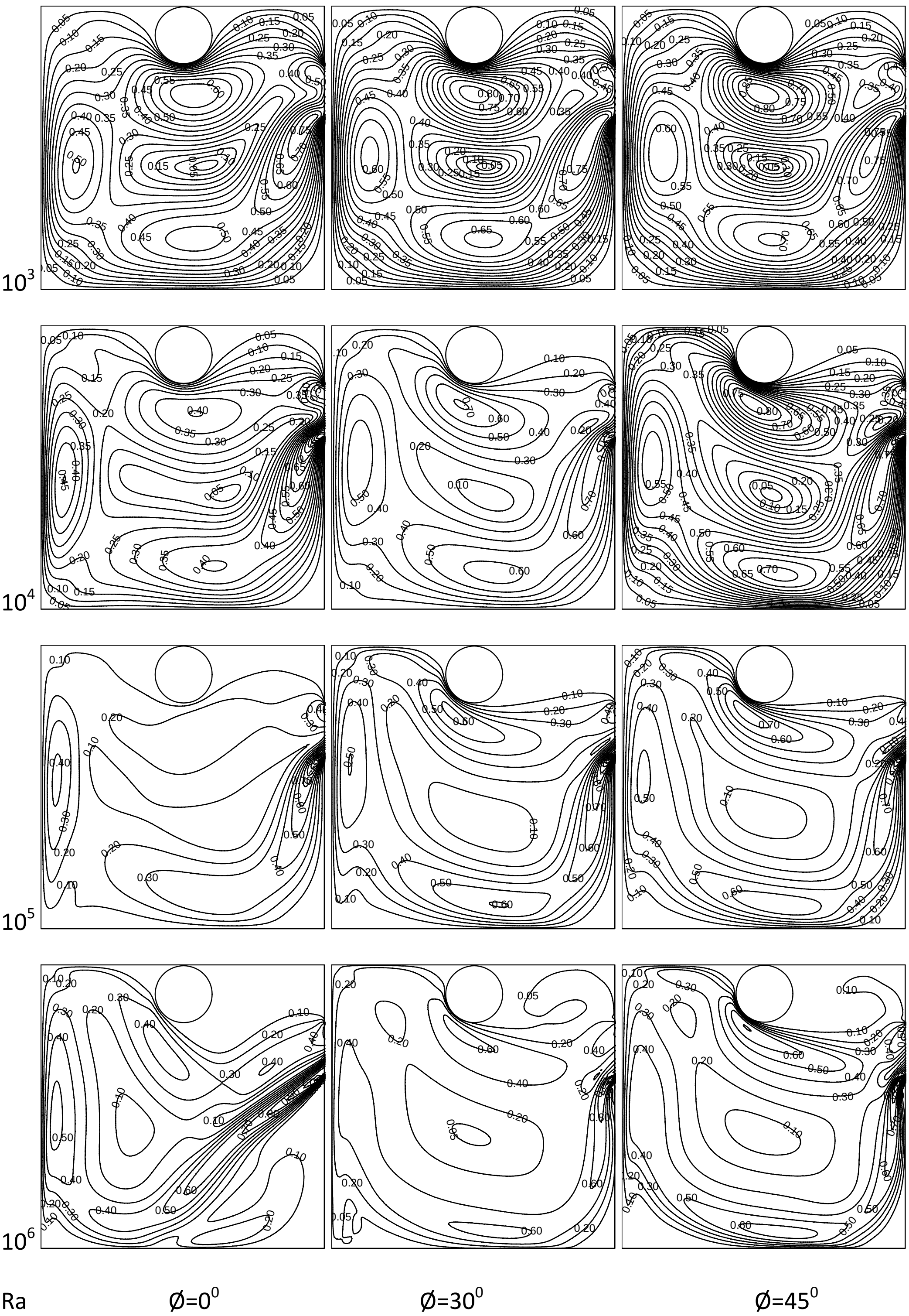

Fig-3.8: Streamline patterns for different angles and Rayleigh numbers where circular cylinder at Top wall and Pr=0.72

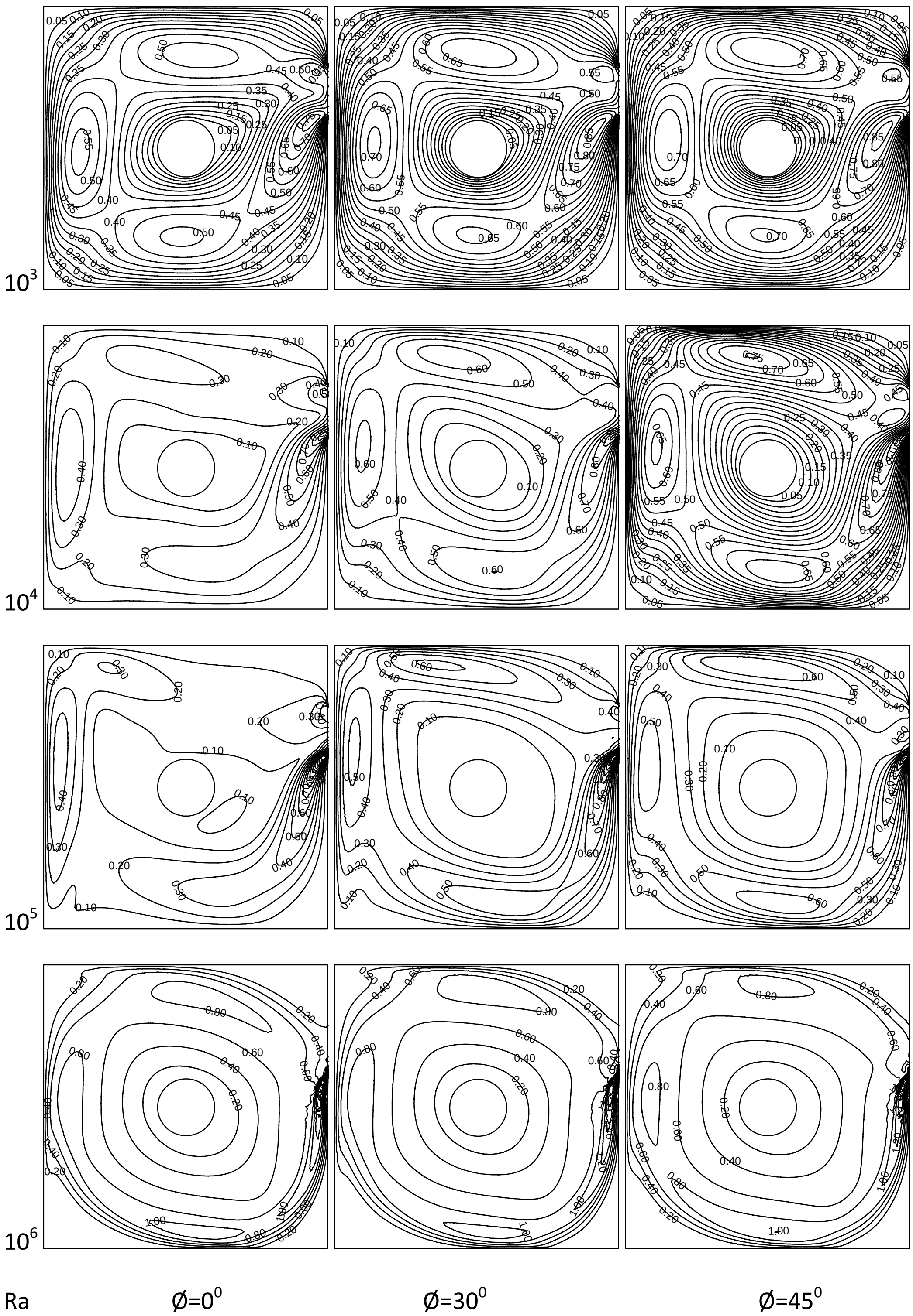

Fig-3.9: Streamline patterns for different angles and Rayleigh numbers where circular cylinder at Centre and Pr=0.72

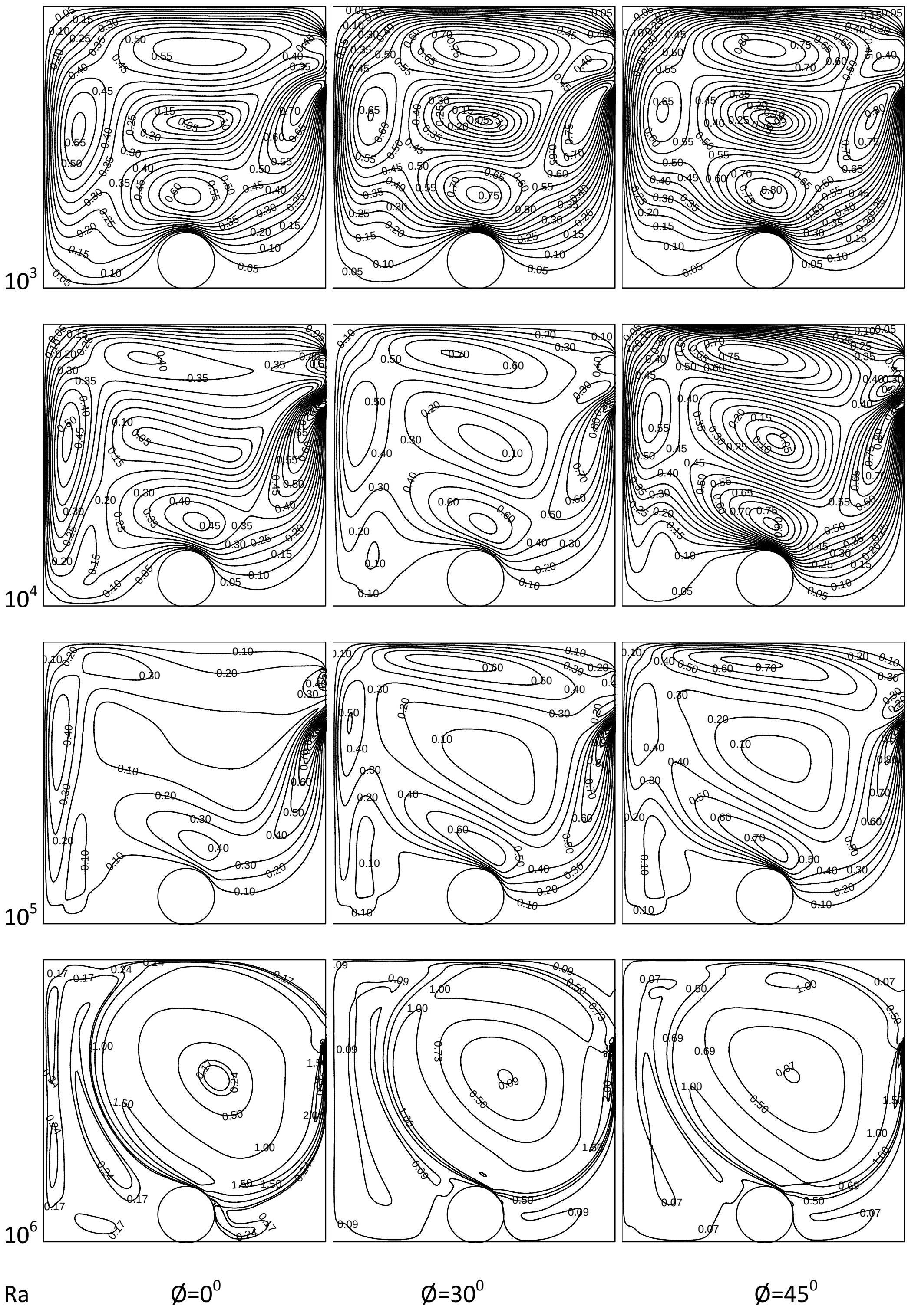

Fig-3.10: Streamline patterns for different angles and Rayleigh numbers where circular cylinder at bottom wall and Pr=0.72

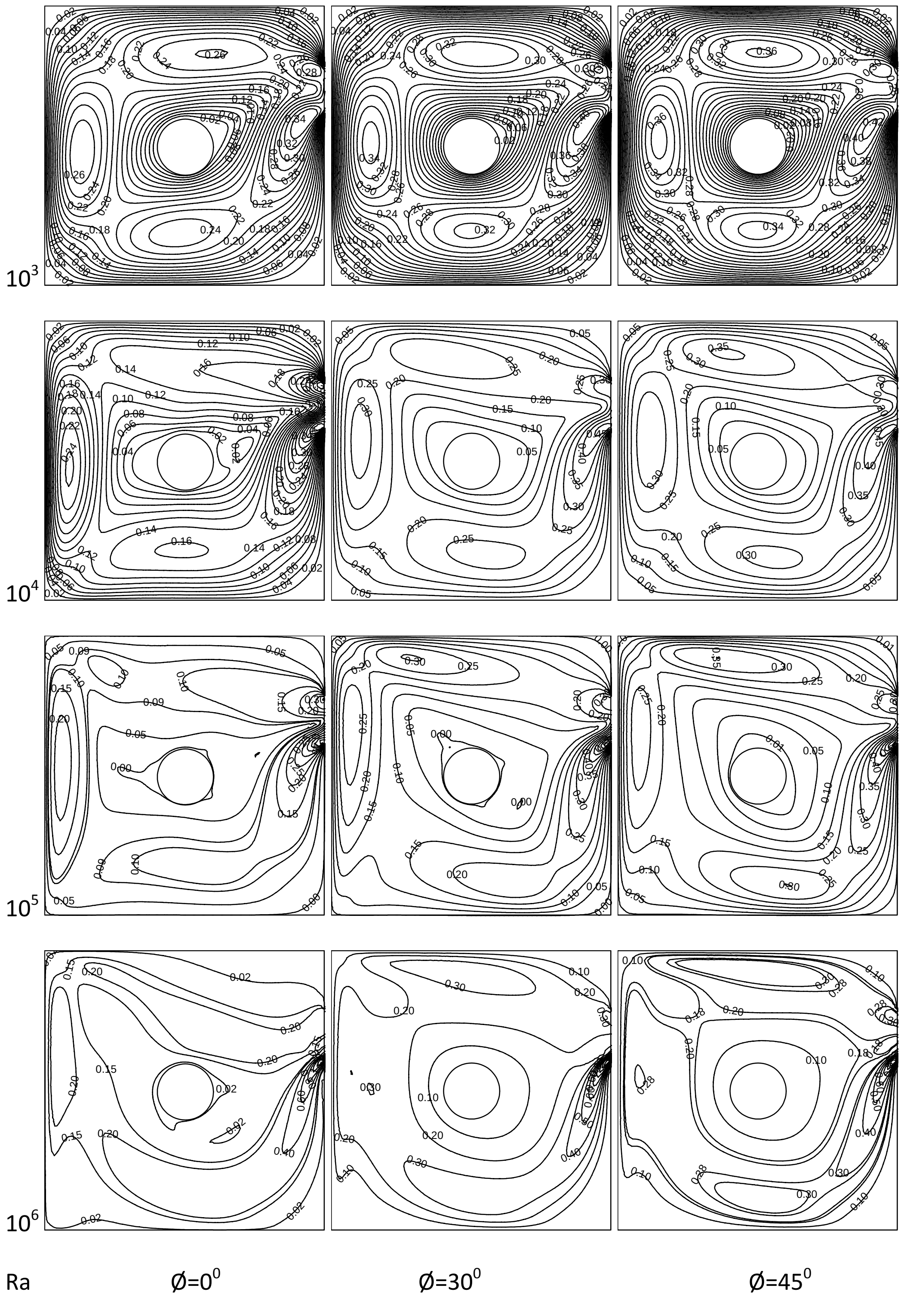

Fig-3.11: Streamline patterns for different angles and Rayleigh numbers where circular cylinder at Centre and Pr=3.0

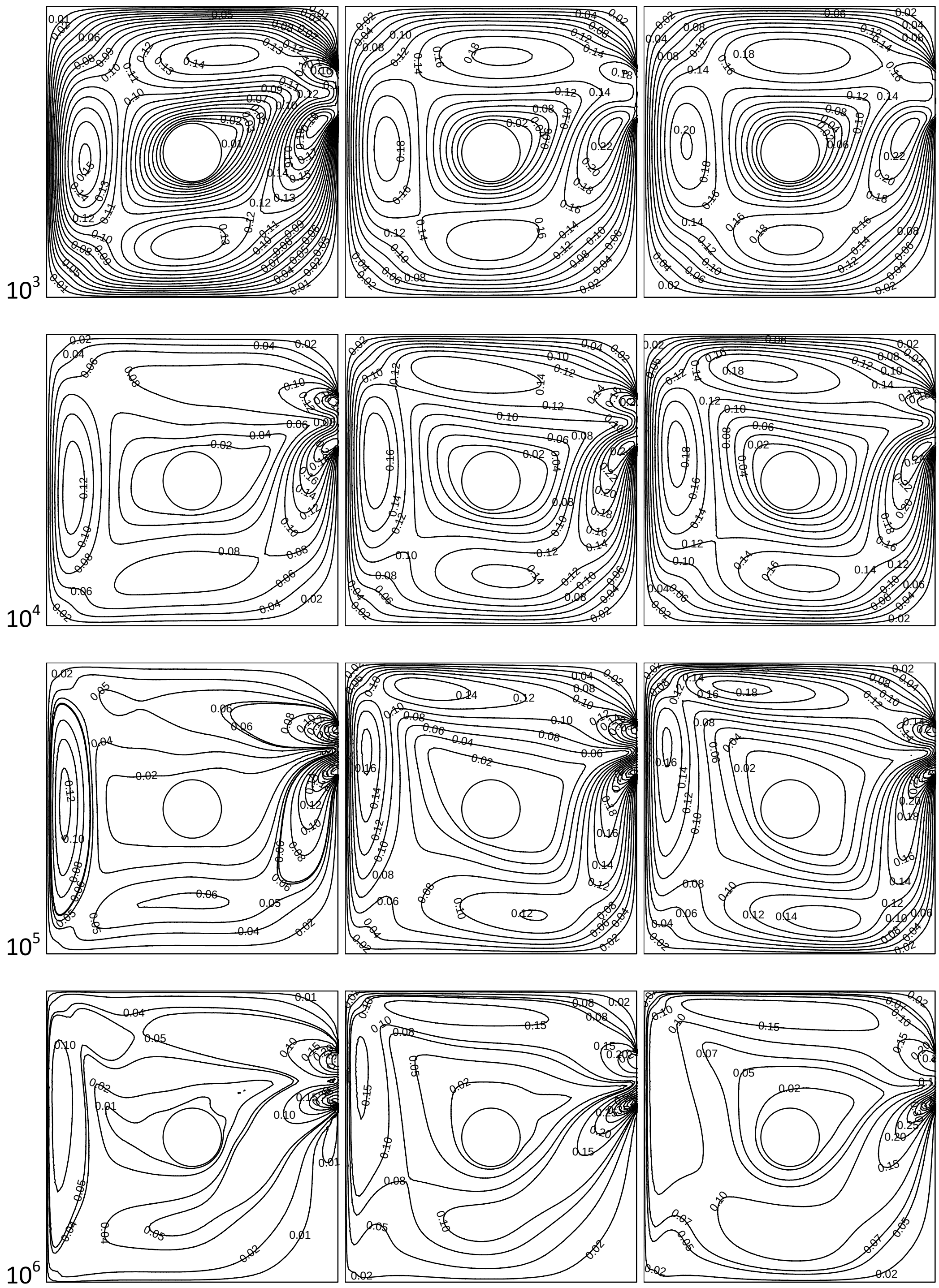

Ra Ø=0⁰ Ø=30⁰ Ø=45⁰

Fig-3.12: Streamline patterns for different angles and Rayleigh numbers where circular cylinder at Centre and Pr=10.0

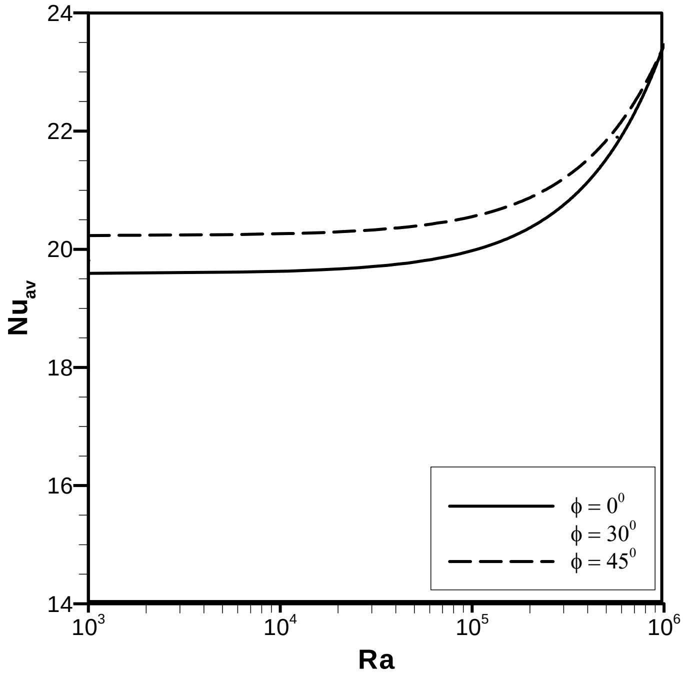

Fig-3.13: Average Nusselt figure for different angles and Rayleigh numbers for Top cylinder when Pr = 0.72

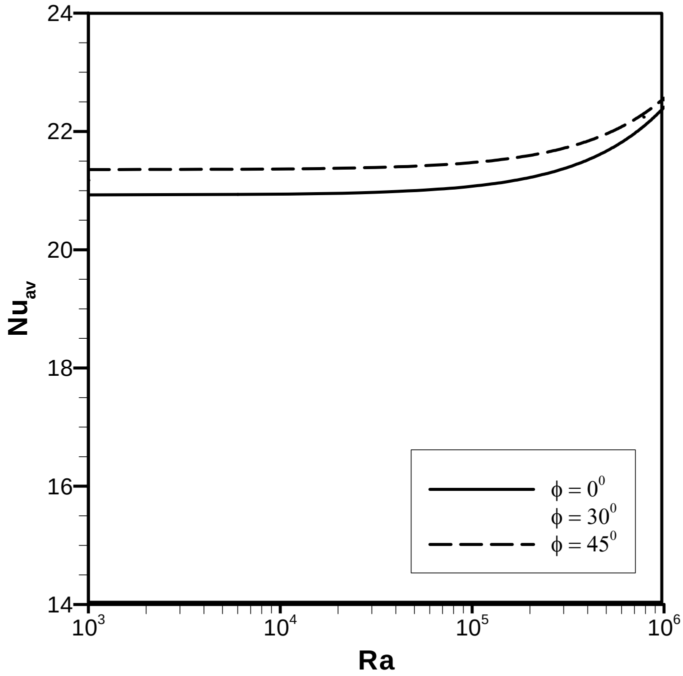

Fig-3.14: Average Nusselt figure for different angles and Rayleigh numbers for Centre cylinder when Pr = 0.72

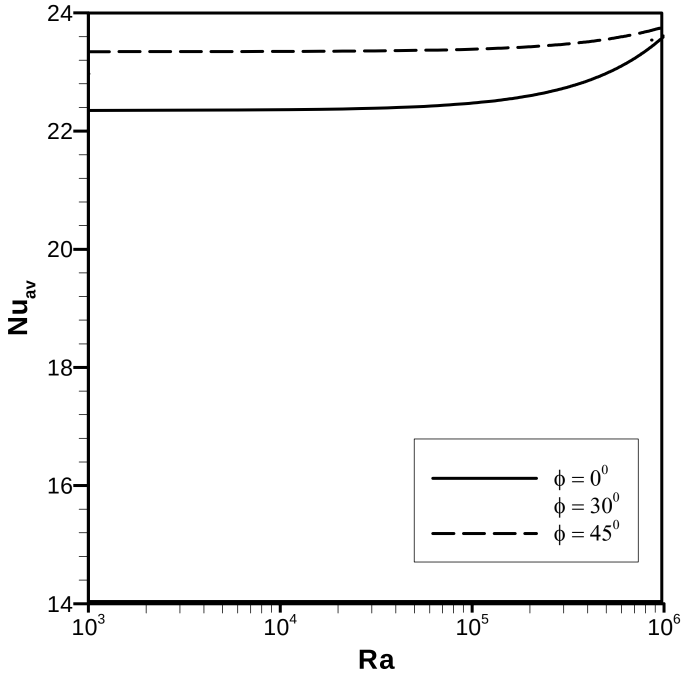

Fig-3.15: Average Nusselt figure for different angles and Rayleigh numbers for Bottom cylinder when Pr = 0.72

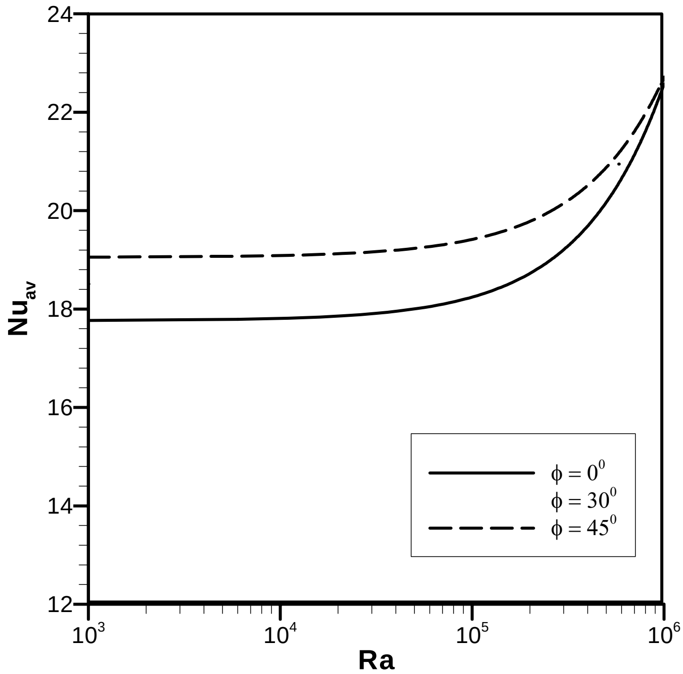

Fig-3.16: Average Nusselt figure for different angles and Rayleigh numbers for Centre cylinder when Pr = 3.0

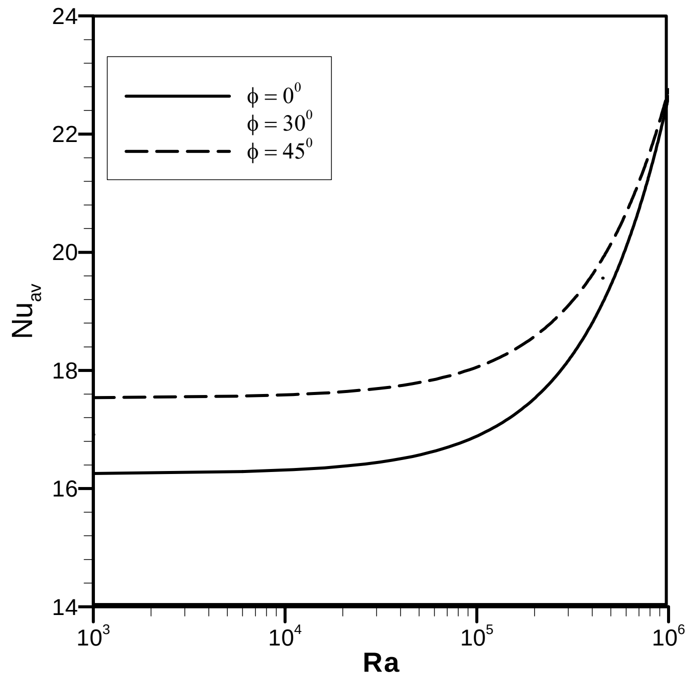

Fig-3.17: Average Nusselt figure for different angles and Rayleigh numbers for Centre cylinder when Pr = 10.0

3.4.2 Effects of Cylinder Location

The effect of cylinder location on the thermal transport has greater importance and is shown in figure 3.18 to 3.23. The isotherm lines and stream lines for various cylinder locations have been shown in fig 3.18 to 3.23 for aspect ratio (AR) = 1.00, Ra = 10^3- 10^6, dr = 0.2, Pr = 0.72 and angle 0^0- 45^0.

For Isotherm Patterns: The figures show that as the Ra number increases, the buoyancy force increases and the thermal boundary layers become thinner at heated wall. We observe that the heat transfer in the cavity is conductive at Ra = 10^3 and becomes dominated by convective regime as Ra increases to 10^6 in fig: 3.18 to 3.20. As Ra increased to 10^6, the isotherms show that the fluid moves to the heated wall, where steep temperature gradients turn into vertical at left wall. At Ra = 10^6 the figure shows that heat transfer rate increases and flow become circular type which dominated most of the part of cavity for all location of cylinder except top cylinder. Then the isotherms become more packed to the left wall. As increasing the Rayleigh numbers the conduction intensified. This suggests that the flow moves faster as natural convection is rigorous.

For streamline Patterns: The figure shows that the fluid moves and create circulate in a clock wise direction following the shape of the cavity. At the bottom cylinder location, a large circulation cell with inner vortex has confined at the top side of cavity at Ra= 10^3. With the increases of Ra = 10^3 – 10^5 the circulation cell becomes flat and also create secondary vortex near the cylinder. At Ra = 10^6 the dramatically change in circulation cell which dominate most of the part of cavity and also create more secondary vortex in cavity. At the center cylinder location, a large circulation cell with inner vortex has confined at the centre of cavity at Ra= 10^3. The circulation cell becomes flat with the increases of Ra = 10^3 – 10^5 and also create secondary vortex near the cylinder. For Ra = 10^6, the flow pattern become more circular which dominate most of the part of cavity. At the top cylinder location, a small circulation cell becomes large with the increase of Ra = 10^3 – 10^5 which confined at the bottom of cavity. The flow pattern becomes faunal shape with the increases of Ra = 10^3 – 10^5 and also create secondary vortex near the cylinder and right-bottom corner.

The average Nusselt numbers (Nu_{av}) at the heated surface in the cavity are plotted against Ra for different cylinder locations have been shown in fig. 3.24 to 3.26. From this figure it is seen that the Nu_{av} is the lowest when the cylinder moves closer to the top adiabatic wall along the mid-vertical plane.

Table 3.8: Average Nusselt number Nu for different locations (Top, Centre and Bottom) and Rayleigh numbers at $\Phi=0^0$ for Pr =0.72

Nu_{av}				
Cylinder location	Ra=10^3	Ra=10^4	Ra=10^5	Ra=10^6
Top	15.47878136	22.09227947	22.46611881	23.19581808
Centre	20.40250621	21.30193788	21.51197329	22.36279026
Bottom	21.31163357	22.88931537	23.04394247	23.54447156

Table 3.9: Average Nusselt number Nu for different locations (Top, Centre and Bottom) and Rayleigh numbers at $\Phi=30^0$ for Pr =0.72

Nu_{av}				
Cylinder location	$Ra=10^3$	$Ra=10^4$	$Ra=10^5$	$Ra=10^6$
Top	14.95883729	22.04043181	22.50841718	23.2414453
Centre	20.17243983	21.58317925	21.91566822	22.48039619
Bottom	22.6864705	22.90042721	23.43104014	23.59416481

Table 3.10: Average Nusselt number Nu for different locations(Top, Centre and Bottom) and Rayleigh numbers at $\Phi=45^0$ for Pr =0.72

Nu_{av}				
Cylinder location	$Ra=10^3$	$Ra=10^4$	$Ra=10^5$	$Ra=10^6$
Top	16.51195327	22.23765696	23.23131258	23.23131258
Centre	20.23971823	21.57393913	22.29072279	22.4763611
Bottom	22.87433423	23.57987663	23.65229046	23.73532059

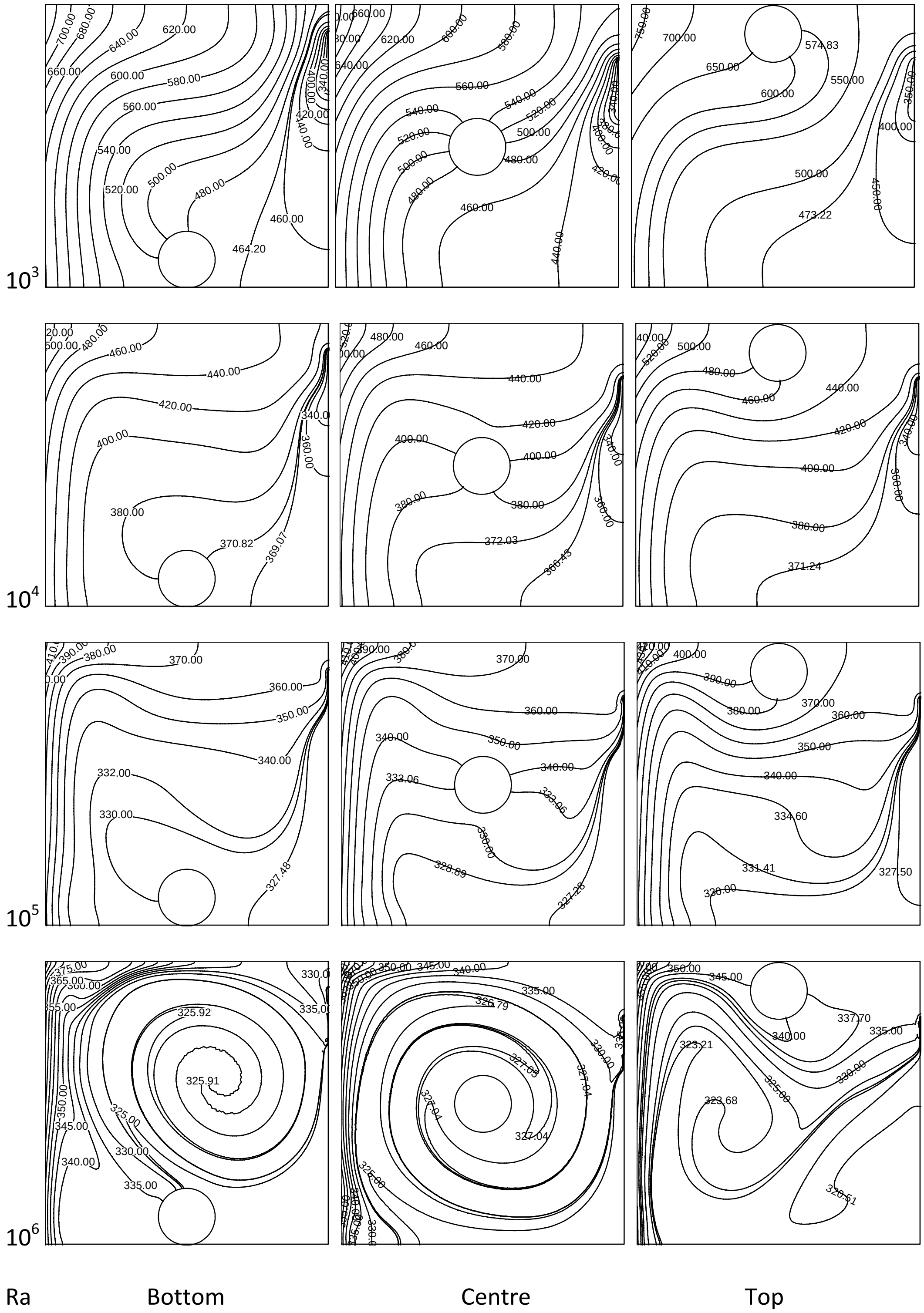

Fig-3.18: Isotherm lines for different Rayleigh numbers Ra and cylinder locations at an angle $\Phi=0^0$ when Pr = 0.72

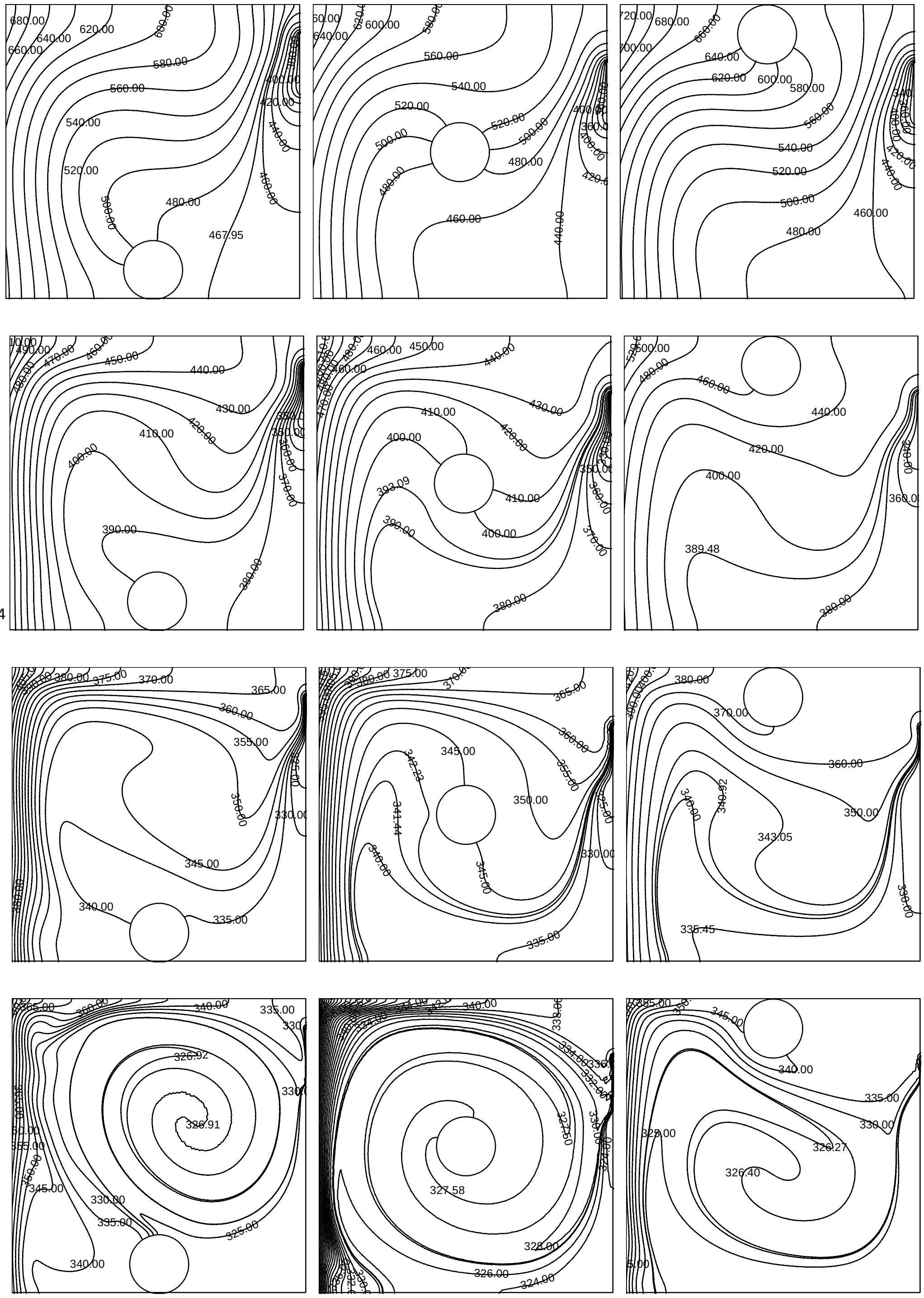

10^3

10^4

10^5

10^6

Ra Bottom Centre Top

Fig-3.19: Isotherm lines for different Rayleigh numbers Ra and cylinder locations at an angle $\Phi=30^0$ when Pr = 0.72

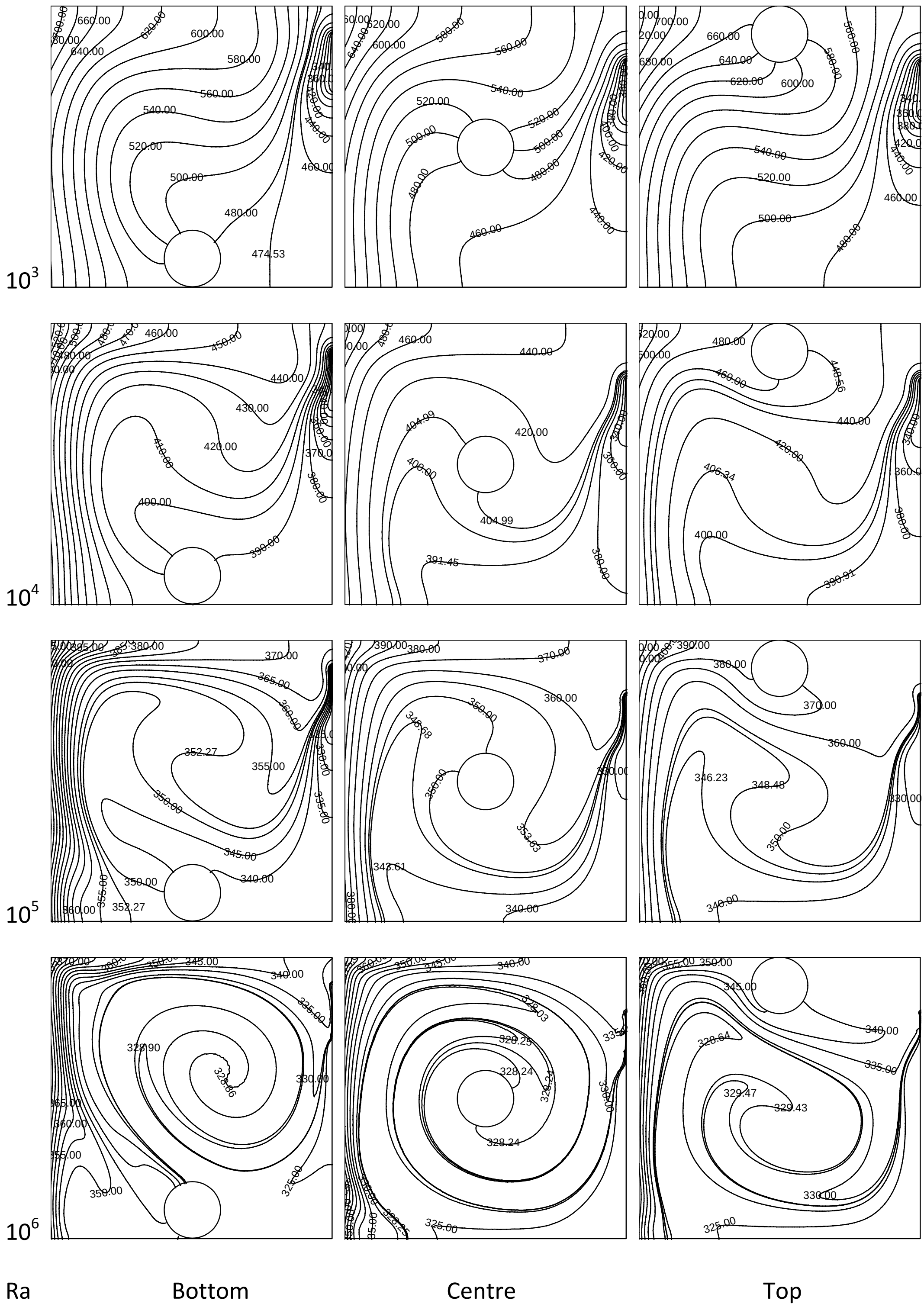

Fig-3.20: Isotherm lines for different Rayleigh numbers Ra and cylinder locations at an angle $\Phi=45^0$ when Pr = 0.72

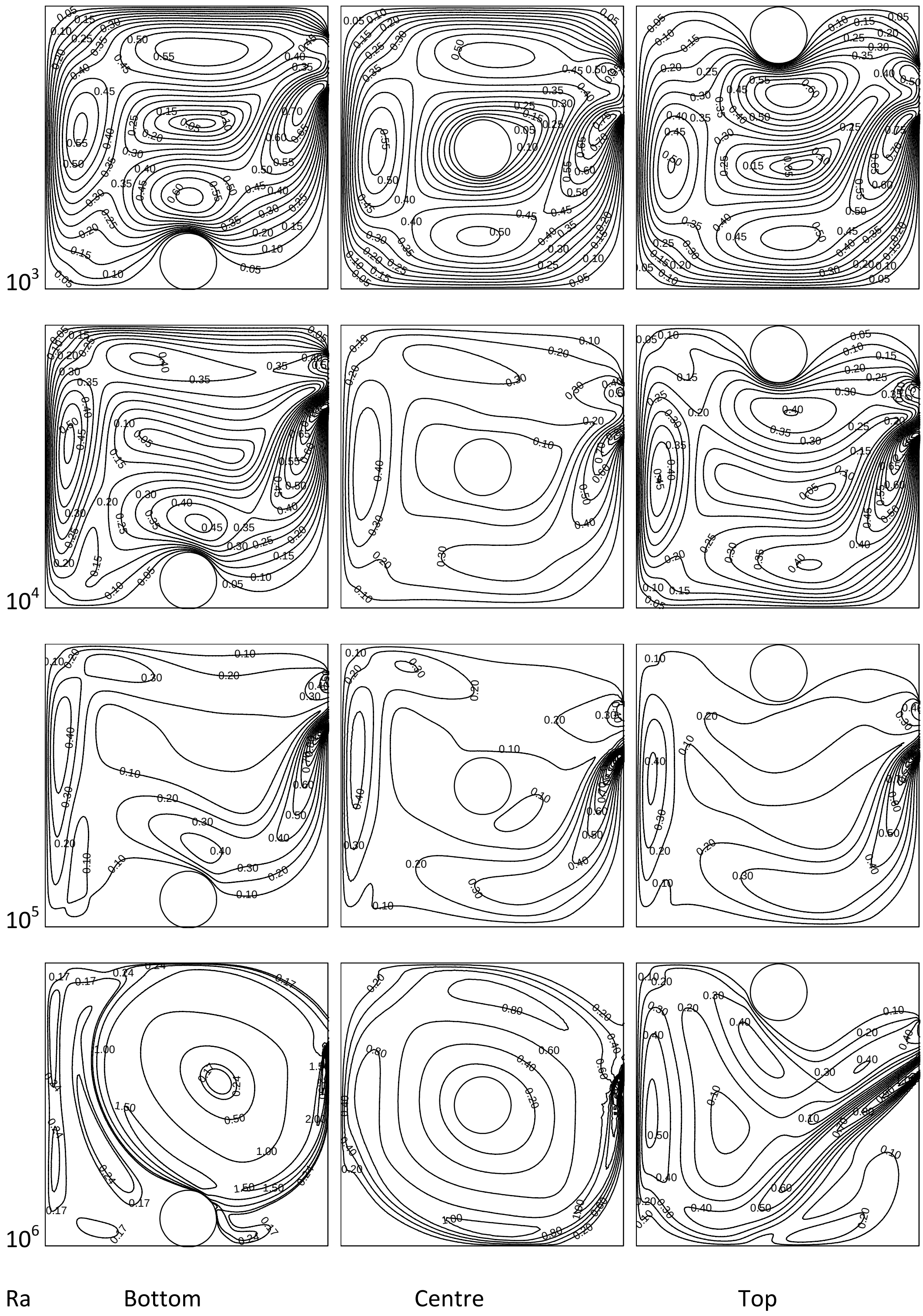

Fig-3.21: Stream lines for different Rayleigh numbers Ra and cylinder locations at an angle $\Phi=0^0$ when Pr = 0.72

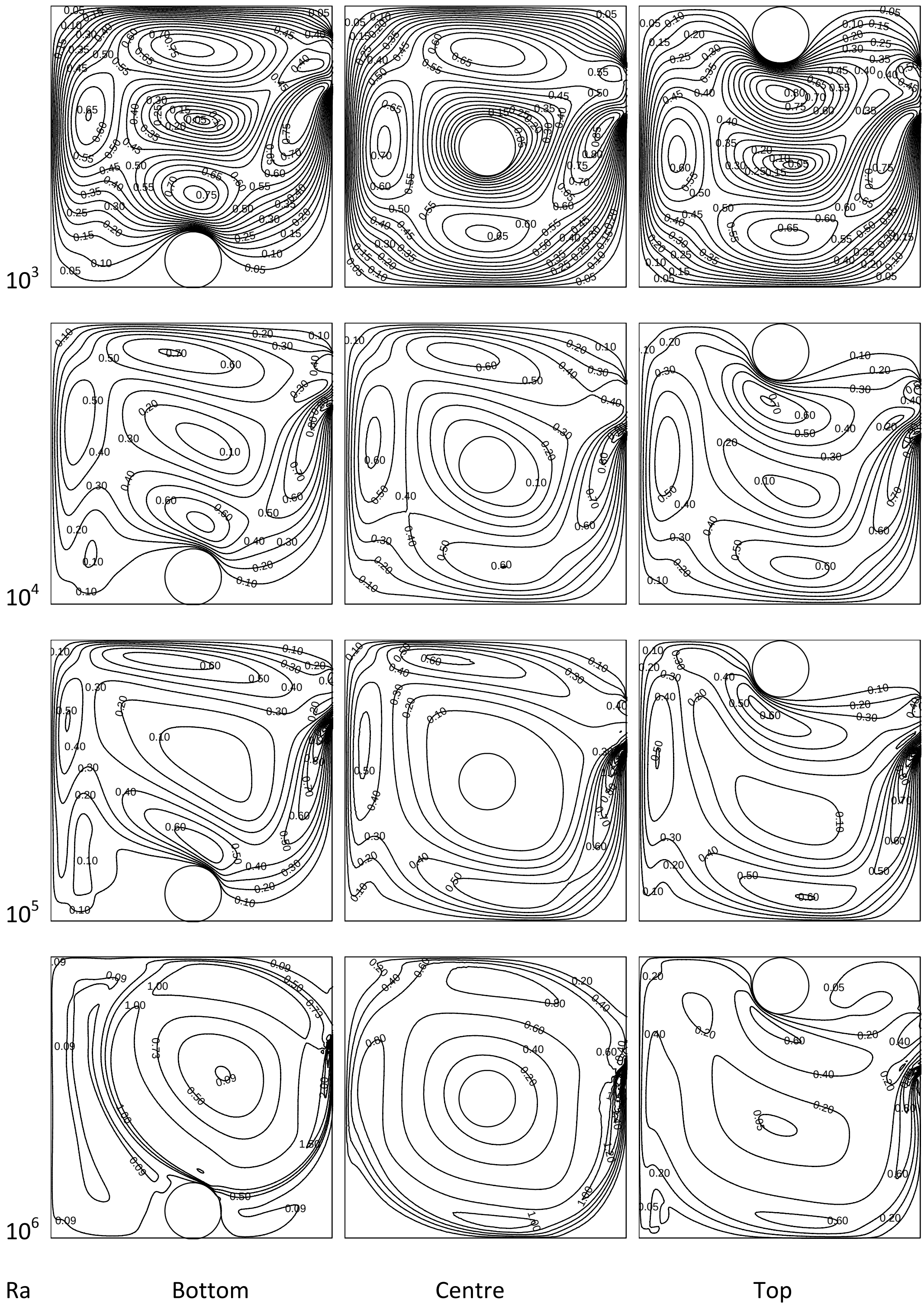

Fig-3.22: Stream lines for different Rayleigh numbers Ra and cylinder locations at an angle $\Phi=30^0$ when Pr = 0.72

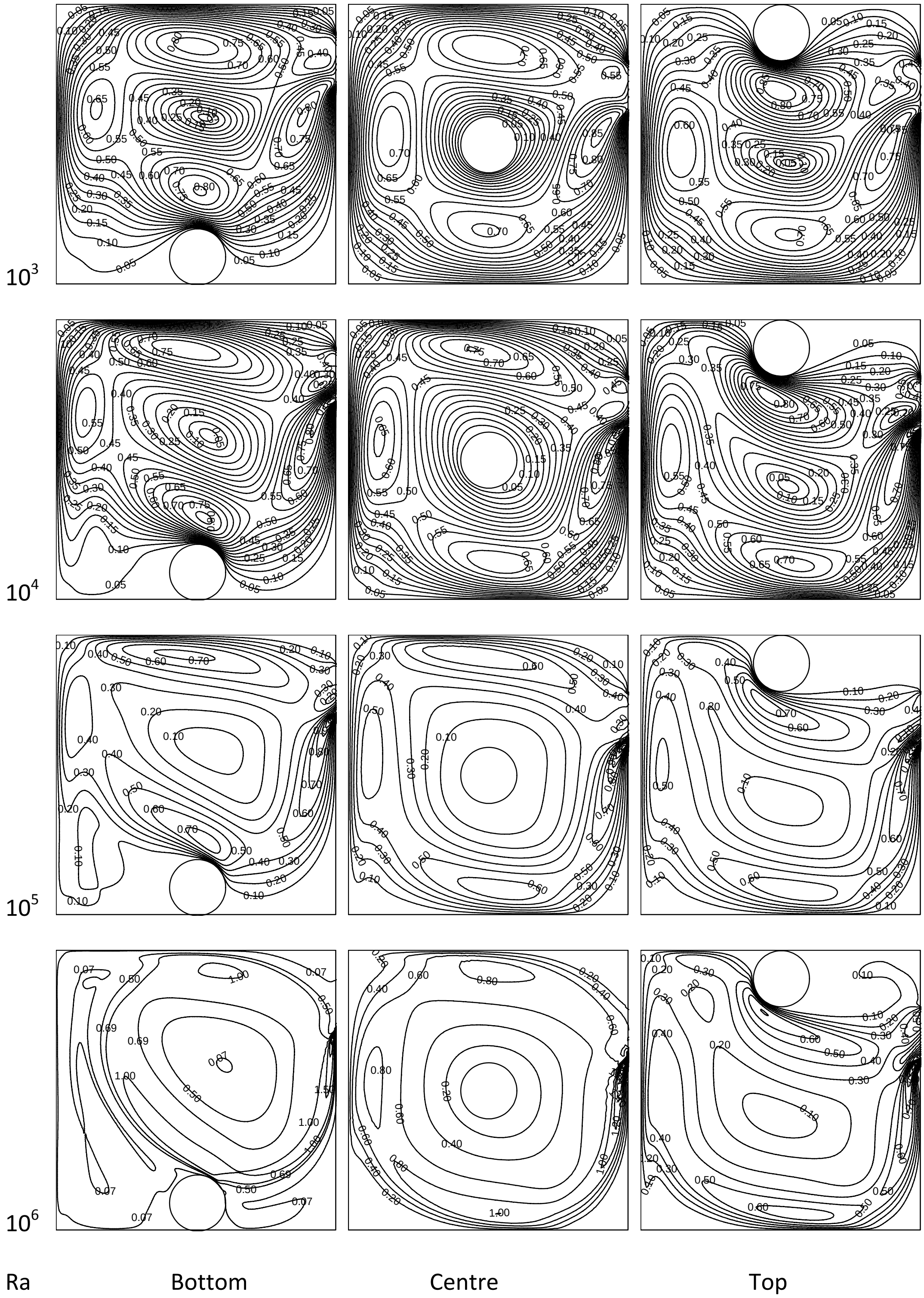

Fig-3.23: Stream lines for different Rayleigh numbers Ra and cylinder locations at an angle $\Phi=45^0$ when Pr = 0.72

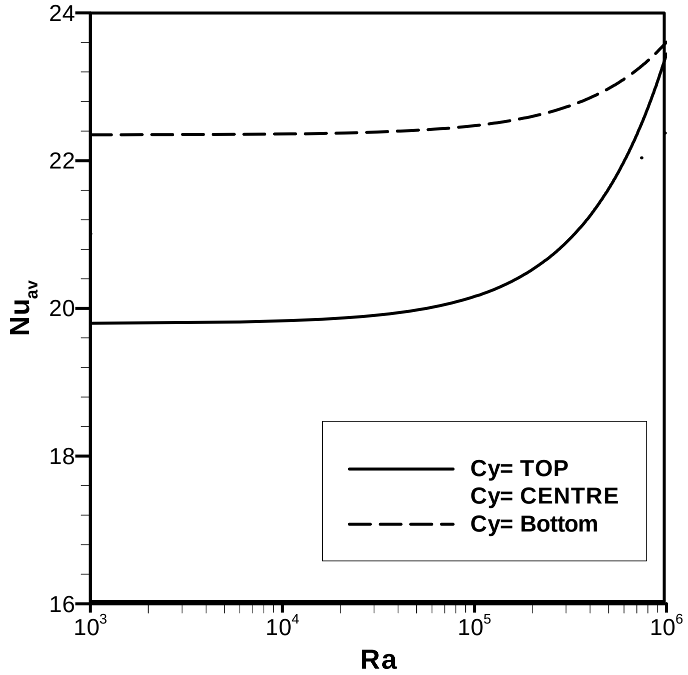

Fig-3.24: Average Nusselt figure for different cylinder locations (Top, Centre & Bottom) and Rayleigh numbers at an angle $\Phi=0^0$ for Pr=0.72

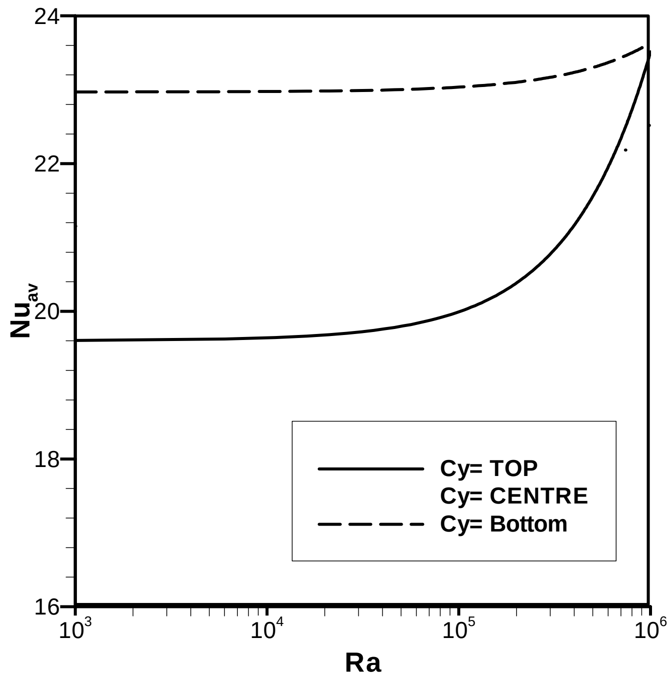

Fig-3.25: Average Nusselt figure for different cylinder locations (Top, Centre & Bottom) and Rayleigh numbers at an angle $\Phi=30^0$ for Pr=0.72

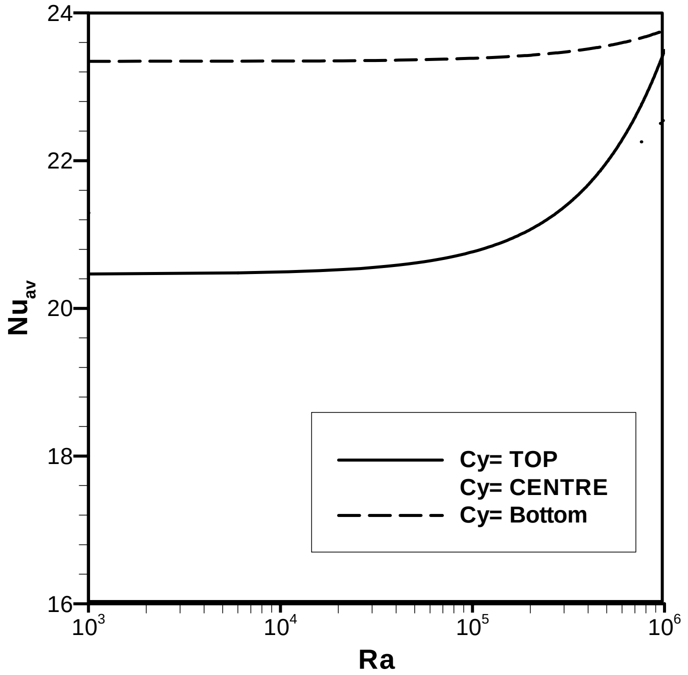

Fig-3.26: Average Nusselt figure for different cylinder locations (Top, Centre & Bottom) and Rayleigh numbers at an angle $\Phi=45^0$ for Pr=0.72

3.4.3 Effects of Prandtl Number

The influence of Prandtl number on isotherms as well as streamlines for centre cylinder location configuration at AR = 1.0, Ra = 10^3 - 10^6, dr = 0.2, Pr = 0.72 and angle 0^0- 45^0 has been demonstrated in fig 3.27 to 3.32.

For Isotherm Patterns: The isotherms illustrate the temperature field in the separated flow region has been shown in fig 3.27 to 3.29. We observe that the flow patterns become more of a boundary layer type at the left wall for Ra = 10^3- 10^6 with the increasing Prandtl number Pr. This implies that the flow becomes faster and temperature gradient increases as conduction is intensified.

For streamline Patterns: It is seen that the fluid that moves clock wise around the cylinder and creates vortices in the cavity. At Ra= 10^3, the flow patterns are very similar for different Prandtl number. At Ra= 10^4-10^5, the flow with small Prandtl number (Pr=0.72) has been affected by the buoyancy force, thus creating a clockwise recirculation region near the cylinder as shown in fig 3.30 to 3.32. This recirculation region decreases with the increasing Prandtl number.

The variation of average Nusselt number at the heated wall in the cavity along with Ra for different Prandtl numbers has been presented in fig 3.33 to 3.35. In Table 3.11 to 3.13 average Nusselt numbers for different Prandtl numbers (*Pr* = 0.72, 3.0 and 10.0) and Rayleigh numbers, obtained with the present model for angle ($\Phi = 0^o - 45^0$) is presented. Figures 3.33 to 3.35 shows the average Nusselt number variation for different Prandtl numbers (*Pr*= 0.72, 3.0, 10.0). We observed that the average Nusselt number *Nu* increases with increasing Rayleigh number Ra and average Nusselt number decreases with the increasing Prandtl number *Pr*, that is, heat transfer characteristics become low for higher Prandtl number *Pr* = 10 and high for lower *Pr* = 0.72. This is, because, the fluid with *Pr* = 10 has a higher thermal diffusivity than that of the fluid with *Pr* = 0.72. Hence, the fluid with *Pr* = 10 will tend to exchange more heat with surrounding fluid by diffusion.

Table 3.11**:** Average Nusselt number for different Prandtl numbers (Pr = 0.72, 3.0 & 10.0) and Rayleigh numbers at an angle $\Phi = 0^o$

Nu_{av}				
Pr	Ra=10^3	Ra=10^4	Ra=10^5	Ra=10^6
0.72	20.40250621	21.30193788	21.51197329	22.36279026
3.0	12.63859595	20.07549464	21.44009634	22.24093084
10.0	8.96380401	19.55421272	21.41617059	22.16082597

Table 3.12: Average Nusselt number for different Prandtl numbers (Pr = 0.72, 3.0 & 10.0) and Rayleigh numbers at an angle $\Phi = 30^o$

Nu_{av}				
Pr	$Ra=10^3$	$Ra=10^4$	$Ra=10^5$	$Ra=10^6$
0.72	20.17243983	21.58317925	21.91566822	22.48039619
3.0	13.99251657	20.75348129	21.51449017	22.44059645
10.0	10.44347108	19.86945846	21.48540366	22.34484008

Table 3.13: Average Nusselt number for different Prandtl numbers (Pr = 0.72, 3.0 & 10.0) and Rayleigh numbers at an angle $\Phi = 45^o$

Nu_{av}				
Pr	$Ra=10^3$	$Ra=10^4$	$Ra=10^5$	$Ra=10^6$
0.72	20.23971823	21.57393913	22.29072279	22.4763611
3.0	14.96348202	21.3112681	21.50929871	22.47750561
10.0	11.69442281	20.36985093	21.48010234	22.38447703

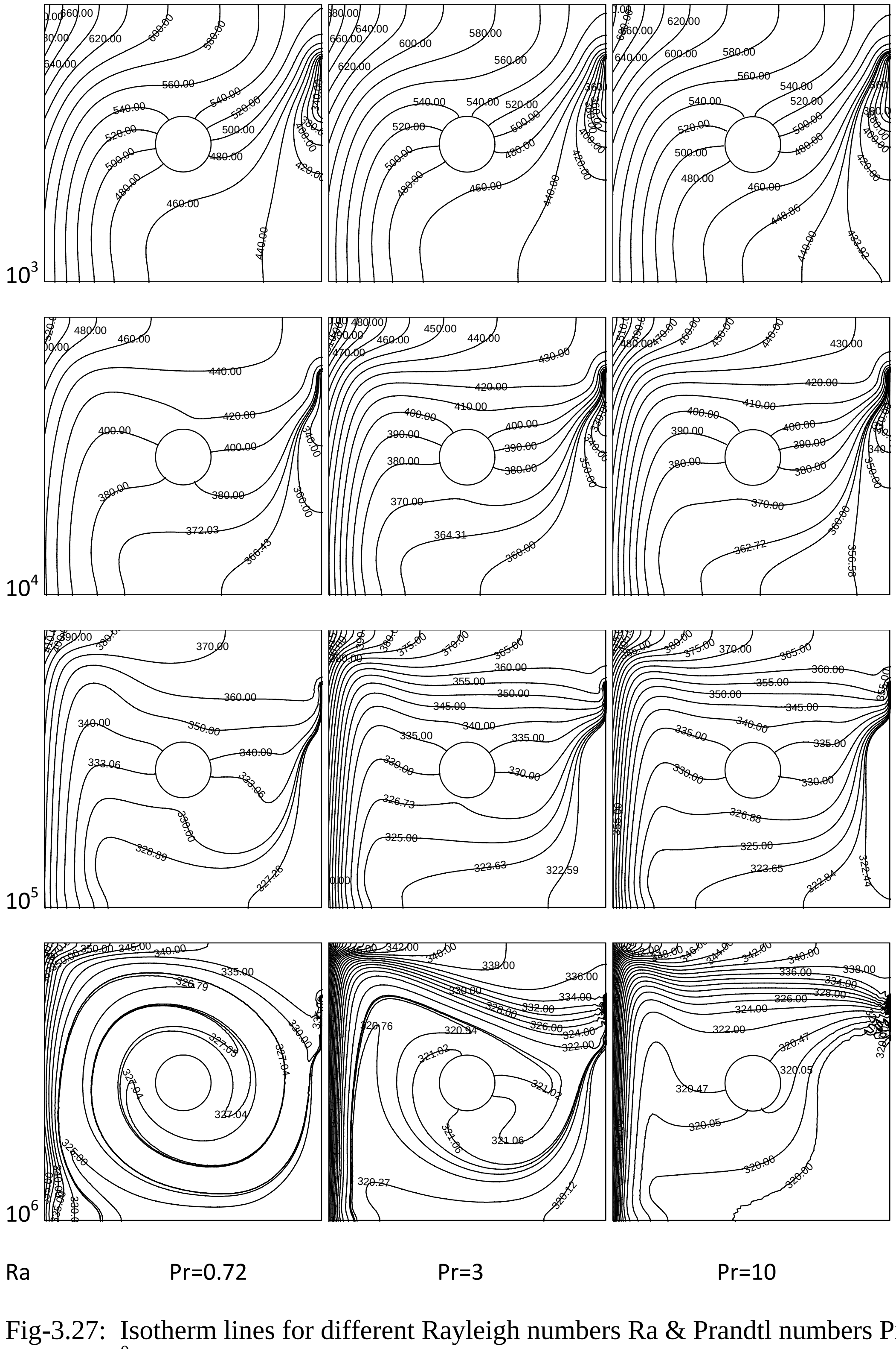

Fig-3.27: Isotherm lines for different Rayleigh numbers Ra & Prandtl numbers Pr at an angle $\Phi=0^0$

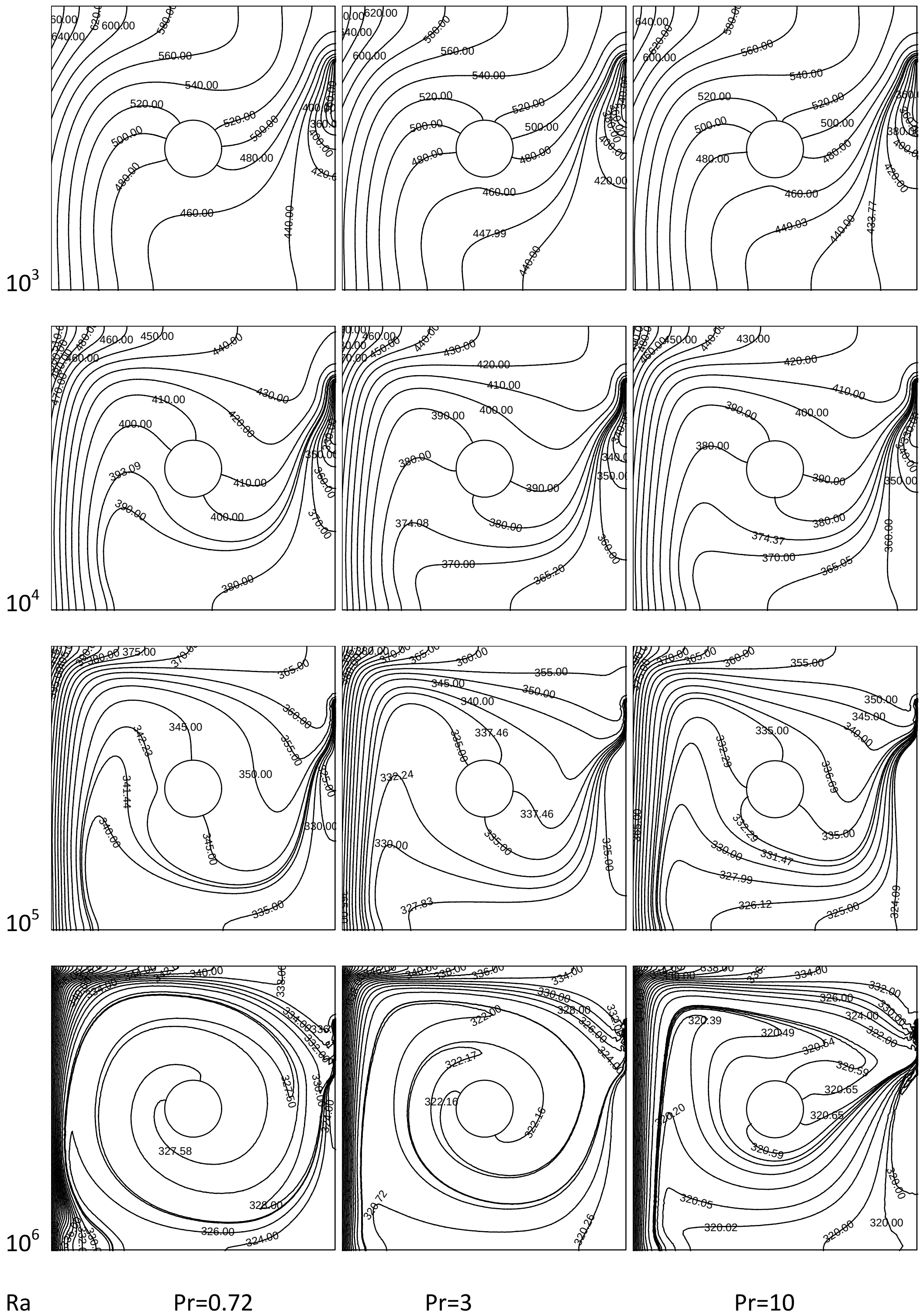

Fig-3.28: Isotherm lines for different Rayleigh numbers Ra & Prandtl numbers Pr at an angle $\Phi=30^0$

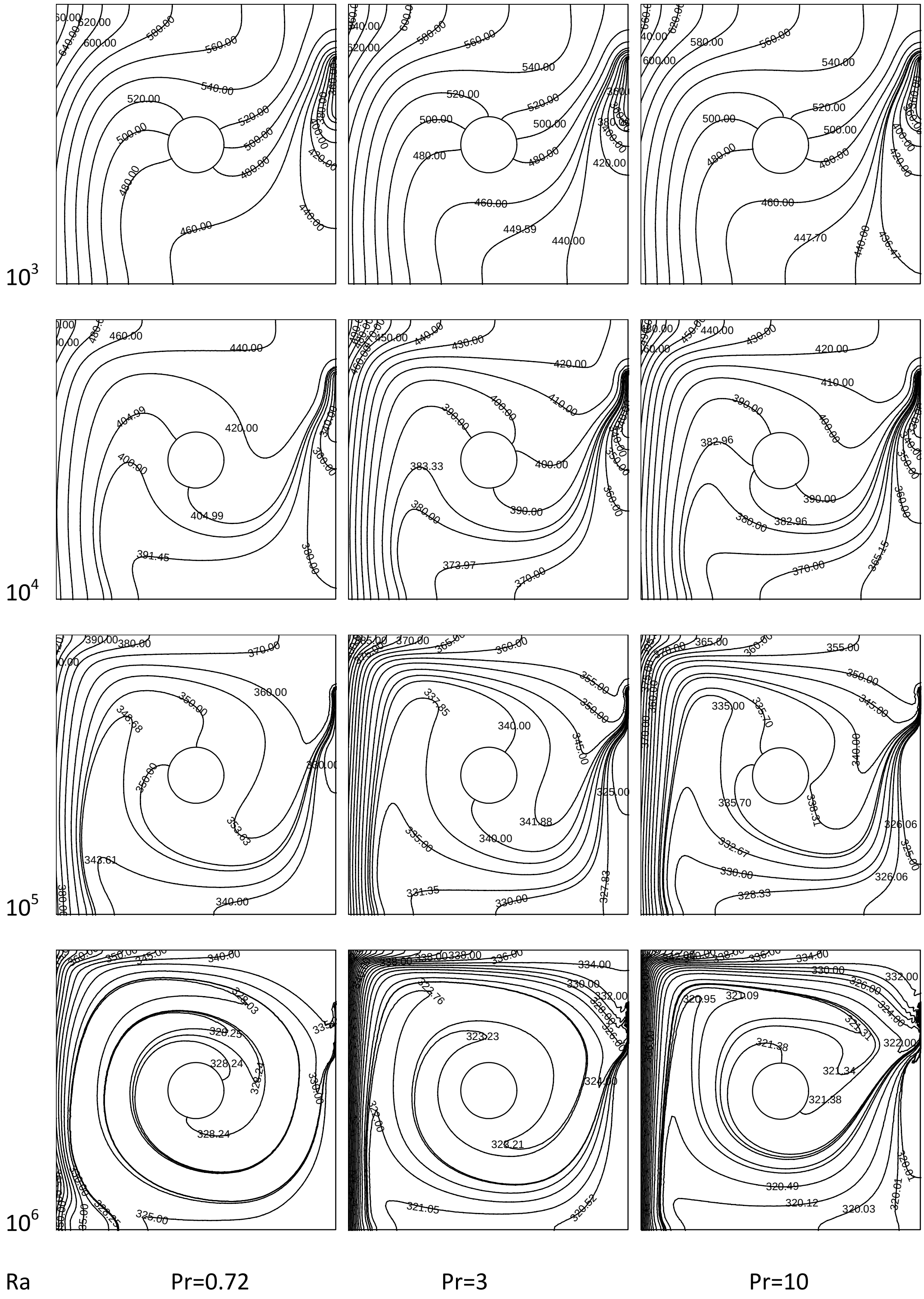

Fig-3.29: Isotherm lines for different Rayleigh numbers Ra & Prandtl numbers Pr at an angle $\Phi=45^0$

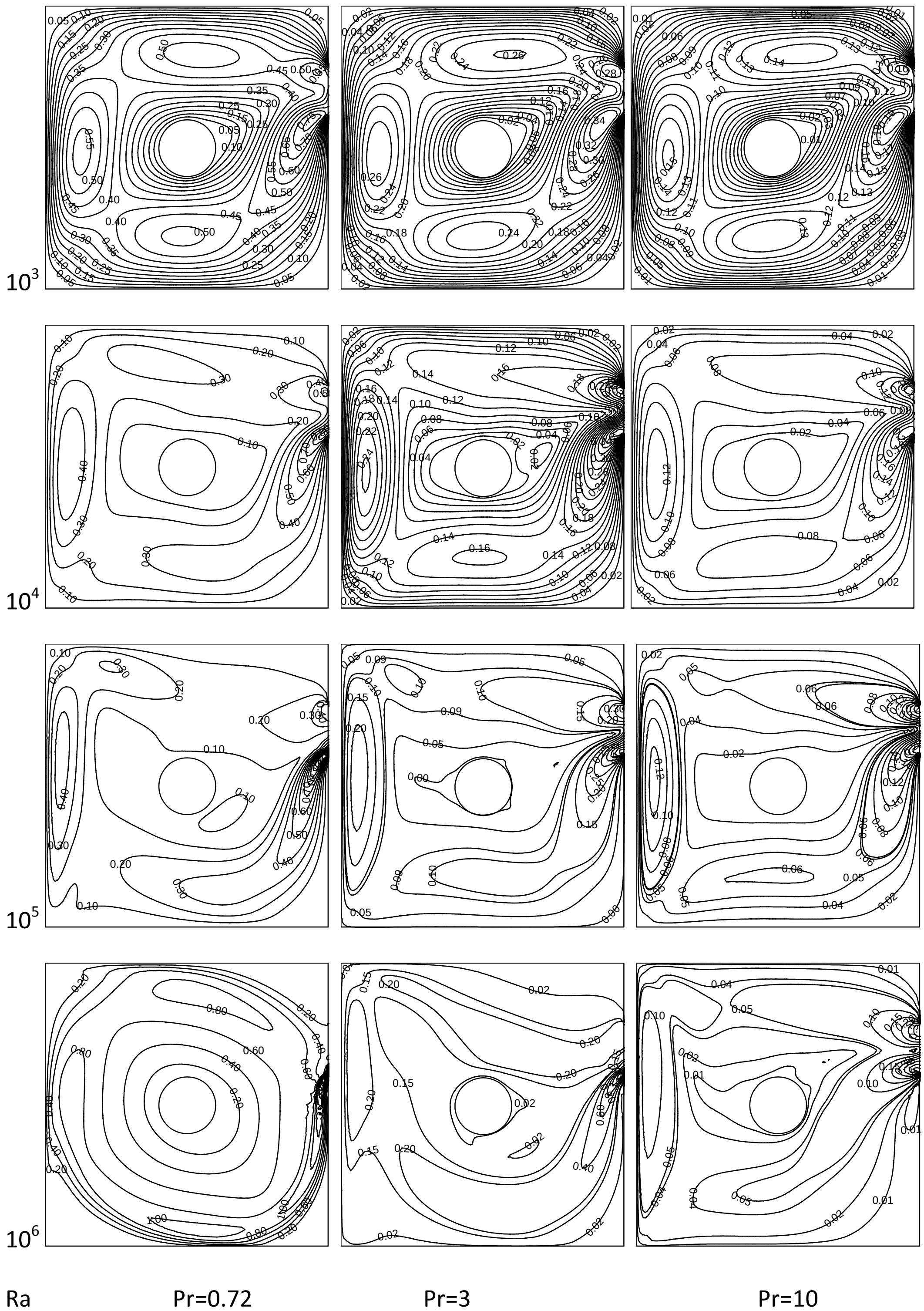

Fig-3.30: Stream lines for different Rayleigh numbers Ra & Prandtl numbers Pr at an angle $\Phi=0^0$

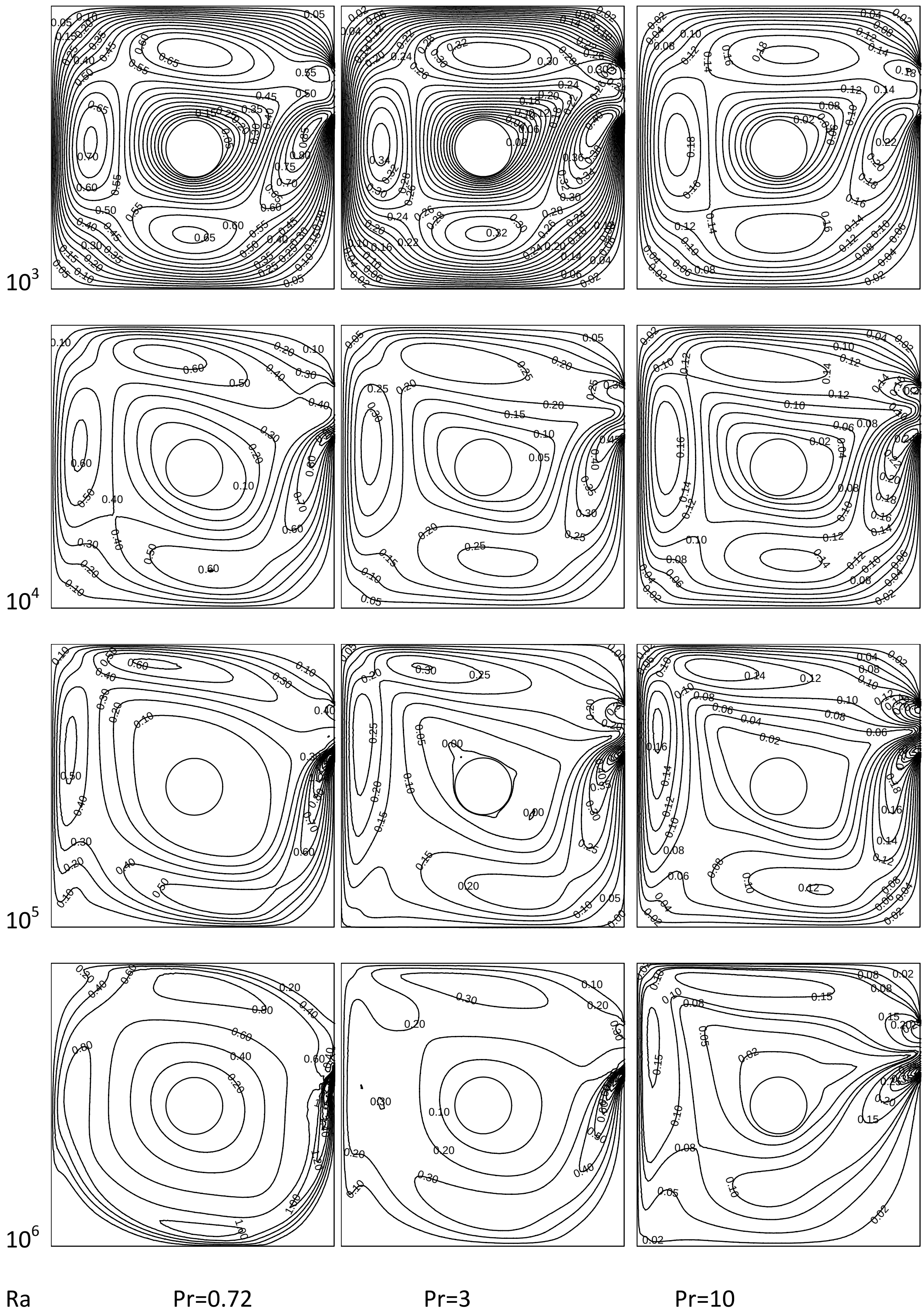

Fig-3.31: Stream lines for different Rayleigh numbers Ra & Prandtl numbers Pr at an angle $\Phi=30^0$

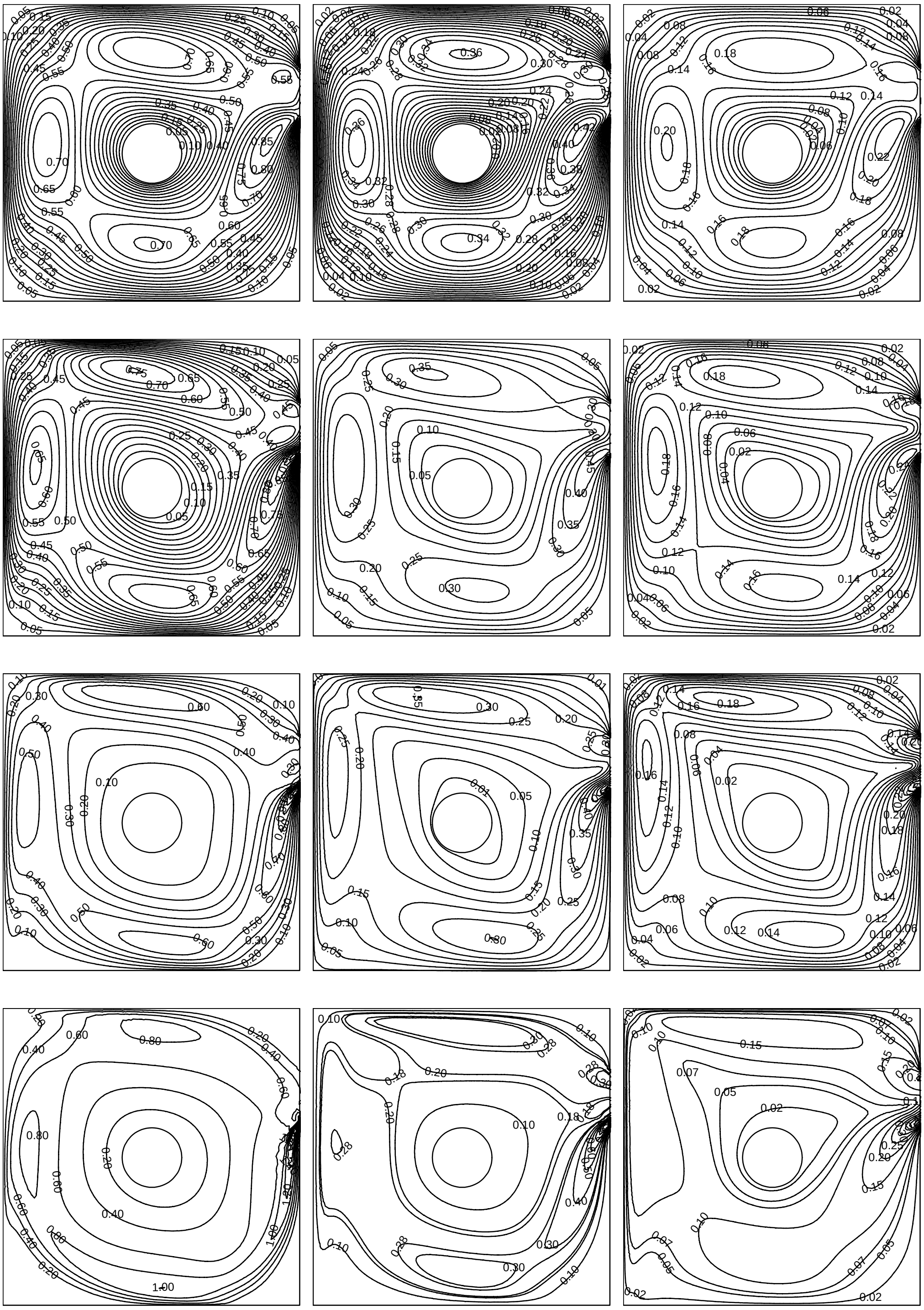

10^3 10^4 10^5 10^6

Ra Pr=0.72 Pr=3 Pr=10

Fig-3.32: Stream lines for different Rayleigh numbers Ra & Prandtl numbers Pr at an angle $\Phi=45^0$

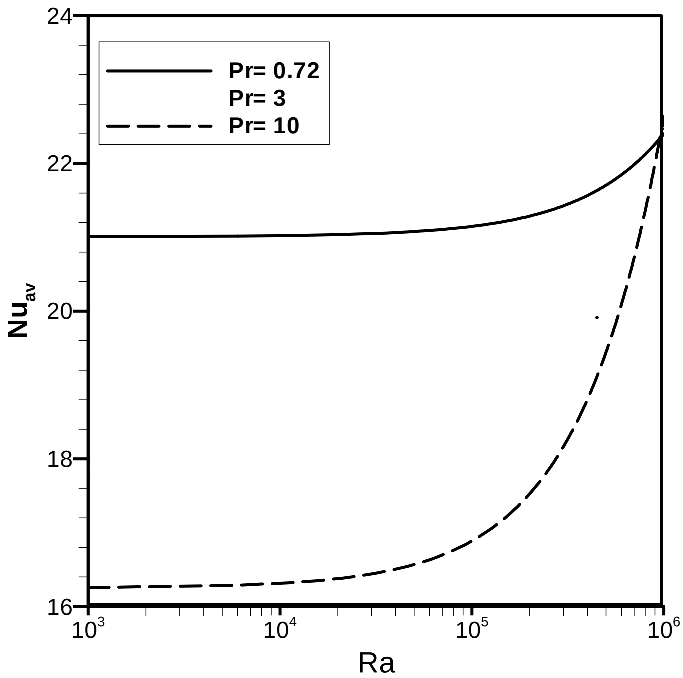

Fig-3.33: Average Nusselt figure for different Prandtl numbers Pr and Rayleigh numbers Ra at an angle $\Phi=0^0$ for centre cylinder

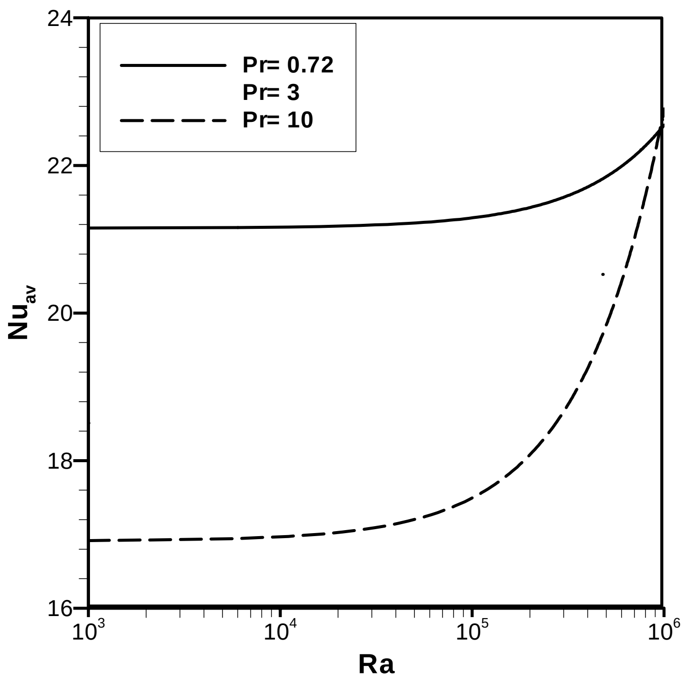

Fig-3.34: Average Nusselt figure for different Prandtl numbers Pr and Rayleigh numbers Ra at an angle $\Phi=30^0$ for centre cylinder

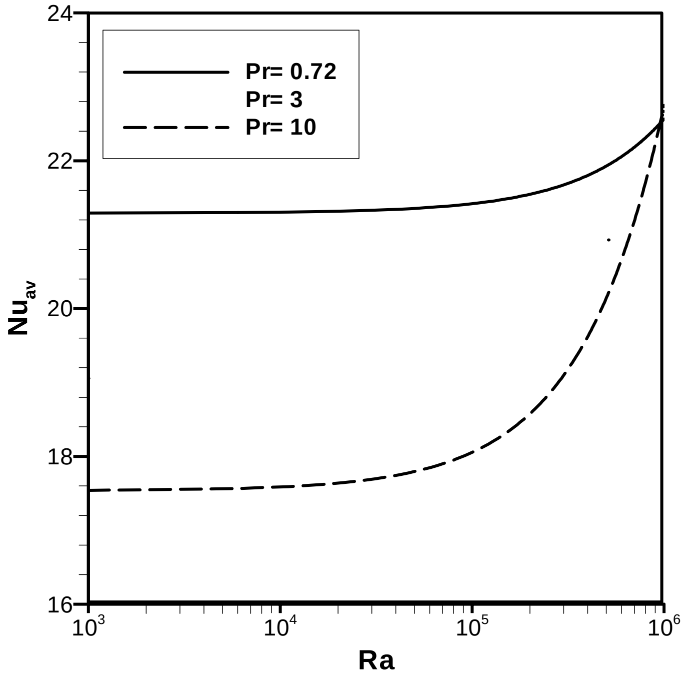

Fig-3.35: Average Nusselt figure for different Prandtl numbers Pr and Rayleigh numbers Ra at an angle $\Phi=45^0$ for centre cylinder

3.4.4 Effects of Diameter Ratio

The effect of diameter ratio of a centre cylinder on the thermal transport has greater importance and has shown in figure 3.36 to 3.41. The isotherm lines and stream lines for various diameter of a centre cylinder for aspect ratio (AR) = 1.00, Ra = 10^3- 10^6, diameter ratio dr= 0.0 - 0.2, Pr = 0.72 and angle $\Phi=0^0$- 45^0 has been demonstrated in fig 3.36 to 3.41.

For Isotherm Patterns: In fig 3.36 to 3.38, when Pr=0.72 the flow patterns become more packed to the left boundary wall for all diameter ratios with increase of Rayleigh numbers Ra. As a result, Thermal Boundary Layer becomes thinner and also temperature gradient increases. Besides, flow patterns for dr=0.2 at $\Phi=0^0$ distorted and circulated at Ra = 10^6. We also observed that the flow patterns become more of a boundary layer type at the left wall for Ra = 10^3- 10^6 with the increasing of diameter ratios. This implies that the flow becomes faster and temperature gradient increases as conduction is intensified.

For Streamline Patterns: In fig 3.39 to 3.41, when Pr=0.72 the streamline patterns become boundary type with increase of Ra. There are more vortices in the cavity for $Ra=10^3$-10^4 and vortex gradually converted to boundary type. As a result, Velocity Boundary Layer becomes thinner and also Velocity gradient increases. Hence, conduction dominated at 10^3 and convection intensified with increase of Ra. Streamline patterns from the right side become more horizontal for Ra = 10^3 - 10^5 but circulate at 10^6 for all diameter ratios. The flow pattern becomes faunal shape with the increases of Ra = 10^3 – 10^5 and also create secondary vortex near the cylinder. Velocity gradient decreases with diameter ratio at heated wall. Entering fluid flow patterns become flat and create more vortices with the increases of diameter ratio. At Rayleigh number Ra = 10^4, fluid flow more packed at diameter ratio dr = 0.2 than other diameter ratio dr and the flow type is boundary layer.

In Table 3.14 to 3.16, average Nusselt numbers for different diameter ratios (*dr* = 0.0, 0.1 and 0.2) and Rayleigh numbers, obtained with the present model for angle $\Phi = 0^o - 45^0$ and Prandlt number Pr= 0.72 are presented. Figure 3.42 to 3.44 shows average Nusselt number decreases with increasing of diameter ratio of the cylinder for $Ra=10^3$ to 10^6. At Ra = 10^3 – 10^5, thermal boundary layer increases along with the increase of diameter ratio (dr) because of the restriction of heat flow from bottom to upper in the cavity. But at Ra = 10^6, the thermal boundary layer decreases with the increase of diameter ratio due to the increase of convective heat transfer.

Table 3.14: Average Nusselt number for different diameter ratios (*dr* = 0.0, 0.1 & 0.2) and Rayleigh numbers Ra at an angle $\Phi = 0^o$ when *Pr* = 0.72

Nu_{av}				
dr	$Ra=10^3$	$Ra=10^4$	$Ra=10^5$	$Ra=10^6$
0.0	20.402506	21.914341	22.0982	22.821992
0.1	20.170982	21.301938	21.612121	22.36279
0.2	11.355765	19.50749	21.511973	22.199985

Table 3.15: Average Nusselt number for different diameter ratios (dr = 0.0, 0.1 & 0.2) and Rayleigh numbers Ra at an angle $\Phi = 30^o$ when Pr = 0.72

Nu_{av}				
dr	$Ra=10^3$	$Ra=10^4$	$Ra=10^5$	$Ra=10^6$
0.0	20.698809	21.969422	22.653885	22.928894
0.1	20.17244	21.583179	21.915668	22.480396
0.2	16.763687	20.368344	21.693392	22.368809

Table 3.16: Average Nusselt number for different diameter ratios (dr = 0.0, 0.1 & 0.2) and Rayleigh numbers Ra at an angle $\Phi = 45^o$ when Pr = 0.72

Nu_{av}				
dr	$Ra=10^3$	$Ra=10^4$	$Ra=10^5$	$Ra=10^6$
0.0	20.837624	21.952324	22.917878	22.969117
0.1	20.239718	21.573939	22.290723	22.476361
0.2	17.263107	21.102933	21.686445	22.428129

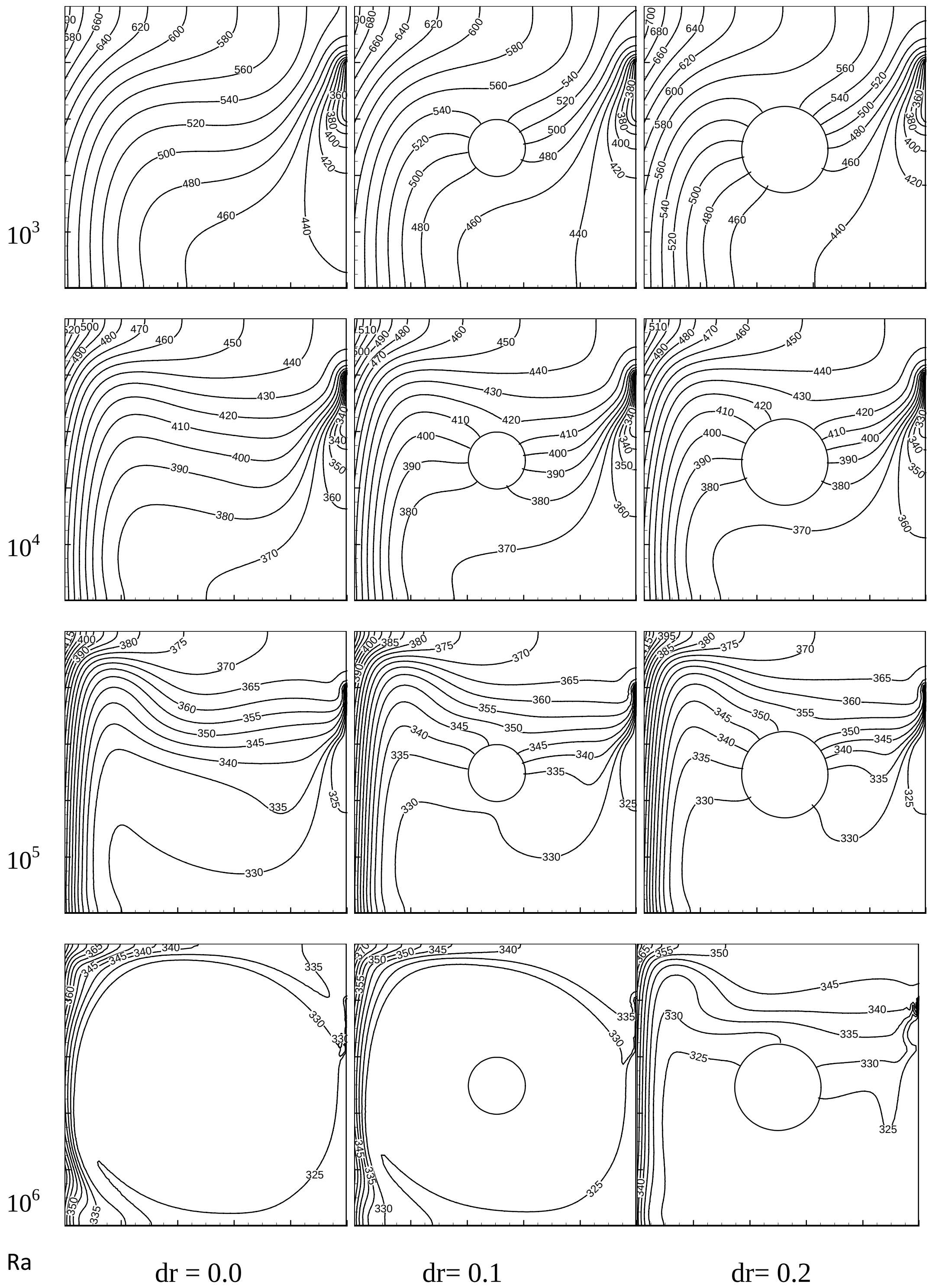

Fig-3.36: Isotherm patterns for different diameter ratios dr and Rayleigh numbers Ra at an angle $\Phi = 0^0$ when Pr = 0.72

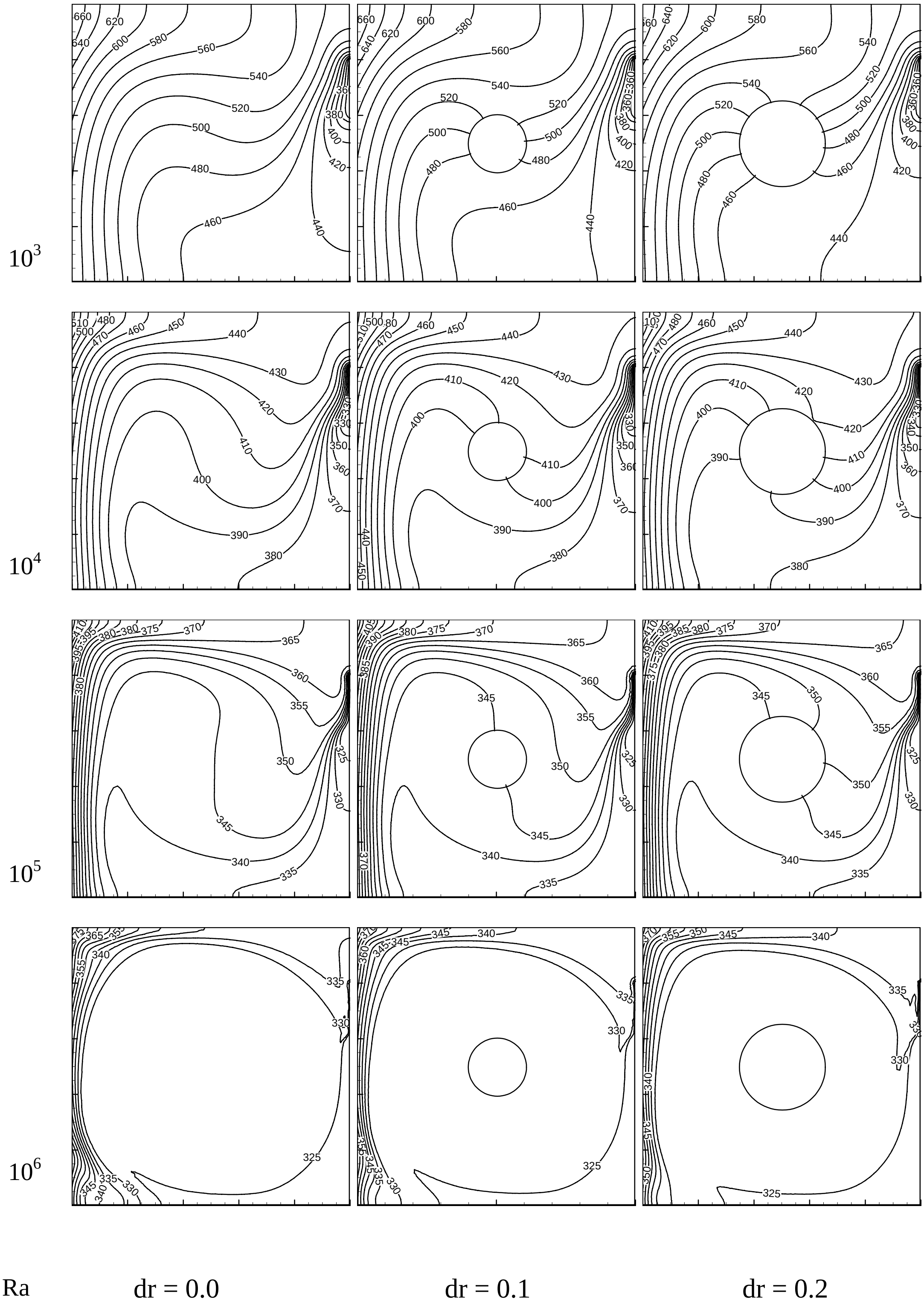

Fig-3.37: Isotherm patterns for different diameter ratios dr and Rayleigh numbers Ra at an angle $\Phi = 30^0$ when Pr = 0.72

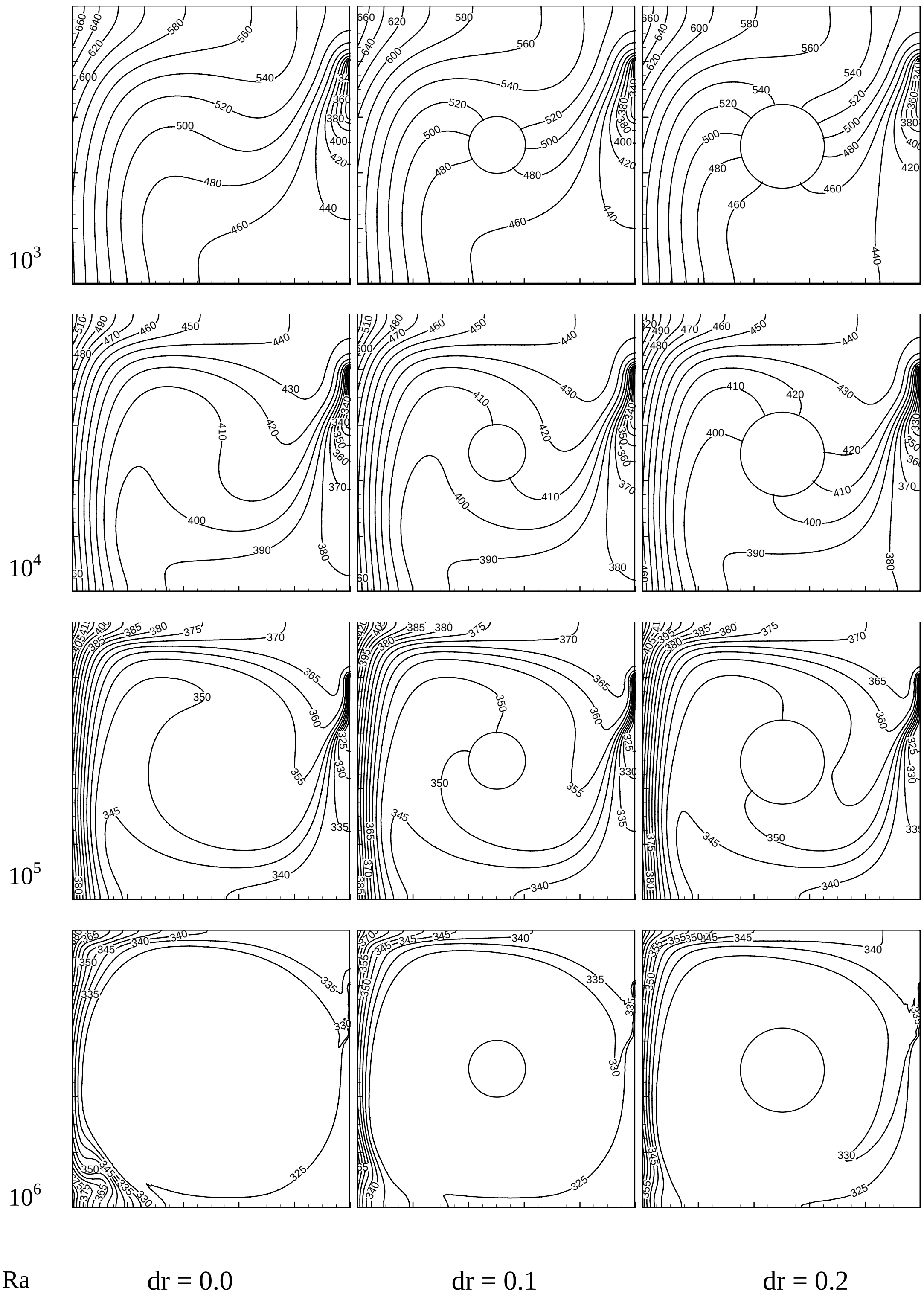

Fig-3.38: Isotherm patterns for different diameter ratios dr and Rayleigh numbers Ra at an angle $\Phi = 45^0$ when Pr = 0.72

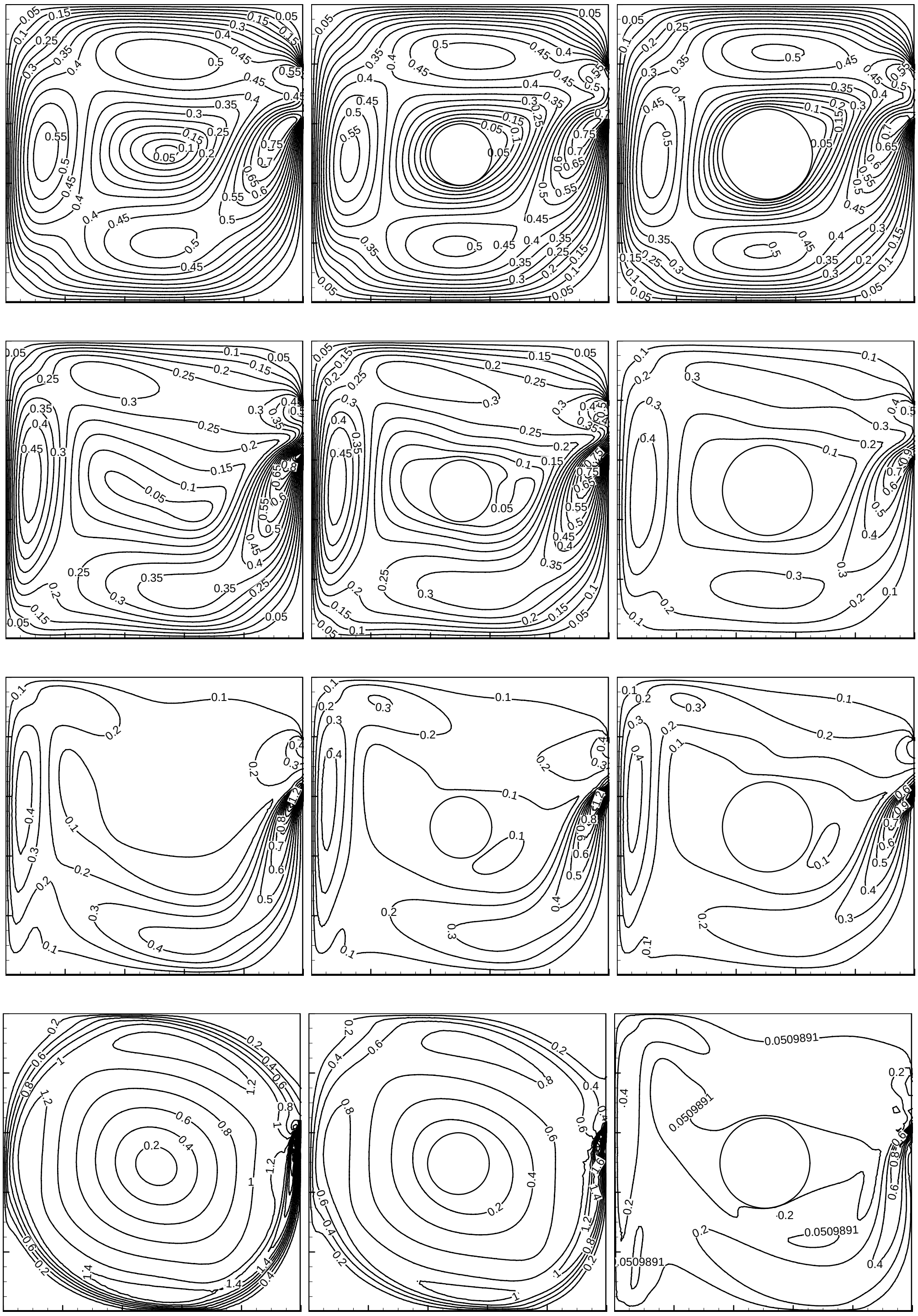

10^3

10^4

10^5

10^6

Ra   dr = 0.0   dr = 0.1   dr = 0.2

Fig-3.39: Streamline patterns for different diameter ratios dr and Rayleigh numbers Ra at an angle $\Phi = 0^0$ when Pr = 0.72

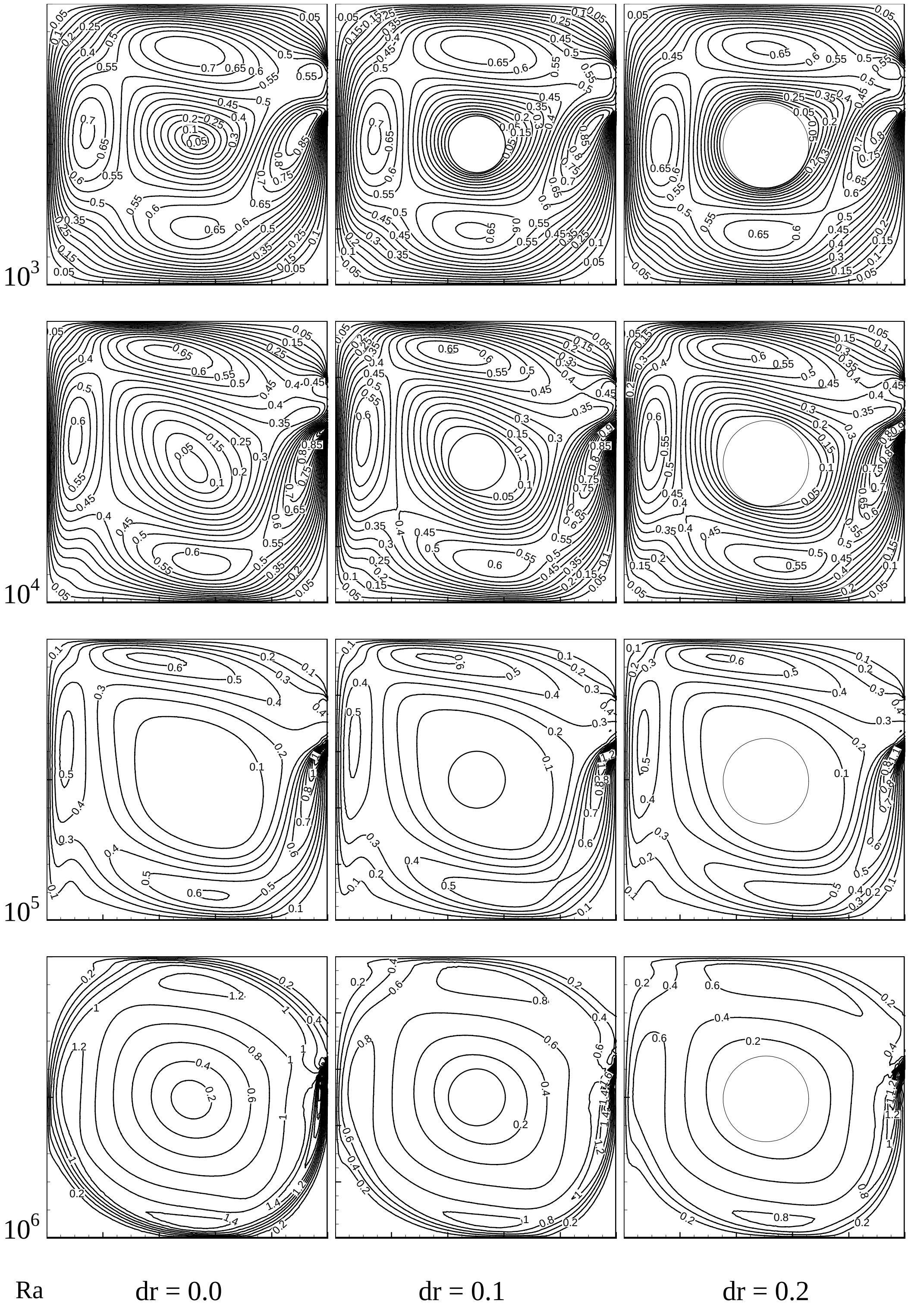

Fig-3.40: Streamline patterns for different diameter ratios dr and Rayleigh numbers Ra at an angle $\Phi = 30^0$ when Pr = 0.72

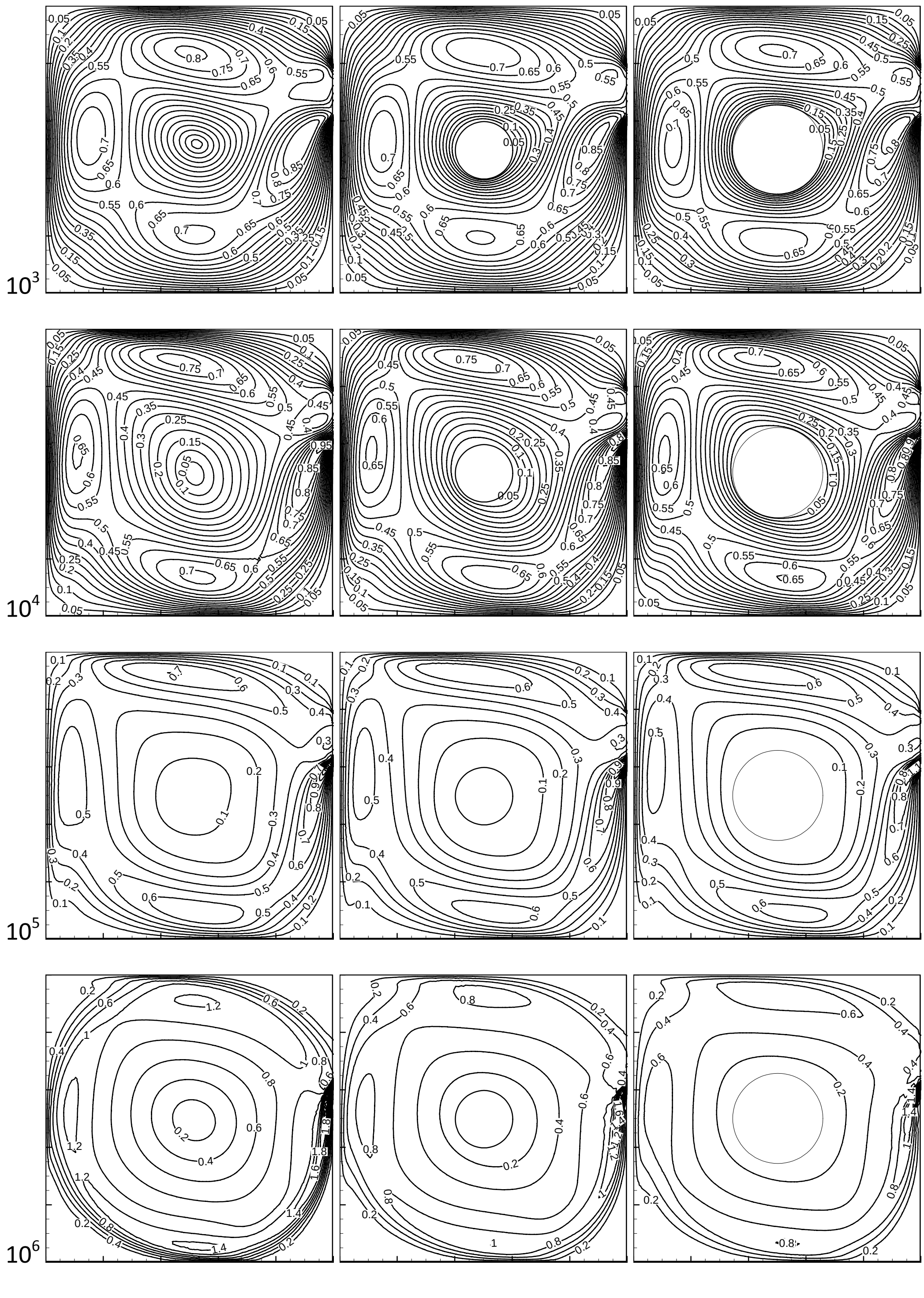

Fig-3.41: Streamline patterns for different diameter ratios dr and Rayleigh numbers Ra at an angle $\Phi = 45^0$ when Pr = 0.72

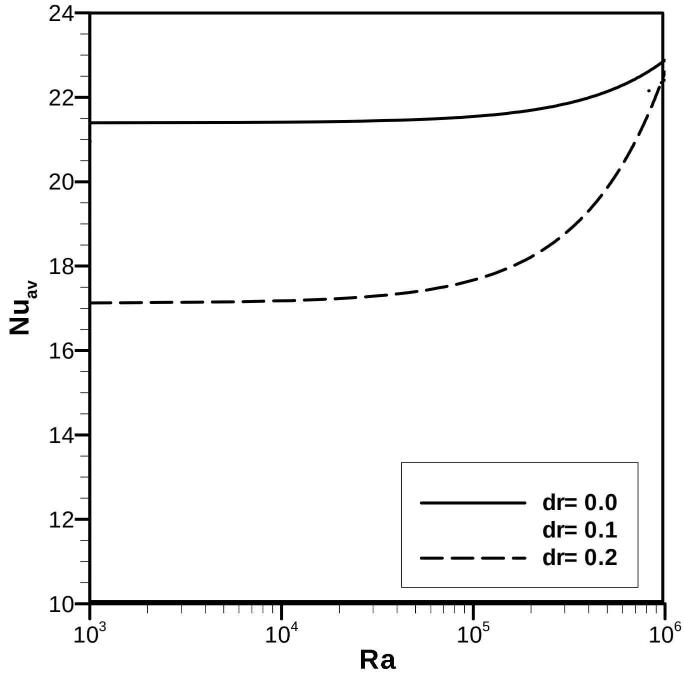

Fig-3.42: Average Nusselt figure for different diameter ratios dr and Rayleigh numbers Ra at an angle $\Phi = 0^0$ when Pr = 0.72 for centre cylinder

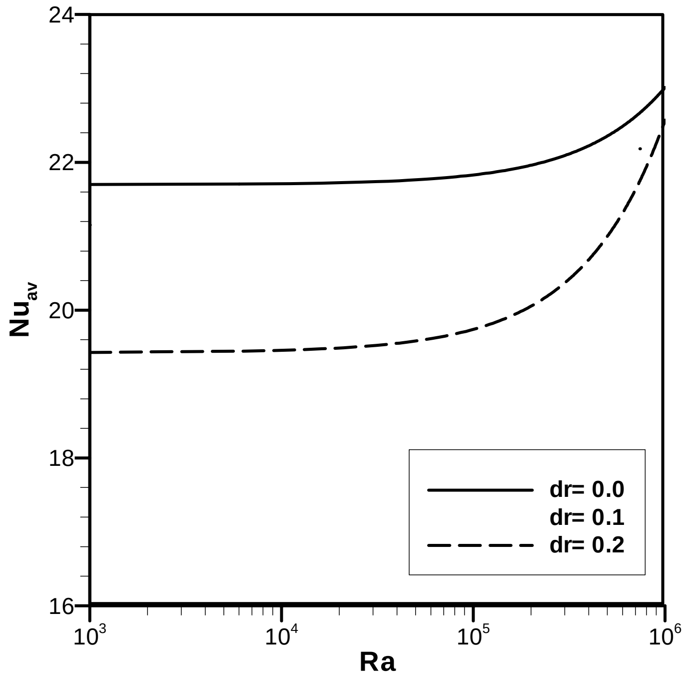

Fig-3.43: Average Nusselt figure for different diameter ratios dr and Rayleigh numbers Ra at an angle $\Phi = 30^0$ when Pr = 0.72 for centre cylinder

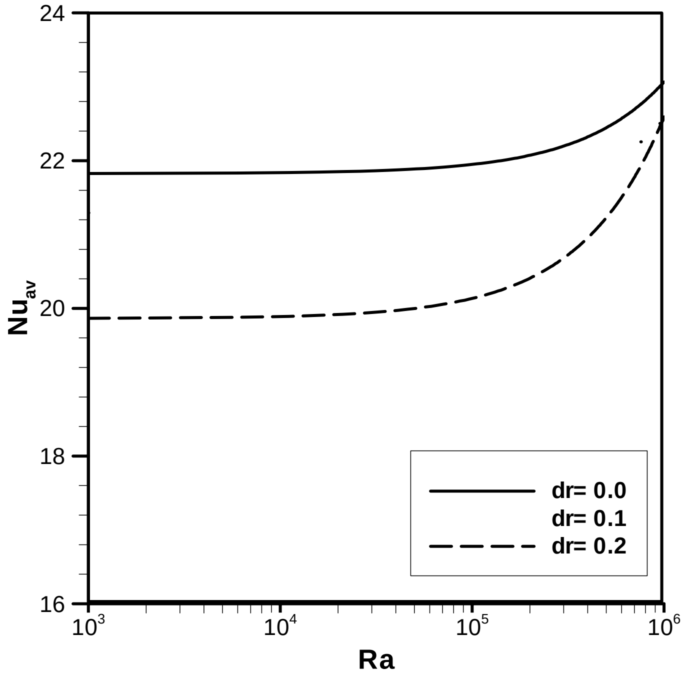

Fig-3.44: Average Nusselt figure for different diameter ratios dr and Rayleigh numbers Ra at an angle $\Phi = 45^0$ when Pr = 0.72 for centre cylinder

3.5 Chapter Summary

Two-dimensional laminar steady state natural convection flow in a partially heated square cavity with the left vertical wall at iso-heat flux has been studied numerically. A finite element method for steady-state incompressible natural convection flow is presented. The finite element equations derived from the governing flow equations that consist of the conservation of mass, momentum, and energy equations. The derived finite element equations are non-linear requiring an iterative technique solver. The Newton-Raphson iteration method has been applied to solve these nonlinear equations for solutions of the nodal velocity component, temperature, and pressure by considering Prandtl numbers of 0.72, 3.00 and 10.00 and Rayleigh numbers of 10^3 to 10^6. The results show the following aspects:

a. Heat transfer depends on Prandtl number and heat transfer rate decreases for higher Prandtl number.

b. Thermal boundary layer becomes thinner due to the increasing of Rayleigh number.

c. The heat transfer rate Nu_{av} increases with the increasing of inclination angles as well as Rayleigh numbers.

d. The heat transfer rate Nu_{av} decreases with the increasing of diameter ratio and Ra.

e. Various vortices entering the flow field and a secondary vortex at the centre and bottom wall of the cavity are seen in the streamlines.

f. The average Nusselt number Nu_{av} is higher for the location of bottom cylinder.

CHAPTER 4

4.1 Summary of Major Outcomes

The study has been confined to cases of an adiabatic circular cylinder in a partially heated square cavity. In cases of an adiabatic circular cylinder, the stream line of flow and thermal fields as well as characteristics of heat transfer process particularly its expansion has been evaluated in chapter 3. On the basis of the analysis the following conclusions have been drawn:

a. An adiabatic circular cylinder has significant effect on the flow and thermal distributions in a partially heated square cavity. The average Nusselt number (Nu_{av}) at the hot wall is the highest for the angle 45^0 when Rayleigh number 10^6, whereas the lowest heat transfer rate for the angle 0^0 when Rayleigh number 10^3.

b. The heat transfer rate Nu_{av} decreases with the increasing of diameter ratio for Ra10^3 – 10^6.

c. Heat transfer depends on Prandtl number and heat transfer rate decreases for higher Prandtl number but increases for lower prandtl number.

d. Various vortices entering into the flow field and a secondary vortex at the centre and bottom wall of the cavity is seen in the streamlines for centre cylinder.

e. The heat transfer rate is higher for location of Bottom cylinder

4.2 Extension of Works

The consequent can be ahead for the additional works on the base of the present research as.

a. The study can be extended by dissimilar physics like radiation effects, heat generation and tube effects.

b. Effect of conduction on mixed convection flow in a square open cavity with a heat conducting square cylinder.

c. Effect of conduction on mixed convection flow in a square open cavity with a heat conducting circular cylinder.

d. The study can be extended for non-uniform surface temperature using different fluids

e. The study can be performed by using magnetic circular cylinder instead of adiabatic circular cylinder.

f. Investigation can be performed by using magnetic fluid within the porous medium and changing the boundary conditions of the cavity's walls.

g. Investigation can be performed by using inlet-outlet with various places in the cavity.

h. Two-dimensional fluid flow and heat transfer has been analyzed in this thesis. So this consideration may be extended to three-dimensional analyses to explore the effects of parameters on flow fields and heat transfer in cavities. In addition, the problem of fluid flow and heat transfer along with heat generating cylinder may be studied in three-dimensional cases.

References

[1] Arnold, J. N., Catton, I., and Edwards, D. K., “Experimental Investigation of Natural Convection in Inclined Rectangular Regions of Differing Aspect Ratios,” Journal of Heat Transfer, Vol. 98, pp.67-71, 1976.

[2] Bilgen, E., and Oztop, H., “Natural convection heat transfer in partially open inclined square cavities”, Int. J. of Heat and Mass Transfer, Vol. 48, pp. 1470-1479, 2005.

[3] Chan,Y. L. and Tien, C. L., “A Numerical study of two-dimensional laminar natural convection in a shallow open cavity”, Int. J. Heat Mass Transfer, Vol. 28, pp. 603-612,1985.

[4] Chan,Y. L. and Tien, C. L., “A Numerical study of two-dimensional natural convection in square open cavities”, Numerical Heat Transfer, Vol. 8, pp. 65-80, 1985.

[5] Chen, C. J. and Talaie, V., “Finite Analytic Numerical Solutions of Laminar Natural Convection in Two-Dimensional Inclined Rectangular Enclosures,” ASME paper 85-HT-10, 1985.

[6] Cook, R. D., Malkus, D. S., and Plesha, M. E., “Concepts and applications of finite element analysis”, Third Ed., John Wiley & Sons, New York, 1989.

[7] Chung.T.J.,“Computational Fluid Dynamices”, Second Ed., Cambridge, 2002.

[8] Dechaumphai, P. Adaptive finite element technique for heat transfer problems, Energy, Heat & Mass transfer, Vol. 17, pp. 87-94, 1995.

[9] Dechaumphai, P., Finite Element Method in Engineering, second Ed., Chulalongkorn University Press, Bangkok,1999.

[10] Elsherbiny, S.M., Raithby, G. D., and Hollands, K. G. T., “Heat Transfer by Natural Convection across Vertical and Incline Air Layers”, Transactions of the ASME, Vol. 104, pp. 96-102, 1982.

[11] Frederick, R. L. “Natural convection in an inclined square enclosure with a partition attached to its cold wall”, Int. J. Heat and Mass Transfer,Vol. 32, pp. 87–94, 1989.

[12] Ferziger, J. H. and Perić, M., “Computational methods for fluid dynamics”, Second Ed., Springer Verlag, Berlin Hedelberg, 1997.

[13] Gallagher, R. H., Simon, B. R., Johnson, P. C. and Gross, J. F., Finite elements in biomechanics, John Wiley & Sons, New York, 1982.

[14] Goutam Saha, Sumon Saha and Md. Arif Hasan Mamun, “A Finite Element Method for Steady-State Natural Convection in a Square Tilt Open Cavity”, ARPN Journal of Engineering and Applied Sciences, Vol. 2, No. 2, pp. 41-49, 2007.

[15] Hamady, F. J., Lloyd, J. R., Yang, H. Q., and Yang, K. T., “Study of Local Natural convection Heat Transfer in an Inclined Enclosure,” International Journal of Heat and Mass Transfer, Vol. 32, pp.1697-1708, 1989.

[16] Hinojosa, J. F., Estrada, C. E., Cabanillas, R. E., and Alvarez, G., “Nusselt number for the natural convection and surface thermal radiation in a square tilted open cavity”, Int. Com. In Heat and Mass Transfer, Vol. 32, pp. 1184-1192, 2005.

[17] Jini, J., The finite element method in electromagnetics, John Wiley & Sons, New York, 1993.

[18] Kangni, A., Ben, R. and Bilgen, E. “Natural convection and conduction in enclosure with multiplevertical partitions”, Int. J. Heat and Mass Transfer,Vol. 34, pp. 2819–2825, 1991.

[19] Kuhn, D. and Oosthuizen, P. H., “Unsteady natural convection in a partially heated rectangular cavity”, ASME Journal of Heat Transfer, Vol. 109, pp. 789–801, 1987.

[20] Kuyper, R.A., Van Der Meer, Th. H., Hoogendoorn, C. J., and Henkes, R. A. W. M., “Numerical Study of Laminar and Turbulent Natural Convection in an Inclined Square Cavity,” International Journal of Heat and Mass Transfer, Vol. 36, No. 11, pp. 2899-2911, 1992.

[21] Lakhal, E. K., Hasnaoui, M.and Vasseur, P., “Numerical study of transient natural convection in a cavity heated periodically with different types of excitations”, International Journal of Heat and Mass Transfer, Vol. 42, No. 21, pp. 3927–3941, 1999.

[22] Le Quere, P., Humphery, J. A., and Sherman, F.S. ”Numerical calculation of thermally driven two-dimensional unsteady laminar flow in cavities of rectangular cross section”, Numerical Heat Transfer, Vol. 4, pp. 249-283,1981.

[23] Lewis, R.W., Morgan, K., Thomas, H. R. and Seetharamu, K. N., The Finite element method in heat transfer analysis, John Wiley & Sons, New York, 1996.

[24] Linthorst, S.J.M., Schinkel, W. M. M., and Hoogendorn, C. J., “Flow Structure with Natural convection in Inclined Air-filled Enclosures,” Journal of Heat Transfer. Vol. 103, pp.535-539, 1981.

[25] Mohamad, A., “Natural convection in open cavities and slots”, Numerical Heat Transfer, Vol. 27, pp. 705-716, 1995.

[26] Ozoe, H., Sayama, H., and Churchill, S. W., “Natural Circulation in an Inclined Rectangular channel at Various Aspect Ratios and Angles—Experimental Measurements,” International Journal of Heat and Mass Transfer, Vol.18, pp.1425-1420, 1975.

[27] Ozoe, H., Sayama, H., and Churchill, S. W., “Natural Convection in an Inclined Square Channel,” International Journal of Heat and Mass Transfer, Vol. 17, pp.401-406,1974.

[28] Patankar, S. V., Numerical Heat Transfer and Fluid Flow, Hemisphere, Washington, DC; McGraw-Hill, New York, 1980.

[29] Penot, F., “Numerical calculation of two-dimensional natural convection in isothermal open cavities”, Numerical Heat Transfer, Vol. 5, pp. 421-437, 1982.

[30] Peraire, J., Vahidati, M., Morgan, K., and Zienkiewicz, O. C. Adaptive remeshing for compressible flow computation, Journal of Computational Physics, Vol.72, pp. 449-466, 1987.

[31] Polat, O. and Bilgen, E. “Laminar natural convection in inclined open shallow cavities”, Int. J. Therm Sci, Vol. 41, pp. 360-368, 2002.

[32] Reddy J.N. and Gartling, “Fundamentals of the Finite Element Method in Heat Transfer”, Second Ed., CRC Press, 2001.

[33] Showole, R.A. and Tarasuk, J.D., “Experimental and numerical studies of natural convection with flow separation in upward-facing inclined open cavities”,Journal of Heat Transfer, Vol. 115, pp. 592-605, 1993.

[34] Soong, C. Y., Tzeng, P. Y., Chiang, D. C., and Sheu, T. S., "Numerical Study on Mode-transition on Natural Convection in Differentially Heated Inclined Enclosures", International Journal of Heat and Mass Transfer, Vol. 39, No. 14, pp. 2869-2882, 1996.

[35] Tasnim, S. T. and Collins, M.R. "Numerical analysis of heat transfer in a square cavity with a baffle on the hot wall", Int. Com. Heat and Mass Transfer, Vol. 31, pp. 639–650, 2004.

[36] Zhong, Z.Y., Yang, K. T., and Lloyd, J. R., "Variable-property Natural convection in tilted Enclosures with Thermal Radiation", Numerical Methods in Heat Transfer, Vol. III, pp. 195-214, 1985.

[37] Zienkiewicz, O. C. and Taylor, R. L. The finite element method, Fourth Ed., McGraw-Hill. 1991.